Geographic Range Shifts under Climate Warming

Ying Zhou

A dissertation
submitted in partial fulfillment of the
requirements for the degree of

Doctor of Philosophy

University of Washington

2013

Reading Committee:

Mark Kot, Chair

Eric Shea-Brown

Loyce Adams

Program Authorized to Offer Degree:
Applied Mathematics

University of Washington

Abstract

Geographic Range Shifts under Climate Warming

Ying Zhou

Chair of the Supervisory Committee:
Professor Mark Kot
Department of Applied Mathematics

Rapid climate warming has caused species across the globe to shift their geographic ranges, and ecologists are increasingly concerned about whether species are able to track climate warming. Early efforts to predict species ranges used statistical correlation models that neglected population dynamics. Recently, theoretical ecologists have begun to incorporate both population growth and dispersal in their models.

Integrodifference equations are useful in describing spatiotemporal dynamics of species with distinct growth and dispersal stages. These equations can accommodate a diverse assortment of dispersal mechanisms. I incorporated climate warming into some classic examples of integrodifference equations by letting the *niche curve*, a curve describing environmental suitability for population growth on a spatial gradient, shift in one direction. The equations thus become non-autonomous. Using a series of these non-autonomous integrodifference equations, I investigate the impact of changing climatic conditions on a single-species population. These integrodifference equations can prescribe climate-warming scenarios and environmental heterogeneity in a versatile way.

These new models capture the range-shift phenomenon. A population experiencing niche-curve shifts exhibits traveling pulse solutions when it persists. The population may, however, lag behind the shifting niche curve, and carry a *niche deficit*. The niche deficit may stabilize at a level, or keep accumulating, depending on the acceleration of climate warming. Acceleration of climate warming is shown to impose extra burden on the species,

compared with constant-speed warming, even if the amount of warming is the same over the same period of time for a fair comparison.

The population experiencing climate warming may also fail to persist, and go extinct, if climate warming is too rapid. The threshold speed for persistence, or the critical speed, c^*, can be viewed as the species' ability to keep up with climate warming. This critical speed depends both on the species' growth or recruitment, and its dispersal.

TABLE OF CONTENTS

LIST OF FIGURES

ACKNOWLEDGMENTS

I wish to express my deep appreciation to my advisor, Dr. Mark Kot, whose mentorship was one of the most wonderful gifts I have received. I would also like to thank Dr. Eric Shea-Brown, Dr. Janneke Hille Ris Lambers, and Dr. Loyce Adams for their patient guidance, constructive suggestions, and enthusiastic championship.

I have benefited significantly from interacting with many ecologists on campus. I wish to thank the Janneke lab and the Kot lab for many inspiring conversations. I would like to also thank my home department, Department of Applied Mathematics at University of Washington, for a much-appreciated graduate school experience.

DEDICATION

To my friend John K. Adams

Chapter 1

INTRODUCTION

Climate change has been a powerful driving force for species range changes. Paleoclimate and paleoecological records have demonstrated extensive species range changes during the glacial and interglacial alternations in the Quaternary Period [55, 88]. Recent warming in the Earth's climate has also caused well-documented ecological changes in species ranges [21, 20, 51, 54, 67, 80, 88, 100, 116, 119, 153]. With further warming projected [58], studying the impacts of climate warming on species ranges is an imperative task.

Range changes are complicated processes that may involve population growth and decline, dispersal, interspecific interactions, etc. Mathematical models are therefore useful in separating the complicated processes into simple, fundamental components. For example, models for single-species populations may provide important insights for multi-species populations and community ecology. Simple models can then be extended to increase their complexity.

This dissertation aims at studying climate-induced range shifts for a single-species population. Models in this dissertation consider species with distinct growth and dispersal stages in their life cycles. Some annual plants, for example, may germinate in spring, flower in summer, and set seeds in autumn. The seeds then disperse, and give rise to new individuals. For these species, integrodifference equations are powerful tools to incorporate growth and dispersal, and hence spatiotemporal population dynamics, in the study of range shifts.

1.1 Discrete-time population dynamics and difference equations

For many species, birth and death are episodic rather than continuous, and occur in well-defined time periods within their life cycles. These time periods are often well-synchronized within a population of the species. Population censuses for these species are often conducted at discrete time points (e.g., annually), and their population dynamics are better captured

by discrete-time models, such as difference equations, rather than by continuous-time models such as differential equations.

Difference equations have been used extensively to model population dynamics. Many difference equations reveal amazingly rich, chaotic dynamics despite the simple forms of these equations. A well-known example of a simple equation with chaotic dynamics can be seen in early studies by May [95, 96, 97] and Li and Yorke [84] of the discrete-time logistic map

$$n_{t+1} = n_t \left[1 + r\left(1 - \frac{n_t}{K}\right)\right]. \tag{1.1}$$

In addition to the plethora of simple mappings with complex and often chaotic behaviors, there are also many difference equations with simple dynamics. One example is the equation

$$n_{t+1} = \frac{R_0 n_t}{1 + [(R_0 - 1)/K]n_t}. \tag{1.2}$$

Here, n_t stands for population density at the t-th time step. The right-hand side of equation (1.2) is the Beverton−Holt stock-recruitment curve [12]. The Beverton−Holt stock-recruitment curve is a classic depiction of density-dependent recruitment that involves an increasing limitation on recruitment as the population becomes more dense, but without an actual decline in recruitment.

Equilibria of mapping (1.2) can be found by solving the equation

$$n^* = \frac{R_0 n^*}{1 + [(R_0 - 1)/K]n^*} \tag{1.3}$$

for n^*. At an equilibrium n^*, the variable n_t is locked at n^* and does not change, hence the population neither grows or declines. Equation (1.2) has two equilibria, $n_1^* = 0$ and $n_2^* = K$. The equilibrium n_1^* is referred to as the trivial equilibrium. The non-trivial equilibrium $n_2^* = K$ describes the state where birth and death still occur but equal each other. The population density at this state, K, is referred to as the *carrying capacity*.

The parameter R_0, referred to as the *net reproductive rate*, is the highest possible per capita recruitment rate for the population. Depending on R_0, difference map (1.2) exhibits two fundamentally different types of dynamics. When $R_0 < 1$, the trivial equilibrium is *asymptotically stable*. That is, with any initial population density n_0, the consequent population density n_t approaches the trivial equilibrium over time, and the population

approaches extinction. When $R_0 > 1$, the trivial equilibrium becomes *unstable* while the non-trivial equilibrium becomes asymptotically stable: the population density approaches the carry capacity K with any positive initial density n_0. Therefore the population is said to be *persistent* when $R_0 > 1$.

1.2 Modeling growth and dispersal with integrodifference equations

The process of individuals or of parts of individuals moving away from a natal site to give rise to new individuals, referred to as *dispersal*, plays a crucial role in population ecology. While difference equations capture temporal dynamics of a population, they neglect the spatial spread of the population. To incorporate dispersal into the model and capture spatiotemporal dynamics of the population, integrodifference equations are often useful.

Integrodifference equations are discrete-time, continuous-space models. They are increasingly used by ecologists for organisms with distinct growth and dispersal stages. For example, the equation

$$n_{t+1}(x) = \int_{\Omega} k(x,y) f[n_t(y)]\, dy \tag{1.4}$$

describes a single, unstructured population living on a one-dimensional spatial habitat Ω. The variable $n_t(x)$ is the population density at the t-th time step at location x. Equation (1.4) maps $n_t(x)$, the population density at time step t, to $n_{t+1}(x)$, the population density at the next time step, in two stages: the sedentary growth stage and the dispersal stage. During the sedentary stage, individuals may grow, reproduce, or die. The local population density $n_t(y)$ at location y within spatial domain Ω, is replaced by the density of propagules, $f[n_t(y)]$. Individuals outside the spatial domain Ω do not reproduce. The function f is the growth or recruitment function. The right hand side expressions in the difference equations (1.1) and (1.2) are all candidates for f.

The propagules then disperse during the dispersal stage. The integral kernel $k(x,y)$ quantifies dispersal, and is referred to as the *dispersal kernel*. For a fixed source of propagules y, the dispersal kernel is a probability density function for the destination, x, of the propagules. The integral in equation (1.4) then tallies all propagules from the habitat Ω that have x as their final destination.

The dispersal kernel is protean, and depends, in general, on both the source y and the destination x. For simplicity, it is assumed throughout this thesis that space is homogeneous and isotropic for dispersal. The kernel $k(x, y)$ can therefore be written as the difference kernel $k(|x - y|)$, and the integrodifference equation becomes

$$n_{t+1}(x) = \int_{\Omega} k(|x - y|) f[n_t(y)]\, dy. \tag{1.5}$$

The difference kernel $k(|x - y|)$ can be understood as the probability density function for the displacement of the propagules. Well-known candidates of difference kernels include the Gaussian, Laplace, and Cauchy distributions.

One classic problem in integrodifference-equation models is the study of population persistence [72, 77, 78, 87, 151, 152]. Latore et al. [77], for example, studied the integrodifference equation

$$n_{t+1}(x) = \int_{-\frac{L}{2}}^{\frac{L}{2}} k(x - y) f[n_t(y)]\, dy, \tag{1.6}$$

for a population on a finite, homogeneous patch of length L. Since individuals cannot reproduce outside the domain $[-L/2, L/2]$, they fail to contribute to the next generation if they disperse across patch boundaries. The smaller the patch size L, the larger the proportion of lost individuals. There is, therefore, a critical patch size below which the population cannot persist. Latore et al. later extended model (1.6) to model

$$n_{t+1} = Q(x) \int_{-\infty}^{\infty} k(x - y) f[n_t(y)]\, dy, \tag{1.7}$$

to include spatial heterogeneity in recruitment rate. In equation (1.7), Q(x) is a habitat quality function that prescribes post-dispersal habitat quality, such as habitat quality for seedling recruitment, at location x. They found that the shape of the habitat quality function $Q(x)$ affects population persistence as well.

If the habitat quality function is the constant function $Q(x) \equiv 1$ for $x \in (-\infty, \infty)$, model (1.7) reduces to equation

$$n_{t+1} = \int_{-\infty}^{\infty} k(x - y) f[n_t(y)]\, dy. \tag{1.8}$$

Equation (1.8) was used to study invasive organisms by Kot et al. [70], and was extended to other integrodifference equations in the invasive organisms literature [37, 83, 104, 107].

Equation (1.8) is known to exhibit traveling wave solutions when the population can persist [156, 157]. Depending on the dispersal kernel, the traveling waves may have a constant speed [48, 69, 89, 156, 157], or accelerated speeds [23, 70, 82].

1.3 Incorporating climate warming

Equations (1.6) and (1.7) are autonomous. The spatial domain $[-L/2, L/2]$ and the habitat quality function $Q(x)$ do not depend on time t. Under climate warming, however, environmental conditions change over time. In chapters 2 and 3, I examine the non-autonomous model

$$n_{t+1}(x) = \int_{-\frac{L}{2}+ct}^{\frac{L}{2}+ct} k(x-y) f[n_t(y)]\, dy. \tag{1.9}$$

Model (1.9) is built upon model (1.6), but with a shifting spatial domain $[-L/2+ct, L/2+ct]$. Rather than living in a fixed patch $[-L/2, L/2]$, the population now resides on a patch that moves, because of climate warming, to the right, at a constant speed c. It is found in Chapter 2 that the speed of shift, c, affects population persistence profoundly. If the speed c is larger than a critical speed c^*, the population cannot persist. The existence of such a "tipping point" is supported by models in other frameworks, such as reaction-diffusion equations [9, 122] and stochastic simulations [148]. Numerical calculations of the critical speed of shift indicates that c^* depends on the patch size L, the dispersal kernel $k(x-y)$, and the growth or recruitment function f. One can understand the critical speed c^* as a quantification of a species' ability to keep up with climate warming while living in a patch of a fixed size L. Following the numerical calculations, I propose a dimension-reduction method in Chapter 3 to obtain analytic approximations of the critical speed c^*. Applications of this method on many examples demonstrate that a close approximation of the critical speed can often be obtained even when the reduced dimensions are very low.

Even though most models in climate-induced range shifts assume the simplest case of constant-speed warming [9, 122, 148, 161], climate warming is projected to accelerate [58]. In Chapter 4, I extend model (1.9) to a more universal form,

$$n_{t+1} = \int_{-\infty}^{\infty} k(x-y) Q[y-s(t)]\, f[n_t(y)]\, dy. \tag{1.10}$$

Here, $Q(y)$ is a pre-dispersal habitat suitability function that describes environmental conditions for pre-dispersal population growth along a spatial gradient. The function $s(t)$ causes the curve of $Q(y)$ to shift, and prescribes climate-induced changes in the environmental conditions. This model accommodates a variety of climate-warming scenarios. When $s(t) = ct$, for example, the speed of climate warming is constant, while $s(t) = c_1 t + c_2 t^2/2$ prescribes accelerated warming.

Model (1.9) is a special case of model (1.10). When $s(t) = ct$, and the habitat suitability function $Q(y)$ is a hat function

$$Q(y) = \begin{cases} 1, & y \in [-L/2, L/2], \\ \\ 0, & y \notin [-L/2, L/2], \end{cases} \tag{1.11}$$

model (1.10) reduces to model (1.9). On the other hand, Model (1.10) is also similar to model (1.7), but modifies and extends it to include climate warming. In chapter 4, both scenarios $s(t) = ct$ and $s(t) = c_1 t + c_2 t^2/2$ are considered. This is, to the best of my knowledge, the first attempt to model range shifts under accelerated climate warming. Results within Chapter 4 are alarming. Compared with a constant-speed warming, an acceleration in climate warming is found to impose extra burden on the species, even if the amount of warming is the same over the same period of time for a fair comparison.

Chapter 2

DISCRETE-TIME GROWTH-DISPERSAL MODELS WITH SHIFTING SPECIES RANGES

2.1 Introduction

The Earth's climate is warming. Global average temperatures have increased by 0.13 °C per decade over the last 50 years (1956–2005). Further warming, at an even faster rate, is expected over the next 50 years [58]. This warming is expected to cause species to shift their ranges poleward in latitude or upward in elevation [54, 88, 100, 116, 153]. Ecologists must now face the challenge of predicting the range-shifting responses of the Earth's biota.

Bioclimate envelope models are commonly used to assess the impacts of climate change on species distributions [5, 13, 42, 60, 120]. These statistical models correlate the current distribution of a species with climatic variables such as degree-days, maximum and minimum temperatures, and water balance. Ideally, scientists can combine a species' climate envelope with projections of climate change to predict a species' new distribution.

The use of bioclimate envelope models has, however, been contentious [62, 118]. One (of several) criticisms is that bioclimate envelope models do not account for species dispersal [41, 102, 118]. Rather, they predict the *potential* ranges of species. Poor dispersers may, in general, fail to live up to their potential.

Can a species keep pace with climate-induced range shifts? We believe that one must use a mathematical model that incorporates growth, dispersal, and climate-driven spatial shifts to answer this question.

There are many mathematical models that describe the growth and dispersal of biological populations [64, 66, 141]. The use of reaction-diffusion equations [18, 38, 109, 140, 142] is especially common. For reaction-diffusion models, space and time are continuous. Growth and diffusion, moreover, are assumed to occur simultaneously. Recently, Potapov and Lewis [122] and Berestycki et al. [9] used reaction-diffusion models to study the effects of climate

change on the ranges of plants and animals. Berestycki et al. [9], in particular, showed that if a habitat shifts too rapidly, species may go extinct.

Many species have distinct growth and dispersal stages. Summer annuals, for example, may germinate in spring, flower in summer, and disperse their seeds in autumn. Insects typically disperse as adults, and only less so as larvae [111]. For these species, ecologists increasingly use integrodifference equations [50, 70, 72, 77, 83, 87, 90, 104, 105, 151] instead of reaction-diffusion models. Integrodifference equations are discrete-time, continuous-space models. In the simplest case, with discrete, nonoverlapping generations, one writes

$$n_{t+1}(x) = \int_{\Omega} k(x,y)\, f[n_t(y)]\, dy. \tag{2.1}$$

Here, $n_t(x)$ is the population density in generation t at location x, Ω is the spatial domain, $f(n)$ is the recruitment or growth function, and $k(x,y)$ is the redistribution or dispersal kernel.

Integrodifference equations can, because of their protean kernel, handle a diverse assortment of dispersal mechanisms [105]. These equations have, as a result, been used for a wide variety of applications. Two of these applications are especially relevant to the current problem. The first application is the study of population persistence [72, 77, 78, 87, 151, 152]. Latore et al. [77, 78], for example, studied persistence on a finite, homogeneous, one-dimensional patch of size or length L using the integrodifference equation

$$n_{t+1}(x) = \int_{-\frac{L}{2}}^{\frac{L}{2}} k(x,y)\, f[n_t(y)]\, dy. \tag{2.2}$$

Since individuals disperse and are lost across patch boundaries, there is a critical patch size below which the patch's population cannot persist. This critical size depends on both the population's growth rate and on the kernel $k(x,y)$, which implicitly defines the boundary conditions.

The other application is the study of invasive organisms [37, 70, 83, 104, 107]. These studies typically start with an integrodifference equation on an infinite domain,

$$n_{t+1}(x) = \int_{-\infty}^{\infty} k(x,y)\, f[n_t(y)]\, dy. \tag{2.3}$$

Integrodifference equations can, like reaction-diffusion equations, generate constant-speed traveling waves [48, 69, 89, 156, 157]. They may, however, also generate accelerating invasions [23, 70, 82].

The problem we consider involves both population persistence and invasion. We examine an integrodifference equation in which all growth occurs on a finite domain that moves at a constant speed, mimicking a climate-driven range shift. (In future work, we also hope to examine accelerating range shifts.) Warming may, of course, affect different parts of the life cycle. In this paper, we focus on the impact of warming on reproductive processes because of the demonstrated effect of climate change on phenology and reproductive biology [41, 81, 100, 115, 153]. We do not, in contrast, consider direct effects of warming on dispersal since this is thought to be less important (but see section 2.6). In the next section, we describe our model in detail, provide mathematical background, and give a numerical example of how the speed with which a patch shifts affects persistence. Section 2.3 contains mathematical analyses that explain the phenomena observed in section 2.2. Sections 2.4 and 2.5 focus on analytically and numerically tractable examples. In section 2.6, we illustrate our ideas using data for Fender's blue butterfly (*Icaricia icarioides fenderi*), an endangered subspecies of Oregon's Willamette Valley [133]. Finally, section 2.7 contains our discussion and concluding remarks.

2.2 Model

We begin by considering the integrodifference equation

$$n_{t+1}(x) = \int_{-\frac{L}{2}+ct}^{\frac{L}{2}+ct} k(x,y)\, f[n_t(y)]\, dy. \tag{2.4}$$

This equation differs from a model on a stationary domain, equation (2.2), in its limits of integration, and hence, its habitat boundaries. Our population is no longer restricted to an immobile one-dimensional patch. Rather, our population reproduces on an interval, initially $[-L/2, L/2]$, that moves, because of climate change, to the right, at constant speed c. We will use this formulation for both latitudinal and elevational range shifts.

Equation (2.4) maps the density of the population in generation t, $n_t(x)$, $x \in (-\infty, \infty)$, to the density in the next generation, $n_{t+1}(x)$, in two stages. The first stage accounts for the

sedentary part of the organism's life cycle. During this stage, individuals inside the interval $[-(L/2)+ct,(L/2)+ct]$ grow, reproduce, and die. The local density inside the interval, $n_t(x)$, is replaced by a new density, $f[n_t(x)]$, of propagules. Individuals outside the interval fail to reproduce.

The function f is the growth or recruitment function. Well-known choices for f include the right-hand sides of the Beverton–Holt [12] stock-recruitment curve,

$$n_{t+1} = \frac{R_0 n_t}{1+[(R_0-1)/K]n_t}, \tag{2.5}$$

the logistic difference equation [94, 99],

$$n_{t+1} = (1+r)n_t - \frac{r}{K}n_t^2, \tag{2.6}$$

and the Ricker [127] curve,

$$n_{t+1} = n_t e^{r(1-\frac{n_t}{K})}. \tag{2.7}$$

Here, K is the carrying capacity of the environment, R_0 is the net reproductive rate, and r is the intrinsic rate of growth. In this paper, we only consider nonnegative growth functions that satisfy

$$f(n) \le f'(0)\, n. \tag{2.8}$$

That is, we explicitly exclude growth functions with Allee [1] effects.

In the second (or dispersal) stage, propagules disseminate. This movement is described by the dispersal kernel $k(x,y)$. For a fixed source y, we may think of the kernel as the probability density function for the destination, x, of the propagules. In this paper, we consider dispersal to be homogeneous and isotropic. We thus assume that our dispersal kernel is both a difference kernel, $k(x,y) = k(x-y)$, and symmetric. Equation (2.4) can now be written as the convolution equation

$$n_{t+1}(x) = \int_{-\frac{L}{2}+ct}^{\frac{L}{2}+ct} k(x-y)\, f[n_t(y)]\, dy. \tag{2.9}$$

Our difference kernel acts as a probability density function for the displacement of the propagules. Well-known examples of symmetric difference kernels include the Gaussian, Laplace, and Cauchy distributions. The convolution integral tallies all propagules within the shifted patch $[-(L/2)+ct,(L/2)+ct]$ that have x as their final destination.

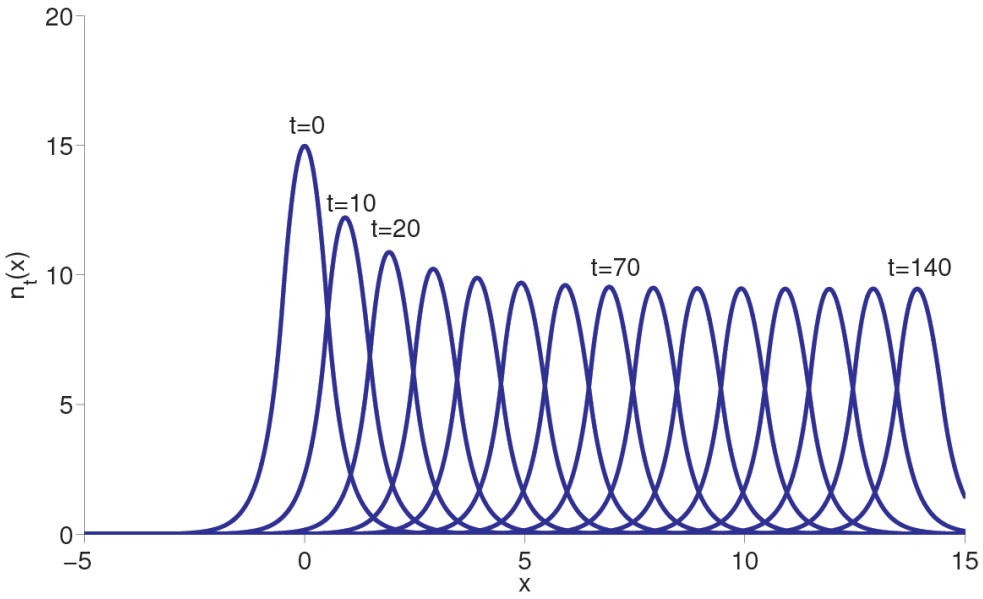

(a)

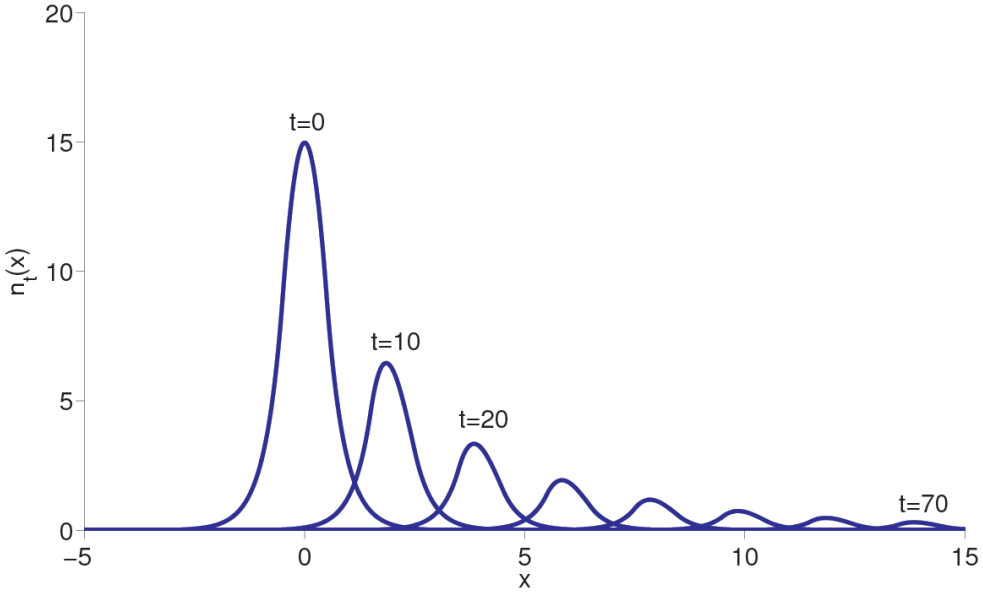

(b)

Figure 2.1: Simulations of the distribution of a population on a one-dimensional patch of size $L = 1$ show that the population will die out when the speed c is large. For this simulation, we used Laplace dispersal kernel (2.10), with $b = 2.5$, and Beverton–Holt stock-recruitment curve (2.5), with $R_0 = 1.7$ and $K = 100$. The initial distribution, marked $t = 0$, was obtained by iterating convolution equation (2.9), with $c = 0$, for a point release of 50 individuals at $x = 0$ for 120 generations, so that the population converged to a steady distribution. We then iterated equation (2.9) with (a) $c = 0.1$ and (b) $c = 0.2$. In (a), the population persisted. In (b), the population went extinct. The distribution is displayed every 10 generations and was computed using an FFT-assisted implementation of the extended trapezoidal rule with 2^{16} nodes.

The presence of a shifting or moving range can have a profound effect on the dynamics of a population. Figure 2.1 shows that an increase in the speed c can cause extinction. This figure was obtained by simulating equation (2.9) with the Laplace kernel,

$$k(x-y) = \frac{1}{2}\, b\, \exp\left(-b\,|x-y|\right), \tag{2.10}$$

and the Beverton–Holt stock-recruitment curve, equation (2.5). For $L = 1$, $b = 2.5$, $R_0 = 1.7$, $K = 100$, and a small speed of translation ($c = 0.1$), the population persists (Figure 2.1a). When we increase the speed to $c = 0.2$, however, the population cannot keep up with climate change and goes extinct (Figure 2.1b). Berestycki et al. [9] observed similar events for their reaction-diffusion model.

Our simulations suggest that there is an upper limit on the speed, $c = c^*$, with which a population can move. Beyond this critical speed, a population cannot persist unless other parameters also change. Increasing the net reproductive rate or the patch size permits a larger critical speed. Changing the shape or scale of the dispersal kernel has, in contrast, a less consistent effect.

What is the relationship between the critical speed and the other parameters in our model? To answer this question, we turn to a mathematical analysis of the condition for population persistence.

2.3 Analysis of population persistence

Since the habitat is moving with constant speed c, we will look for a traveling pulse,

$$n_t(x) = n^*(\bar{x}) \equiv n^*(x - ct). \tag{2.11}$$

After substituting this solution into convolution equation (2.9), we find that

$$n^*(x - ct - c) = \int_{-\frac{L}{2}+ct}^{\frac{L}{2}+ct} k(x-y)\, f[n^*(y-ct)]\, dy. \tag{2.12}$$

If we change variables, so that $\bar{y} = y - ct$ and $\bar{x} = x - ct$, and shift $\bar{x}$ by c, we find that our traveling pulse must satisfy the integral equation

$$n^*(\bar{x}) = \int_{-\frac{L}{2}}^{\frac{L}{2}} k(\bar{x} + c - \bar{y})\, f[n^*(\bar{y})]\, d\bar{y}. \tag{2.13}$$

For the growth functions for the Beverton–Holt curve, equation (2.5), the logistic equation, equation (2.6), and the Ricker curve, equation (2.7), $n^*(\bar{x}) = 0$ is a trivial solution. We would like to study the stability of this solution, since population persistence is equivalent to the instability of the trivial solution.

In general, the stability of a traveling pulse can be studied by adding a small perturbation, $\xi_t(x)$, to the pulse,

$$n_t(x) = n^*(\bar{x}) + \xi_t(x). \tag{2.14}$$

Because restriction (2.8) excludes Allee effects, we may linearize the right hand side of equation (2.9) about the traveling pulse to obtain

$$\xi_{t+1}(x) = \int_{-\frac{L}{2}+ct}^{\frac{L}{2}+ct} k(x-y)\, f'[n^*(\bar{y})]\, \xi_t(y)\, dy. \tag{2.15}$$

For the trivial solution, equation (2.15) reduces to

$$\xi_{t+1}(x) = f'(0) \int_{-\frac{L}{2}+ct}^{\frac{L}{2}+ct} k(x-y)\, \xi_t(y)\, dy. \tag{2.16}$$

We now write our perturbation as

$$\xi_t(x) = \lambda^t\, u(x-ct). \tag{2.17}$$

After substituting this expression into equation (2.16), we change variables, so that $\bar{y} = y - ct$ and $\bar{x} = x - ct$, and shift $\bar{x}$ by c, to obtain

$$\lambda\, u(\bar{x}) = f'(0) \int_{-\frac{L}{2}}^{\frac{L}{2}} k(\bar{x}+c-\bar{y})\, u(\bar{y})\, d\bar{y}. \tag{2.18}$$

λ is an eigenvalue of the integral operator with eigenfunction $u(\bar{x})$.

The stability of the trivial solution is determined by the dominant eigenvalue, i.e., by the eigenvalue λ with largest magnitude. The trivial solution loses stability when the magnitude of the dominant eigenvalue exceeds one.

We now restrict our domain to $(\bar{x}, \bar{y})$ that satisfy $\bar{x} \in [-L/2, L/2]$ and $\bar{y} \in [-L/2, L/2]$. If our dispersal kernel is continuous on this domain and if the interval $[-L/2, L/2]$ is finite, then the linear integral operator on the right-hand side of equation (2.18) is compact (or completely continuous). The eigenvalues of a compact linear operator form a discrete set.

This set may be finite, countably infinite, or empty [57, 65]. Each eigenvalue is of finite multiplicity and zero is the only possible accumulation point for the eigenvalues. In general, the eigenvalues are complex. If, moreover, the kernel is positive, we may invoke Jentzsche's (1912) theorem [61](see also [53] and [75]). Jentzsch's theorem is an extension of the Perron–Frobenius theorem for positive matrices to integral equations with positive kernels. The theorem guarantees the existence of a simple and positive dominant eigenvalue with positive eigenfunction. If the conditions of the theorem are satisfied, persistence is gained or lost as the dominant eigenvalue passes through $\lambda = 1$.

Continuous dispersal kernels with infinite support, such as the Laplace and Gaussian distributions, always satisfy Jentzsch's theorem for $[-L/2, L/2]$ finite. Continuous dispersal kernels with compact support may also satisfy this theorem, but only if the radius of their support is sufficiently large relative to the patch size L and speed c.

2.4 A simple, separable example

Eigenvalue problem (2.18) simplifies to a finite-dimensional problem in linear algebra if its kernel is separable (or degenerate). A kernel is separable [77, 121] if it can be written as a finite, linear combination of products of a function of x alone and a function of y alone,

$$k(x, y) = \sum_{i=1}^{N} g_i(x)\, h_i(y). \tag{2.19}$$

Consider, for example, the kernel

$$k(x - y) = \begin{cases} \dfrac{\omega}{2} \cos \omega(x - y), & |x - y| \le \dfrac{\pi}{2\omega}, \\ 0, & |x - y| > \dfrac{\pi}{2\omega}, \end{cases} \tag{2.20}$$

with finite radius of dispersal $\pi/(2\omega)$. If we assume, for convenience, that this radius of dispersal is larger than the patch size,

$$\frac{\pi}{2\omega} > L, \tag{2.21}$$

and that the speed c is small,

$$c < \frac{\pi}{2\omega} - L, \tag{2.22}$$

eigenvalue problem (2.18) reduces to an equation,

$$\lambda\, u(\bar{x}) = f'(0) \int_{-\frac{L}{2}}^{\frac{L}{2}} \frac{\omega}{2} \cos\, \omega(\bar{x} + c - \bar{y})\, u(\bar{y})\, d\bar{y}, \tag{2.23}$$

that has a kernel that is positive for all $(\bar{x}, \bar{y})$ such that $\bar{x} \in [-L/2, L/2]$ and $\bar{y} \in [-L/2, L/2]$.

The kernel is also separable, since

$$\frac{\omega}{2} \cos\, \omega(\bar{x} + c - \bar{y}) = \frac{\omega}{2} \left[\cos\, \omega\bar{x}\, \cos\, \omega(\bar{y} - c) + \sin\, \omega\bar{x}\, \sin\, \omega(\bar{y} - c)\right]. \tag{2.24}$$

Our eigenvalue problem now takes the form

$$\begin{aligned} \lambda\, u(\bar{x}) \;&= \frac{\omega R_0}{2} \left[\int_{-\frac{L}{2}}^{\frac{L}{2}} \cos\, \omega\, (\bar{y} - c)\, u(\bar{y})\, d\bar{y}\right] \cos\, \omega\bar{x} \\ &\quad + \frac{\omega R_0}{2} \left[\int_{-\frac{L}{2}}^{\frac{L}{2}} \sin\, \omega\, (\bar{y} - c)\, u(\bar{y})\, d\bar{y}\right] \sin\, \omega\bar{x}, \end{aligned} \tag{2.25}$$

where $R_0 = f'(0)$.

Equation (2.25) implies that the eigenvector $u(\bar{x})$ can be written as a linear combination of $\cos\, \omega\bar{x}$ and $\sin\, \omega\bar{x}$,

$$u(\bar{x}) = c_1\, \cos\, \omega\bar{x} + c_2\, \sin\, \omega\bar{x}, \tag{2.26}$$

where c_1 and c_2 are constants. Inserting this expression into equation (2.25) and equating the coefficients of $\cos\, \omega\bar{x}$ and $\sin\, \omega\bar{x}$ on each side, we obtain the linear system

$$\lambda\, c_1 = a_{11}\, c_1 + a_{12}\, c_2, \tag{28a}$$

$$\lambda\, c_2 = a_{21}\, c_1 + a_{22}\, c_2, \tag{28b}$$

where

$$a_{11} = \frac{\omega R_0}{2} \int_{-\frac{L}{2}}^{\frac{L}{2}} \cos\,\omega(\bar{y}-c)\,\cos\,\omega\bar{y}\,d\bar{y} \tag{29a}$$

$$= \frac{R_0}{4}\,(\omega L + \sin\,\omega L)\,\cos\,\omega c,$$

$$a_{12} = \frac{\omega R_0}{2} \int_{-\frac{L}{2}}^{\frac{L}{2}} \cos\,\omega(\bar{y}-c)\,\sin\,\omega\bar{y}\,d\bar{y} \tag{29b}$$

$$= \frac{R_0}{4}\,(\omega L - \sin\,\omega L)\,\sin\,\omega c,$$

$$a_{21} = \frac{\omega R_0}{2} \int_{-\frac{L}{2}}^{\frac{L}{2}} \sin\,\omega(\bar{y}-c)\,\cos\,\omega\bar{y}\,d\bar{y} \tag{29c}$$

$$= \frac{R_0}{4}\,(-\omega L - \sin\,\omega L)\,\sin\,\omega c,$$

$$a_{22} = \frac{\omega R_0}{2} \int_{-\frac{L}{2}}^{\frac{L}{2}} \sin\,\omega(\bar{y}-c)\,\sin\,\omega\bar{y}\,d\bar{y} \tag{29d}$$

$$= \frac{R_0}{4}\,(\omega L - \sin\,\omega L)\,\cos\,\omega c.$$

Linear system (28) has the characteristic equation

$$\lambda^2 - (a_{11}+a_{22})\,\lambda + (a_{11}a_{22} - a_{12}a_{21}) = 0, \tag{2.29}$$

which reduces to

$$\lambda^2 - \left(\frac{R_0\,\omega L}{2}\cos\,\omega c\right)\,\lambda + \frac{R_0^2}{16}\,(\omega^2 L^2 - \sin^2\,\omega L) = 0. \tag{2.30}$$

Separable kernel (2.20) is continuous and nonnegative. If conditions (2.21) and (2.22) for the patch size, radius of dispersal, and shift speed are satisfied, the kernel is positive and Jentzsch's theorem guarantees us a simple and positive dominant eigenvalue. Stability of the trivial solution is then lost through $\lambda = 1$. Setting $\lambda = 1$ allows us to determine the critical speed c^*. Thus,

$$1 - \left(\frac{R_0\,\omega L}{2}\,\cos\,\omega c^*\right) + \frac{R_0^2}{16}\,(\omega^2 L^2 - \sin^2\,\omega L) = 0. \tag{2.31}$$

The added condition

$$\frac{R_0^2}{16}\,(\omega^2 L^2 - \sin^2\,\omega L) < 1 \tag{2.32}$$

ensures that $\lambda = 1$ is, in fact, the dominant eigenvalue. The critical speed c^* occurs within just one function of equation (2.31) and, if we solve for c^*, we quickly find that

$$c^* = \frac{1}{\omega} \cos^{-1} \left[\frac{16 + R_0^2 \left(\omega^2 L^2 - \sin^2 \omega L\right)}{8 R_0 \omega L} \right], \tag{2.33}$$

for

$$\frac{4}{\omega L + \sin \omega L} < R_0 < R_{\max}. \tag{2.34}$$

The critical speed is zero for smaller values of R_0. The upper limit on R_0 for our analysis, $R_{\max}$, is determined by the more stringent of conditions (2.22), for $c = c^*$, or (2.32).

For separable kernel (2.20) and conditions (2.21) and (2.22), we can also say something about the shape of any traveling pulses. Pulse equation (2.13) now takes the form

$$n^*(\bar{x}) = \frac{\omega}{2} \int_{-\frac{L}{2}}^{\frac{L}{2}} \cos \omega \left(\bar{x} + c - \bar{y}\right) f[n^*(\bar{y})] \, d\bar{y}, \tag{2.35}$$

which, because of our separable kernel, reduces to

$$\begin{aligned} n^*(\bar{x}) \; = & \frac{\omega}{2} \left\{ \int_{-\frac{L}{2}}^{\frac{L}{2}} \cos \omega \left(\bar{y} - c\right) f[n^*(\bar{y})] \, d\bar{y} \right\} \cos \omega \bar{x} \\ & + \frac{\omega}{2} \left\{ \int_{-\frac{L}{2}}^{\frac{L}{2}} \sin \omega \left(\bar{y} - c\right) f[n^*(\bar{y})] \, d\bar{y} \right\} \sin \omega \bar{x}. \end{aligned} \tag{2.36}$$

It is clear from this last equation that any traveling pulse $n^*(\bar{x})$ is a linear combination of $\cos \omega\bar{x}$ and $\sin \omega\bar{x}$. We thus let

$$n^*(\bar{x}) = a_1 \cos \omega\bar{x} + a_2 \sin \omega\bar{x}, \tag{2.37}$$

with constant coefficients a_1 and a_2. After substituting this expression into equation (2.36) and equating the coefficients of $\cos \omega\bar{x}$ and $\sin \omega\bar{x}$ on each side, we discover that a_1 and a_2 must satisfy

$$a_1 = \frac{\omega}{2} \int_{-\frac{L}{2}}^{\frac{L}{2}} \cos \omega \left(\bar{y} - c\right) f(a_1 \cos \omega\bar{y} + a_2 \sin \omega\bar{y}) \, d\bar{y}, \tag{39a}$$

$$a_2 = \frac{\omega}{2} \int_{-\frac{L}{2}}^{\frac{L}{2}} \sin \omega \left(\bar{y} - c\right) f(a_1 \cos \omega\bar{y} + a_2 \sin \omega\bar{y}) \, d\bar{y}. \tag{39b}$$

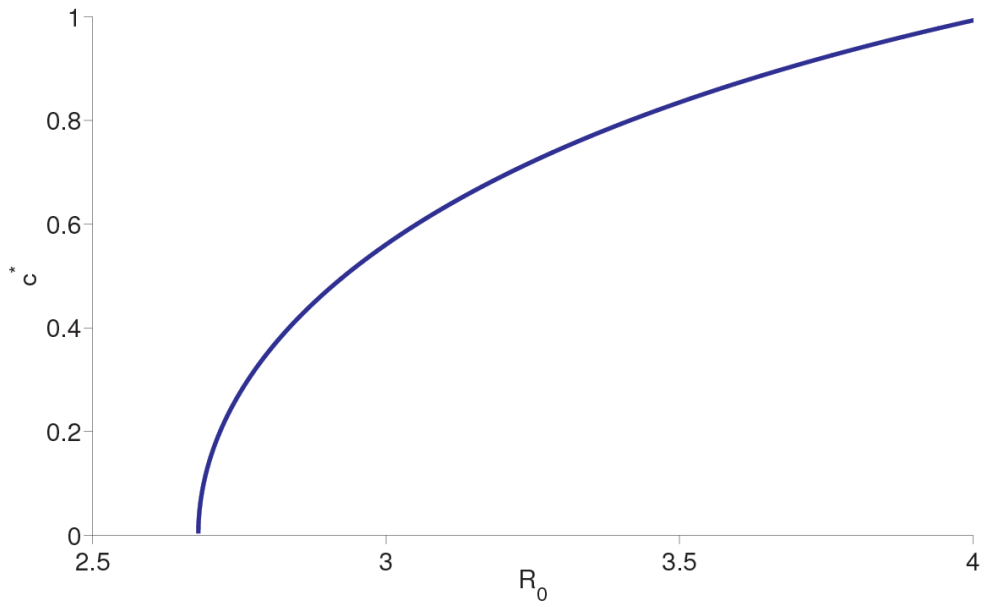

Figure 2.2: A plot of the critical speed (for extinction) as a function of the net reproductive rate R_0 for a population with Beverton–Holt growth, equation (2.5), and separable kernel (2.20). We used critical-speed equation (2.33) with patch size $L = 1$ and $\omega = \pi/4$ to draw this graph. Condition (2.22) requires $c < 1$.

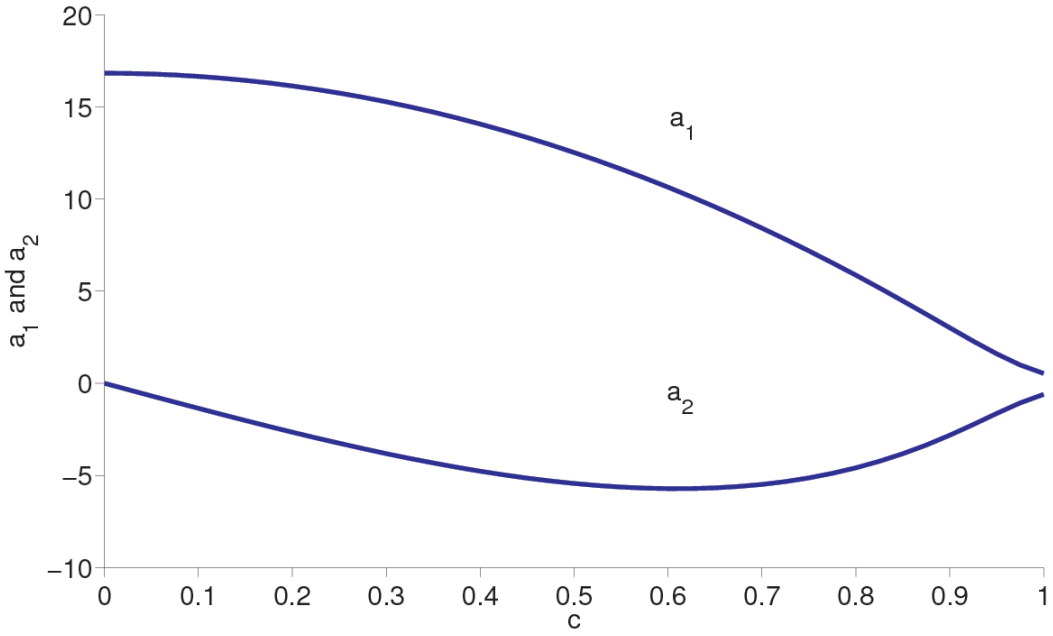

Figure 2.3: Shape coefficients a_1 and a_2 of traveling pulse (2.37) plotted as functions of the speed c. The coefficient a_1 is proportional to the total within-patch population while a_2 introduces asymmetry into the traveling pulse. Here, $L = 1$, $R_0 = 4$, $\omega = \pi/4$, $K = 100$.

For an arbitrary growth function, solving this nonlinear system for a_1 and a_2 is hard. These two equations do, however, provide a useful numerical scheme for calculating these coefficients. Begin by guessing a_1 and a_2, evaluate the right-hand sides of the two equations, and use these values as your new best guesses of a_1 and a_2. Repeat as needed. In our next example, this iterative scheme rapidly converges to the true a_1 and a_2.

To make the above discussion concrete, we focus on a population that obeys the Beverton–Holt stock-recruitment curve, equation (2.5); that has a patch size of one, $L = 1$; and that obeys dispersal kernel (2.20) with a radius of dispersal of two, so that $\omega = \pi/4$. Because of condition (2.22), we assume that $c < 1$. We plot the critical speed c^* as a function of the net reproductive rate R_0 (see Figure 2.2) using equation (2.33). (For higher speeds, the trivial equilibrium is stable and the population goes extinct.) The plotted curve increases monotonically and is concave down. Thus, as the critical speed c^* increases, a population must increase its net reproductive rate faster and faster to persist.

In Figure 2.3, we use system (39) to determine and plot the shape coefficients a_1 and a_2 of traveling pulse (2.37) as a function of the speed c for $0 \leq c \leq 1$, $L = 1$, $\omega = \pi/4$, and $R_0 = 4$. For the traveling pulse, the total population within the moving patch is proportional to the parameter a_1 and we see that this coefficient decreases monotonically as the speed c increases.

The coefficient a_2 introduces asymmetry into the pulse. To see this, we rewrite traveling pulse (2.37) as

$$n^*(\bar{x}) = A \cos(\omega\bar{x} + \phi) \tag{2.40}$$

with amplitude

$$A \equiv \sqrt{a_1^2 + a_2^2} \tag{2.41}$$

and phase lag

$$\phi \equiv \tan^{-1}\left(\frac{-a_2}{a_1}\right). \tag{2.42}$$

As c increases, the phase lag (see Figure 2.4) increases and the distribution of organisms within the habitat is increasingly asymmetric: individuals pile up near the lagging edge of the patch.

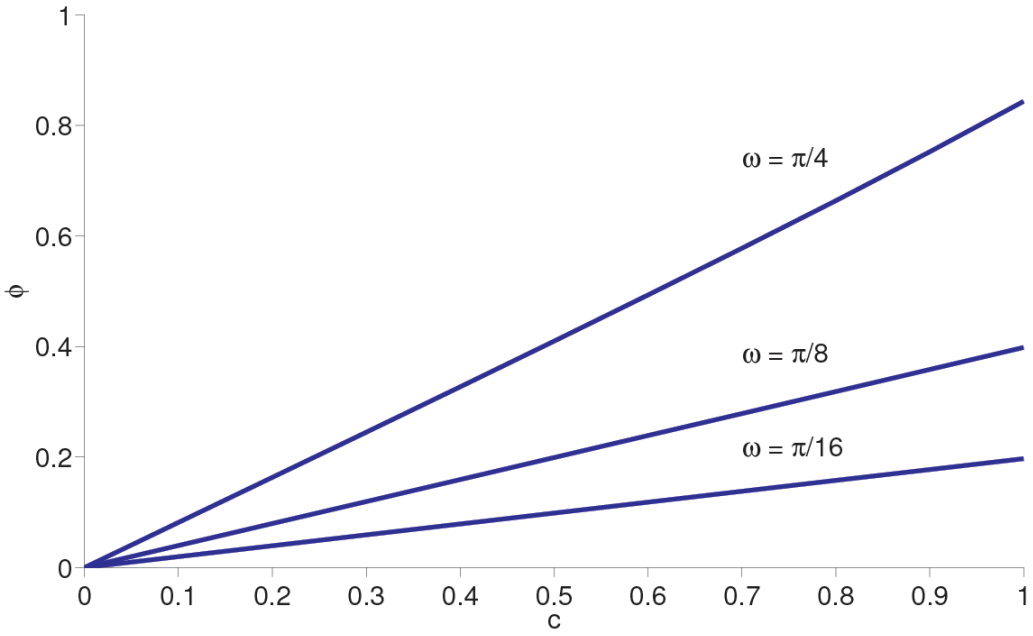

Figure 2.4: Phase lag ϕ, as defined by equation (2.42), plotted as a function of the speed c. As the speed c increases, the phase lag increases more or less linearly. The phase lag was computed for $L = 1$, $R_0 = 4$, and $\omega = \pi/16$, $\pi/8$, and $\pi/4$.

2.5 Numerical methods

Although separable kernels are tractable, they are also relatively rare. For most kernels, we need numerical methods.

The most useful numeric procedures for analyzing eigenvalue problem (2.18) all start with the Nyström method [31, 124]. That is, these procedures all begin by discretizing the integral using a quadrature rule.

The simplest quadrature rule is the repeated trapezoidal rule, which reduces equation (2.18) to

$$\lambda\, u(\bar{x}_i) = f'(0)\,\frac{\Delta\bar{x}}{2}\sum_{j=1}^{N-1}\left[\, k(\bar{x}_i + c - \bar{y}_j)\, u(\bar{y}_j) + k(\bar{x}_i + c - \bar{y}_{j+1})\, u(\bar{y}_{j+1})\,\right] \tag{2.43}$$

for $i = 1, \ldots, N$. Here, the domain of integration is discretized into $N-1$ equal subintervals of length $\Delta\bar{x} = L/(N-1)$. The variables $\bar{x}$ and $\bar{y}$ in equation (2.18) are each replaced by grid points that range from $-L/2$ to $L/2$ in units of $\Delta\bar{x}$ and that are labeled $\bar{x}_i$ and $\bar{y}_j$. If we let $c_i = u(\bar{x}_i)$,

$$A_{i1} = \frac{\Delta\bar{x}}{2}\, k(\bar{x}_i + c - \bar{y}_1), \tag{44a}$$

$$A_{ij} = \Delta\bar{x}\, k(\bar{x}_i + c - \bar{y}_j),\ 2 \le j \le N-1, \tag{44b}$$

$$A_{iN} = \frac{\Delta\bar{x}}{2}\, k(\bar{x}_i + c - \bar{y}_N), \tag{44c}$$

we now obtain the finite-dimensional linear system

$$\lambda\, c_i = f'(0)\sum_{j=1}^{N} A_{ij}\, c_j, \tag{2.45}$$

where $i = 1, \ldots, N$.

We can now analyze linear system (2.45) in one of two ways. The first approach starts by determining the eigenvalues of system (2.45) directly. The eigenvalues may be obtained using commands such as *eigs*, *eigen*, or *spec* in computing environments such as MATLAB, R, or Scilab or by using well-known routines from numerical libraries such as *Numerical Recipes* [124], LAPACK [2], or the GNU Scientific Library [40]. These commands and routines commonly balance a matrix, reduce the balanced matrix to Hessenberg form, and find the

eigenvalues of the Hessenberg matrix using a QR algorithm. (See [124] for details.) Choose the dominant eigenvalue. Since this eigenvalue depends continuously on the parameters of the model, one can find the critical value for a parameter, such as c, corresponding to an important root, such as $\lambda = 1$, using a standard root-finding algorithm, such as the method of bisection or Brent's method [14, 124].

As an alternative, set λ, in linear system (2.45), equal to one; use an efficient algorithm, such as LU decomposition [124], to evaluate the determinant of the system; and use a numerical root finder to find the value of a chosen parameter that makes the determinant zero. This approach has the advantage of being simpler to implement from scratch, but has the disadvantage that you are not guaranteed that $\lambda = 1$ is always the dominant eigenvalue.

Using these numerical methods, we extended Figure 2.2 for values of R_0 ($R_0 = f'(0)$ for growth function (2.5)) and c^* that violate smallness condition (2.22) (for $c = c^*$). The resulting curve (not shown) continues as before; it is monotonically increasing and concave down. A plot of the critical speed c^* as a function of the radius of dispersal, $\pi/(2\omega)$, for separable kernel (2.20) and $L = 1$ and $R_0 = 4$, in turn, shows (see Figure 2.5) that c^* increases with the dispersal radius when the radius is small, but decreases when the radius is large. When the radius is small, most propagules land within the old patch and increasing the radius helps propagules colonize the newly avaiable habitat in front of the old patch. In contrast, for large radii, most propagules already land outside of the old patch; increasing the radius now leads to overdispersal as more individuals land behind the old patch or in front of the newly available habitat.

The above numerical methods also allow us to determine the critical speed for kernels that are not separable. We will see examples of this in the next section.

2.6 Application

Fender's blue butterfly (*Icaricia icarioides fenderi*) is endemic to the Willamette Valley of Oregon and is listed as endangered by the [150]. This subspecies is, in many ways, poorly suited to our model: it is a habitat specialist, is not vagile, and does not disperse passively. (We will address these issues towards the end of this section.) Populations are, however, univoltine and do live in either isolated patches or in small, isolated clusters of patches

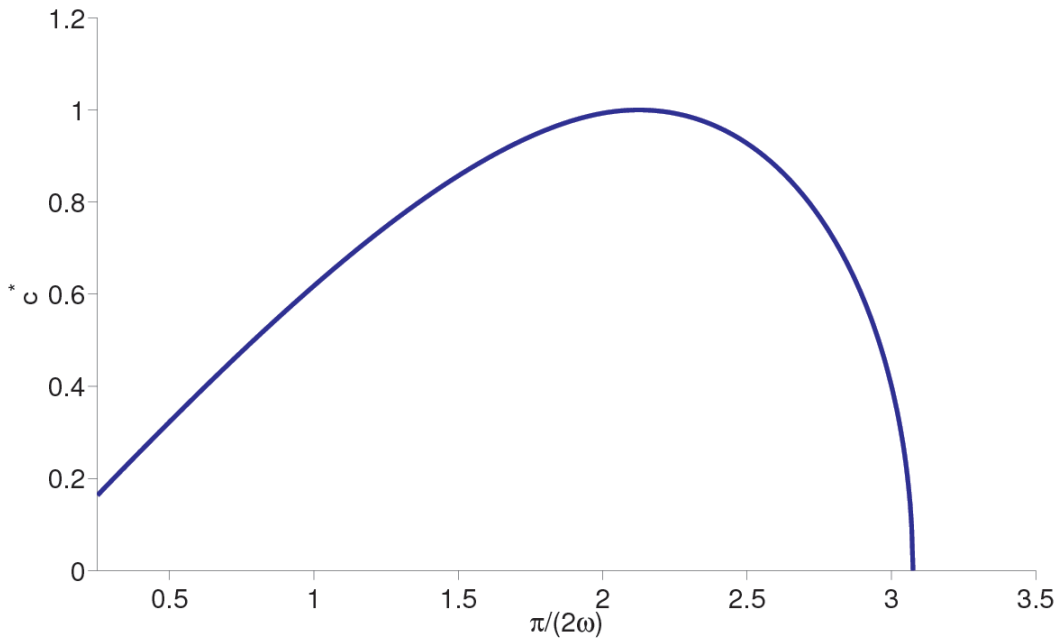

Figure 2.5: A plot of the critical speed as a function of the dispersal radius $\pi/2\omega$ for separable kernel (2.20). The eigenvalue problem, equation (2.18) with kernel (2.20), was discretized using Nyström's method for $L = 1$ and $R_0 = 4$. For each radius of dispersal, we used a root finder (the method of bisection) with tolerance 10^{-8} to determine the critical speed c^* that made the dominant eigenvalue equal to 1.

[129, 28, 133]. In addition, we found good data regarding the critical patch size, growth, and dispersal of this butterfly.

The butterfly is restricted to prairie fragments that contain Kincaid's lupine (*Lupinus sulphureus* ssp. *kincaidii*) and other larval food plants [133]. Prairie has all but disappeared from the Willamette Valley because of the termination of annual burning by Kalapuya Indians [159]. This change in the historical fire regime allowed shrubs and trees to invade and shade out low-growing prairie species. [130] recommended controlled burns as a means of restoring Fender's blue butterfly habitat. Since wildfires are expected to increase with global warming [158], we believe that global warming could have an effect on the distribution of prairie species such as Kincaid's lupine and Fender's blue butterfly.

The sizes of *I. i. fenderi* habitat patches vary from "quite small" (less than 2 ha) to over 50 ha [133, Figure 2.5]. (Small patches often belong to small, isolated clusters.) [28] estimated the minimum patch size for butterfly persistence to be 6 ha. To illustrate the effects of habitat shift, we will consider a patch of 25 ha, a size substantially larger than the estimated minimum patch size. Since we are working in one dimension, we will also assume that our 25 ha patch is square, with a width of 0.5 km.

Fender's blue butterflies display interesting movement patterns. Adult butterflies tend to stay within lupine patches, but occasionally wander out of these patches. Diffusion rates outside of lupine patches are many times greater than those inside lupine patches [129, Table 2]. In addition [29, 131], butterflies exhibit "an intriguing and distinctive looping behavior" at patch boundaries so that movement may, in fact, be a biased, correlated random walk [149], with bias towards habitat patches. These behaviors violate the assumptions underlying our use of a simple difference kernel, that dispersal is homogeneous and isotropic.

Even so, because our goals in this paper are exploratory rather than prescriptive, we will follow Clark [23] and consider the exponential power distribution

$$k(x-y) = \frac{\beta}{2\alpha\Gamma(1/\beta)} \exp\left[-\left(\frac{|x-y|}{\alpha}\right)^{\beta}\right] \tag{2.46}$$

for dispersal, where Γ denotes the gamma function and α and β are positive scale and shape parameters. β controls the kurtosis of the kernel: for $\beta < 2$, the kernel is leptokurtic; for $\beta > 2$, it is platykurtic. For fixed β, α can then be estimated from the mean (absolute)

deviation δ_1 since

$$\delta_1 = \frac{\alpha\Gamma(2/\beta)}{\Gamma(1/\beta)}. \tag{2.47}$$

For the mean deviation, we used Schultz's [129, Table 2] estimate of the net lifetime movement distance for females within lupine of 0.4 km.

Figure 2.6 shows the critical speed c^* (for extinction) as a function of the net reproductive rate R_0 for a leptokurtic dispersal kernel ($\beta = 1$) and a platykurtic dispersal kernel ($\beta = 8$). We determined the critical speeds using eigenvalue equation (2.18) and the numerical methods of section 5 for $R_0 = f'(0)$, size $L = 0.5$ km, and mean deviation $\delta_1 = 0.4$ km. Butterflies with the leptokurtic kernel do better at low and high levels of R_0 (i.e., for lower and higher speeds) while butterflies with the platykurtic kernel cope better at intermediate levels of R_0. This is consistent with the fact that the leptokurtic distribution has more probability in the center peak and in the tails (i.e., for small and large distances) while the platykurtic distribution has more probability in the shoulders.

Schultz and Hammond [132] surveyed Fender's blue butterfly populations across the range of the subspecies and measured growth rates between 0.99 to 2.66 (see their Table 2). The high values of R_0 in Figure 2.6 suggest that most extant populations of Fender's blue butterfly would do poorly with even small amounts of range shift.

The above model, as previously stated, ignores the fact that Fender's blue butterfly is a habitat specialist whose movement is strongly affected by the presence of its host plant, Kincaid's lupine, a long-lived perennial [159]. We can construct a more realistic model at the expense of simplicity. Dwyer and Morris [34] have considered integrodifference equations, built around consumer–resource models, that include resource-dependent dispersal. One can also construct such models for Fender's blue butterfly and Kincaid's lupine.

Discrete-time consumer–resource models often take the form of host–parasitoid models. For these models, the exact order of events is extremely important [63, 98]. In the case of Fender's blue butterfly, adult females lay their eggs on appropriate host plants, plants not overgrown or shaded by taller plants, from May to June [133]. Newly hatched larvae feed for a short time, but then enter diapause until February or March. Most feeding thus takes place after the host has set seed. Larvae spend most of their time on the food plant;

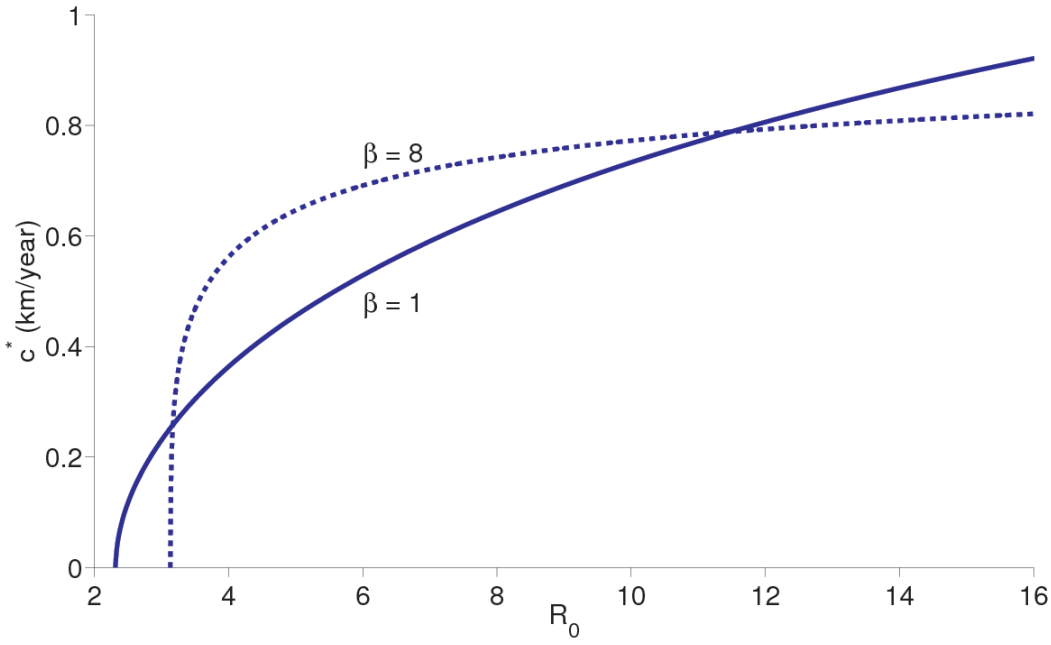

Figure 2.6: Plots of the critical speed c^* as a function of the net reproductive rate R_0 for a leptokurtic and a platykurtic example of exponential power distribution (2.46). The solid curve is for a leptokurtic kernel ($\beta = 1$); the dot-dashed curve is for a platykurtic kernel ($\beta = 8$). The two curves were computed for mean (absolute) deviation $\delta_1 = 0.4$ km and patch width $L = 0.5$ km. For each net reproductive rate (and kernel), we used a root finder (the method of bisection) with tolerance 10^{-8} to determine the critical speed c^* that made the dominant eigenvalue of linear system (2.45) (as found in MATLAB) equal to 1. The effect of kurtosis on the critical speed c^* was different at small, medium, and large values of R_0.

they seldom crawl to the ground (due, perhaps, to a large, predaceous tiger beetle) [133]. For convenience, we will assume that larvae feed only on the plant on which they were oviposited.

A more detailed model for the butterfly–lupine system might thus take the form

$$\begin{cases} R_{t+1}(x) &= \sigma\, f(x, R_t(x), C_t(x)) R_t(x) \,+\, \lambda \int_{-\frac{L}{2}+ct}^{\frac{L}{2}+ct} k(x-y)\, R_t(y)\, g(R_t(y))\, dy\,, \\ C_{t+1}(x) &= \gamma\, \sigma\, [1 - f(x, R_t(x), C_t(x))]\, R_t(x)\,. \end{cases} \tag{2.48}$$

Here, $R_t(x)$ is the density of the lupine population (the resource) before reproduction, $C_t(x)$ is the density of the feeding larvae, σ is the survivorship of adult plants in the absence of consumers, λ is the number of offspring per adult plant in the absence of density dependence, γ is a factor that accounts for the conversion of consumed lupines into butterflies, $k(x-y)$ is the dispersal kernel for the lupine, $g(R_t)$ accounts for density dependence in lupine reproduction, and $f(x, R_t(x), C_t(x))$ is the fraction of adult lupine that survive herbivory. As before, we assume that all reproduction takes place in a patch of size L moving with constant speed c.

The fraction of lupine that survive herbivory ultimately depends on the density and spatial distribution of butterfly eggs. We may thus write

$$f(x, R_t(x), C_t(x)) = \begin{cases} \exp\left[-a \int_{-\frac{L}{2}+ct}^{\frac{L}{2}+ct} h(x-y, R_t(y))\, C_t(y)\, dy\right], & x \in [-\frac{L}{2}+ct, \frac{L}{2}+ct] \\ 1, & x \notin [-\frac{L}{2}+ct, \frac{L}{2}+ct]\,. \end{cases} \tag{2.49}$$

Here, a is the area of discovery [108] and $h(x-y, R_t(y))$ is a dispersal kernel for the butterfly. This kernel now depends on the distribution of host plants as well as on distance. (See Dwyer and Morris [34] for examples of resource-dependent kernels and for other models.)

The analysis of system (2.48) is beyond the scope of this paper, but this example does show how one can extend our basic approach to include more biology. This example also highlights the fact that a species' ability to keep pace with range shifts may, in fact, depend on the dispersal ability of its host.

2.7 Discussion

All species have limits to how frequently and how far they disperse. If these limits are severe, climate change can take a heavy toll. In section 2.2, we introduced a simple model for population growth on a shifting domain. We showed (see Figure 2.1b) that a rapid, climate-induced, shifting species range can cause a population to die out. Even if the population persists (see Figure 2.1a), it may be greatly reduced. Approaches that neglect dispersal, such as bioclimate envelope models, can overestimate the ability of species to survive in the presence of climate change.

For our model, the speed of the range shift determines the toll on the population. For a given growth function, dispersal kernel, and patch size, there is a critical speed beyond which the population cannot survive. In section 2.3, we related population persistence to a simple (integral equation) eigenvalue problem. In section 2.4, we determined the critical speed for a simple separable kernel analytically . In section 2.5, we showed how to determine the critical speed for general dispersal kernels numerically. Other critical values, such as critical patch size and critical growth rate, can also be determined numerically.

Larger growth rates and patch sizes (graph not shown) increase population persistence. Changing the shape or scale of a dispersal kernel has a less consistent effect (see Figures 2.5 and 2.6). Since a population's vulnerability to climate change displays a complicated relationship to its dispersal behavior, we encourage ecologists to use detailed dispersal information in managing populations for conservation. Integrodifference equation are especially useful in this regard since they are built around dispersal kernels and can accommodate varied dispersal mechanisms [105, 107].

In this paper, we started with the simplest reasonable model: we constructed and analyzed a deterministic model with discrete, nonoverlapping generations; compensatory growth; and homogeneous and isotropic dispersal. These assumptions can be relaxed. Instead of a compensatory (Beverton–Holt) growth function, we can easily imagine using growth functions with overcompensation, such as the logistic curve or the Ricker curve. With overcompensation, we expect traveling time-periodic or chaotic pulses. Another alternative is to use a growth function with critical depensation or a strong Allee effect, e.g.,

[145, 154]. Our model might then exhibit bistability and dangerous fold bifurcations. Integrodifference equations have also been extended to accommodate time-periodic, stochastic, density-dependent, and resource-dependent growth and dispersal [34, 49, 71, 90, 106] and age and stage structure [104]. We hope to incorporate these effects into range-shift models in the future.

Chapter 3

LIFE ON THE MOVE: MODELING THE EFFECTS OF CLIMATE-DRIVEN RANGE SHIFTS WITH INTEGRODIFFERENCE EQUATIONS

The geographic ranges of wildlife species constantly respond to changing climates. Paleoecological studies have documented extensive species range changes during the glacial and interglacial alternations in the Quaternary Period [17, 55]. More recently (1956–2005), the Earth has been warming up at the rate of 0.13 °C per decade [58]. Species were expected to shift their ranges during this period, and this has now been documented [21, 51, 67, 80, 116, 119].

One major difference between the current warming event and earlier climatic changes in the Quaternary is that modern anthropogenic activities have created obstacles that make it difficult for the Earth's biota to survive climate change. Species need to shift their ranges to avoid excessive habitat loss during climate change, but, unlike organisms hundreds of thousands of years ago, species now face severe habitat fragmentation that makes shifting their ranges difficult [52, 110, 135]. Invasive exotics introduced by anthropogenic activities further stress indigenous species, since a changing climate creates new opportunities for invasive species to compete with native species. In general, ecologists must now assess the spatial effects of multiple factors in planning conservation strategies. They must, in particular, determine how multiple factors affect species ranges.

Many quantitative tools help us estimate future range shifts. For example, correlation models such as climate envelope models have been used to predict ranges for various climate change scenarios [5, 42, 60]. These models typically correlate species ranges with climatic variables using statistical tools, and then estimate potential ranges by combining correlational information with projections of future climate. These models cannot, however, easily integrate population dynamics, such as growth, dispersal, and interspecific interactions.

Other mathematical models have been used to bridge this gap. Travis [148] and Best

et al. [11] used stochastic, spatially explicit, patch occupancy models to study the effects of range-shift speed on persistence. Potapov and Lewis [122] and Berestycki et al. [9], in turn, used deterministic reaction–diffusion models to study this topic. Reaction–diffusion equations are particularly suitable for organisms with continuous and simultaneous growth and dispersal.

For many organisms, growth and dispersal are discrete episodes in the life cycle. Consider, for example, Edith's checkerspot butterfly (*Euphydryas editha*). In the San Francisco Bay area of California, eggs of this species hatch in April and the larvae feed and develop for 10–14 days. The larvae then enter diapause [47]. Post-diapause larvae feed and grow from December to February. They then pupate and emerge as adults [47]. The adults of *E. editha*, which live some ten days, emerge, fly, mate, search for oviposition sites, and complete their life cycle in March and April [103]. For this univoltine species, adults are the primary dispersers; their dispersal occurs during a very narrow window of time.

The mortality rate of *E. editha*'s larvae depends on synchrony between their life cycle and that of their host plants: larvae must reach their fourth instar and enter diapause before their host plants senesce [114]. This synchrony is strongly affected by climatic variables such as temperature and precipitation [114]. As a result, the population dynamics of *E. editha* are sensitive to climate change. Parmesan [113] examined populations of *E. editha* throughout its range and found that populations along its southern range boundary suffered extinction rates four times higher than those along its northern range boundary. Population extinction rates at lower elevations, meanwhile, were nearly three times as high as those at higher elevations. These drastic differences in extinction rates clarify why the mean location of *E. editha* populations shifted northward and upward [114].

Many other examples of organisms with discrete growth and dispersal occur in the range-shift literature. For these species, population dynamics are more easily described using discrete-time models. We therefore attack the problem of climate-induced range shifts using integrodifference equations (IDEs). IDEs are discrete-time, continuous-space models that combine growth and dispersal [50, 70, 72, 83, 77, 87, 90, 105, 104, 151]. In this chapter, we will describe and analyze an IDE model that includes climate-driven spatial shifts.

In section 3.1, we describe our basic model, apply it to butterflies, and show how over-

dispersal and under-dispersal can both lead to extinction. In section 3.2, we introduce the critical range-shift speed and reduce the problem of finding this speed to an eigenvalue problem. In section 3.3, we survey numerical approaches for solving this problem. In sections 3.4 and 3.6, we use Legendre series and Taylor series to obtain analytic approximations of the critical shift speed. We apply our numerical and analytic approximations to a toy problem, in section 3.5, and to more realistic kernels, in section 3.7. Finally, we summarize and discuss our results in section 3.8.

3.1 Is further better?

Several recent studies suggest that traits such as dispersal ability affect whether a species can successfully shift its range [125, 147, 134, 16, 35, 112]. For example, Pöyry et al. [123] related observed range shifts of butterflies in Finland to 11 butterfly life-history traits, such as mobility, habitat, and host-plant form. They found that habitat availability and dispersal capacity were the two traits most likely to determine whether a butterfly could keep up with climate change by shifting its range.

There is little argument that a sedentary species with little habitat has poor prospects in a world of climate change. But how about a vagile species whose habitat is shifting and fragmenting as we speak? What are its prospects? And, does higher dispersal ability always lead to greater success? We attempt to answer these questions by applying a recently developed IDE model [161] to butterflies.

Without loss of generality, let us assume that we have a univoltine butterfly that thrives on a suitable, spatially continuous patch of habitat in the Northern Hemisphere. Since ranges are expected to shift polewards, we will assume that this patch is a strip or zone bounded by lines of latitude. For mathematical simplicity, we reduce this strip to the one-dimensional interval $[-L/2, L/2]$. The length of this interval, L, in kilometers, represents the patch size. We assume that climate change shifts the two zonal boundaries northwards, at the speed of c km/yr. Thus, t years after the initial time point, the suitable patch is located at $[-L/2 + ct, L/2 + ct]$.

Because the butterfly is univoltine and has well-defined life stages, we can keep track of the population dynamics by censusing the population once a year. If we label the density

of freshly oviposited eggs in year t at location x as $n_t(x)$, then the density of eggs in the next year can be written as

$$n_{t+1}(x) = \int_{-\frac{L}{2}+ct}^{\frac{L}{2}+ct} k(x,y)\, f\left[n_t(y)\right]\, dy. \tag{3.1}$$

The formulation of equation (3.1) can be understood by going through the butterfly's life cycle. Most of the life cycle, from egg hatching to pupal eclosion, is a relatively sedentary stage. The function f describes growth during this stage. It maps the density of eggs (on plants) to a new density of eggs (in emerging adults). To construct the growth function f we might, for example, consider density dependence, larval mortality, clutch size, etc. In this paper, we will use the Beverton–Holt [12] recruitment curve,

$$f(n_t) = \frac{R_0 n_t}{1 + \left[(R_0 - 1)/K\right] n_t}, \tag{3.2}$$

as our growth function. Here, $R_0 = f\,'(0)$ is the net reproductive rate and K is the carrying capacity.

The adult butterflies are the dispersal stage. Eggs produced at y are carried to location x with some probability. For a fixed source of eggs y, we think of the redistribution kernel, $k(x,y)$, as a probability density function for the destination x of propagules. The kernel may depend on only the difference between x and y. In this case, we have a difference kernel, $k(x,y) = k(x-y)$, and we may think of $k(x-y)$ as the probability density function for the displacement (rather than the destination). Kernels can be estimated from mark-release-recapture studies.

Unfortunately, ecologists often lack detailed dispersal data for butterflies. As a result, comparative studies of butterflies often assume mobilities based on expert opinion [26, 68, 123, 144]. Recently, however, Stevens et al. [144] performed a meta-analysis of butterfly studies and summarized dispersal data. They showed that distributions of dispersal distances could be fit with negative exponential curves. These curves engender a 2D probability density function for the deposition of propagules [25, 24]. By taking the marginal distribution of this 2D kernel [83], we obtained [162] the 1D redistribution kernel

$$k(x-y) = \frac{\alpha}{\pi}\, K_0\left(\alpha|x-y|\right), \tag{3.3}$$

for butterflies, where $K_0(x)$ is the modified Bessel function of the second kind of order zero. The parameter α, the reciprocal of the mean dispersal distance, ranges from 0.76 km^{-1} for vagile species to 24.25 km^{-1} for sedentary species [144].

In model (3.1), eggs hatch and grow and adults emerge if they are in the climate-shifted patch for year t. Adults then oviposit their eggs both inside and outside the patch. Equation (3.1) tallies the movement of propagules from sources y within the patch to obtain the density of eggs, $n_{t+1}(x)$, at the start of the next generation.

To explore the effects of dispersal on survival, we numerically iterated equation (3.1) with growth function (3.2) and redistribution kernel (3.3). We set the net reproductive rate, the patch size, and the shift speed to the values $R_0 = 1.9$, $L = 0.5$ km, and $c = 0.1$ km/yr. We then chose three values of α from across the spectrum of observed values [144]. Figures 3.1a, 3.1b, and 3.1c show the dynamics of the three populations. Populations die out for high ($\alpha = 12$ km^{-1}) and low ($\alpha = 2.5$ km^{-1}) values of α. They survive for intermediate α ($\alpha = 6$ km^{-1}).

The causes of the extinctions for high and low α differed. The highly sedentary population ($\alpha = 12$ km^{-1}) in Figure 3.1a was limited by its dispersal ability. It simply could not keep up with its shifting habitat. In contrast, the vagile population ($\alpha = 2.5$ km^{-1}) in Figure 3.1c over-dispersed and was patch-size (or growth-rate) limited (see also [161], Figure 3.5). Thus, climate change and habitat fragmentation can both be important. Conservation efforts need to integrate both factors.

3.2 The critical range-shift speed

Instead of comparing species traits, let us now take a different perspective and look at the severity of climate change. Even if the population in Figure 3.1b is doing fine, will it still prosper if the shift speed c is increased? No! Figure 3.1d demonstrates that our population collapses if we raise the shift speed to $c = 0.125$ km/yr.

The shift speed c clearly has an important effect on the viability of our population. Numerical simulations suggest that for each growth rate, patch size, and redistribution kernel, there may be a critical shift speed c^* beyond which the population goes extinct. We will now employ some simple mathematical analyses to determine this critical shift speed.

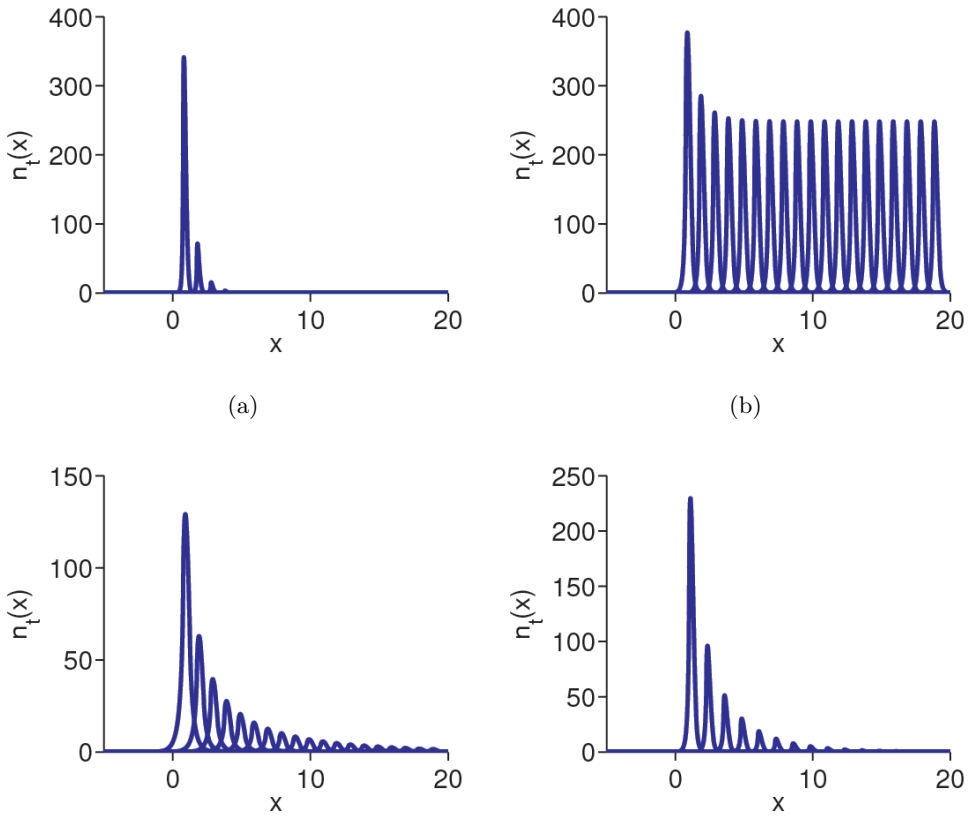

Figure 3.1: Simulations of IDE (3.1) with growth function (3.2) and kernel (3.3) show that a species' ability to survive climate change depends on both its dispersal ability and the speed of climate change. For shift speed $c = 0.1$ km/yr, (a) a sedentary population ($\alpha = 12$ km^{-1}) cannot keep up with its shifting habitat and goes extinct; (b) an intermediate population ($\alpha = 6$ km^{-1}) survives; (c) a vagile population ($\alpha = 2.5$ km^{-1}) over-disperses and goes extinct. For $c = 0.125$ km/yr, (d) the intermediate population ($\alpha = 6$ km^{-1}) also goes extinct. For all four subfigures, $L = 0.5$ km, $R_0 = 1.9$, and $K = 1000$. The initial distribution was $n_0(x) = K \exp(-x^2/2)$. The distribution is displayed every 10 generations and was computed using an FFT-assisted implementation of the extended trapezoidal rule with 2^{16} nodes.

Consider equation (3.1) with a difference kernel,

$$n_{t+1}(x) = \int_{-\frac{L}{2}+ct}^{\frac{L}{2}+ct} k(x-y)\, f\left[n_t(y)\right]\, dy. \tag{3.4}$$

For convenience, we will now assume, throughout the remainder of this paper, that our growth curve is nonnegative, monotonically increasing, and that it satisfies

$$f(n) \leq f'(0)n, \tag{3.5}$$

for $n \geq 0$. In particular, we explicitly exclude Allee effects [1]. These conditions are certainly satisfied by Beverton–Holt curve (3.2) for $R_0 > 1$.

Since the patch moves with constant speed c, we will look for steady states in the moving frame of the patch. This means we will look for moving pulses of the form

$$n_t(x) = n^*(x - ct). \tag{3.6}$$

Using this ansatz,

$$n_{t+1}(x) = n^*(x - ct - c). \tag{3.7}$$

Substituting equations (3.6) and (3.7) into equation (3.4), we find that the moving pulse satisfies

$$n^*(x - ct - c) = \int_{-\frac{L}{2}+ct}^{\frac{L}{2}+ct} k(x-y)\, f[n^*(y - ct)]\, dy. \tag{3.8}$$

Rewriting equation (3.8) in terms of the shifted spatial variables $\bar{x} = x - ct$ and $\bar{y} = y - ct$, we obtain

$$n^*(\bar{x} - c) = \int_{-\frac{L}{2}}^{\frac{L}{2}} k(\bar{x} - \bar{y})\, f\left[n^*(\bar{y})\right]\, d\bar{y}. \tag{3.9}$$

Shifting $\bar{x}$ by c, we find that moving pulse $n^*(\bar{x})$ is a solution of the equation

$$n^*(\bar{x}) = \int_{-\frac{L}{2}}^{\frac{L}{2}} k(\bar{x} + c - \bar{y})\, f\left[n^*(\bar{y})\right]\, d\bar{y}. \tag{3.10}$$

For this derivation to work, our kernel must be a difference kernel.

It is hard, in general, to find closed-form solutions $n^*(\bar{x})$ of equation (3.10). We can, however, identify special solutions in special cases. If the growth curve f has the trivial solution as a fixed-point, then

$$n^*(\bar{x}) \equiv 0 \tag{3.11}$$

is a solution of equation (3.10).

For the simple growth functions that we are using, we expect persistence to be equivalent to instability of solution (3.11) (no bistability). To study the stability of a moving pulse, we add a small, localized perturbation $\xi_t(x)$ to the pulse,

$$n_t(x) = n^*(\bar{x}) + \xi_t(x). \tag{3.12}$$

We then substitute $n_t(x)$ into integrodifference equation (3.4), linearize about $n^*(\bar{x})$,

$$\xi_{t+1}(x) = \int_{-\frac{L}{2}+ct}^{\frac{L}{2}+ct} k(x-y) f'\left[n^*(\bar{y})\right] \xi_t(y)\, dy, \tag{3.13}$$

and study the growth of the perturbation. Equation (3.13) is difficult to analyze in general, but luckily, for the trivial solution, $f'\left[n^*(\bar{y})\right] = f'(0)$ is a constant. As a result, equation (3.13) now reduces to

$$\xi_{t+1}(x) = R_0 \int_{-\frac{L}{2}+ct}^{\frac{L}{2}+ct} k(x-y)\, \xi_t(y)\, dy, \tag{3.14}$$

where $R_0 = f'(0)$ is the net reproductive rate.

Since we are interested in perturbations that persist in the moving frame, we now focus on perturbations that can be written as a product of a growth term λ^t and a traveling term $u(x-ct)$,

$$\xi_t(x) = \lambda^t\, u(\bar{x}) \equiv \lambda^t\, u(x-ct). \tag{3.15}$$

It now follows that

$$\lambda\, u(\bar{x}) = R_0 \int_{-\frac{L}{2}}^{\frac{L}{2}} k(\bar{x}+c-\bar{y})\, u(\bar{y})\, d\bar{y}. \tag{3.16}$$

Finally, for notational convenience, but at great risk of confusing the reader, we drop the bars on $\bar{x}$ and $\bar{y}$,

$$\lambda\, u(x) = R_0 \int_{-\frac{L}{2}}^{\frac{L}{2}} k(x+c-y)\, u(y)\, dy. \tag{3.17}$$

This is the key equation in this paper; we will use it to determine the critical speed c^*. It is a homogeneous Fredholm integral equation of the second kind. Please keep in mind, however, that the x and y in this equation are actually in the moving frame of the habitat. That is, they are really the barred variables.

Equation (3.17) can also be rewritten as the operator equation,

$$\lambda u(x) = K[u(x)], \tag{3.18}$$

where K is the linear operator

$$K: \qquad u(x) \quad \to \quad R_0 \int_{-\frac{L}{2}}^{\frac{L}{2}} k(x+c-y)\, u(y)\, dy. \tag{3.19}$$

The parameter λ is an eigenvalue of the operator, while $u(x) \neq 0$ is the corresponding eigenfunction. In general, this eigenvalue problem is nasty, but if the operator K is compact (or completely continuous), the problem simplifies. The eigenvalues of a compact linear operator form a discrete set, the point spectrum $\Lambda = \{\lambda_0, \lambda_1, \lambda_2, \ldots\}$. This set may be finite, countably infinite, or empty [57, 65]. Each eigenvalue has finite multiplicity and eigenvalues can only accumulate at zero. Compact operators are, in many ways, similar to matrices.

What do we need for K to be compact? It helps if the domain of our problem is closed and bounded. So, for mathematical convenience, let us now impose the restriction that $x \in [-L/2, L/2]$ and $y \in [-L/2, L/2]$ for finite L. In addition, it also helps if our kernel $k(x-y)$ is a continuous function [74] or, more generally, if $k(x-y)$ is a continuous function for $x \neq y$ and if there are numbers, m and $a < 1$, such that $|k(x-y)| \leq m|x-y|^{-a}$ [57]. All of the kernels in this chapter satisfy one or the other of these conditions.

In general, the eigenvalues λ of problem (3.17) are complex. If, however, the kernel is strictly positive, we can take advantage of Jentzsch's 1912 theorem [61] (see also [53] and [75]). This theorem is analogous to the Perron–Frobenius theorem for positive matrices. For our integral operator, it guarantees the existence of a simple, positive eigenvalue of largest modulus that dominates all other eigenvalues. The eigenfunction for this eigenvalue is positive. If the conditions of Jentzsch's theorem are met, the stability of trivial solution (3.11) changes as the dominant eigenvalue passes through $\lambda = 1$. For our problem, this occurs at the critical shift speed c^*.

The restriction that the kernel is strictly positive is important. If the kernel is only nonnegative, eigenvalues need not exist. If they do exist, the spectral radius of the operator

K,

$$r(K) = \max_{\lambda_i \in \Lambda} |\lambda_i|, \tag{3.20}$$

is a (positive) eigenvalue with a nonnegative eigenfunction [65]. In this case, stability of the trivial solution is still lost through $\lambda = 1$.

All the redistribution kernels in this chapter are nonnegative. Continous redistribution kernels with infinite support are positive and satisfy Jentzsch's theorem. Kernels with compact support need not satisfy this theorem. If, however, the radius of support is sufficiently large (relative to the patch size L and speed c), Jentzsch's theorem does apply. We will soon find ourselves approximating kernels of infinite support with kernels of compact support. In these cases, we will try to choose parameters that guarantee that Jentzsch's theorem is still satisfied.

Previously, we [161] showed that eigenvalue problem (3.17) simplifies to a finite-dimensional problem in linear algebra if its kernel is separable. A separable kernel can be written as a finite sum, with each term in the sum the product of a function of x alone and a function of y alone. Taking advantage of this fact, we determined the critical shift speed c^* for a simple, separable toy problem.

Separable kernels are, however, rare. We now consider more general (numerical and analytical) methods that allow us to calculate the dominant eigenvalue and the critical shift speed c^*.

3.3 Numerical approaches

One simple numerical approach for computing the dominant eigenvalue of problem (3.17) is the power method. As with matrix equations, the basic idea is to take an initial guess for the eigenvector and to repetitively rescale and iterate. More precisely, at each step of the process, we take our current estimate of the eigenfunction, $u_t(x)$, rescale this function using its sup norm over $D = [-L/2, L/2]$,

$$\tilde{u}_t(x) = \frac{u_t(x)}{\sup\limits_{x \in D} u_t(x)}\,, \tag{3.21}$$

and use the recurrence relation

$$u_{t+1}(x) = K[\tilde{u}_t(x)], \tag{3.22}$$

to obtain a new, improved estimate of our eigenfunction. Operator K, equation (3.19), accounts for both growth and dispersal. The dominant eigenvalue of the integral operator is now approximated by

$$\sup_{x \in D} u_t(x) \tag{3.23}$$

for large t. The power method is easy to implement, but it can be computationally inefficient.

More efficient approaches are based on Nyström's method [31, 124]. For separable kernels, problem (3.17) simplifies to finding eigenvalues for a finite-dimensional matrix. It makes sense, therefore, to approximate our integral operator with a matrix. To do this, we first discretize our integral using a quadrature rule.

Let us consider, for example, the repeated trapezoidal rule. We divide the domain of integration, $[-L/2, L/2]$, into N equal subintervals of length $\Delta y = L/N$. Replacing the variable y in equation (3.17) with grid points

$$y_j = -\frac{L}{2} + j \cdot \Delta y, \qquad j = 0, 1, \ldots, N, \tag{3.24}$$

we approximate the integral in equation (3.17) using the trapezoidal rule,

$$\begin{aligned} \int_{-\frac{L}{2}}^{\frac{L}{2}} k(x + c - y)\, u(y)\, dy \;\approx\; & \frac{\Delta y}{2} \sum_{j=0}^{N-1} [\, k(x + c - y_j)\, u(y_j) \\ & + k(x + c - y_{j+1})\, u(y_{j+1})\,]. \end{aligned} \tag{3.25}$$

If we now evaluate the function $u(x)$ at the grid points $x_i = y_i$, $i = 0, 1, 2, \ldots, N$, eigenvalue problem (3.17) reduces to

$$\lambda\, u(x_i) = R_0\, \frac{\Delta y}{2} \sum_{j=0}^{N-1} [\, k(x_i + c - y_j)\, u(y_j) + k(x_i + c - y_{j+1})\, u(y_{j+1})\,]. \tag{3.26}$$

Finally, if we denote $u_i = u(x_i)$ and

$$\begin{aligned} A_{i0} &= \frac{\Delta x}{2}\, k(x_i + c - y_0), \\ A_{ij} &= \Delta x\, k(x_i + c - y_j), \qquad 1 \le j \le N - 1, \\ A_{iN} &= \frac{\Delta x}{2}\, k(x_i + c - y_N), \end{aligned} \tag{3.27}$$

we obtain the finite-dimensional linear system

$$\lambda\, u_i = R_0 \sum_{j=0}^{N} A_{ij}\, u_j, \tag{3.28}$$

for $i = 0, \ldots, N$.

Thus, by employing Nyström's method, we transform the analysis of the dominant eigenvalue of an integral operator into the analysis of the dominant eigenvalue λ of linear system (2.45).

We can now analyze linear system (2.45) in one of two ways. The first approach is to determine the eigenvalues of system (2.45) directly. The eigenvalues may be obtained using commands such as *eigs*, *eigen*, or *spec* in computing environments such as MATLAB, R, or Scilab or by using well-known routines from numerical libraries such as *Numerical Recipes* [124], LAPACK [2], or the GNU Scientific Library [40]. These commands and routines commonly balance a matrix, reduce the balanced matrix to Hessenberg form, and find the eigenvalues of the Hessenberg matrix using a QR algorithm. Please see [124] for further details. Having found the eigenvalues, we now choose the dominant eigenvalue. Since this eigenvalue depends continuously on the parameters of the model, we can find the critical value for c, corresponding to $\lambda = 1$, using a standard root-finding algorithm, such as the method of bisection or Brent's method [14, 124].

As an alternative, set λ, in linear system (2.45), equal to one. Then, use an efficient algorithm, such as LU decomposition [124], to evaluate the determinant of the system. Finally, use a numerical root finder to locate the value of c that makes the determinant zero. This last approach has the advantage of being simple to implement from scratch, but has the disadvantage that you are not guaranteed that $\lambda = 1$ is the dominant eigenvalue.

3.4 Analytic approximations

In addition to solving for c^* numerically, we want analytic estimates of the critical speed. The easiest way to obtain these estimates is to assume that the eigenfunction and the kernel in equation (3.17) can be approximated using single or double series of suitably chosen basis functions. These basis functions should be complete and linearly independent. Ideally, they should also be orthogonal. Obvious candidates include trigonometric functions (sines and

cosines) and orthogonal polynomials such as Chebyshev, Hermite, Jacobi, Laguerre, or Legendre polynomials.

For convenience, we now expand the kernel $k(x+c-y)$ in the double series

$$k(x+c-y) \;=\; \sum_{i=0}^{\infty}\sum_{j=0}^{\infty} A_{ij}\;X_i(x)\,X_j(y)\,, \tag{3.29}$$

where $X_i(x)$ and $X_j(y)$ are Legendre polynomials relative to the interval $[-L/2,\ L/2]$. (Please see the appendix for a brief introduction to Legendre polynomials). The coefficients A_{ij}, which depend on c, are, by equation (3.96),

$$A_{ij} \;=\; \frac{(2i+1)\,(2j+1)}{L^2}\int_{-L/2}^{L/2}\int_{-L/2}^{L/2} k(x+c-y)\,X_i(x)\,X_j(y)\,dy\,dx\,. \tag{3.30}$$

If we insert expansion (3.29) into eigenvalue equation (3.17), we see that

$$\lambda\,u(x) \;=\; R_0\sum_{i=0}^{\infty}\left(\sum_{j=0}^{\infty} A_{ij}\int_{-L/2}^{L/2} X_j(y)\,u(y)\,dy\right)\,X_i(x)\,. \tag{3.31}$$

We will treat this equation as an expansion of the eigenfunctions, $u(x)$, in Legendre polynomials relative to the interval $[-L/2,\ L/2]$,

$$u(x) \;=\; \sum_{i=0}^{\infty} a_i\;X_i(x)\,. \tag{3.32}$$

The coefficients a_i clearly satisfy

$$a_i \;=\; \frac{R_0}{\lambda}\sum_{j=0}^{\infty} A_{ij}\int_{-L/2}^{L/2} X_j(y)\,u(y)\,dy\,,\quad i\;=\;0,1,2,.... \tag{3.33}$$

Expansion (3.32) presents the eigenfunctions as a linear combination of the orthogonal polynomials $X_i(x)$. If we use this expansion to eliminate $u(y)$ in coefficient equation (3.33), we see that

$$\begin{aligned}\lambda\,a_i \;&=\; R_0\sum_{j=0}^{\infty} A_{ij}\int_{-L/2}^{L/2} X_j(y)\sum_{k=0}^{\infty} a_k\,X_k(y)\,dy \\ &=\; R_0\sum_{k=0}^{\infty}\left(\sum_{j=0}^{\infty} A_{ij}\int_{-L/2}^{L/2} X_j(y)\,X_k(y)\,dy\right)\,a_k\,.\end{aligned} \tag{3.34}$$

Since our Legendre polynomials are orthogonal and satisfy

$$\int_{-L/2}^{L/2} [X_i(x)]^2 \, dx \;=\; \frac{L}{2i+1} \,, \tag{3.35}$$

it follows that

$$\lambda \, a_i \;=\; R_0 \, L \sum_{j=0}^{\infty} \frac{A_{ij}}{2j+1} \, a_j \tag{3.36}$$

for $i = 0, 1, 2, ...$ and for $j = 0, 1, 2, ...$

System (3.36) is an infinite-dimensional system of linear algebraic equations for the eigenvalues λ of the trivial solution. We can approximate the eigenvalues of largest modulus by truncating this system so that $i = 0, 1, ..., N$ and $j = 0, 1, ..., N$ for finite N. In many cases, N need not be large.

Indeed, in some cases, $N = 0$ will suffice. For $N = 0$, we treat eigenfunctions, by equation (3.32), as constants,

$$u(x) \;\approx\; a_0 \, X_0(x) \;=\; a_0 \,. \tag{3.37}$$

System (3.36), in turn, reduces to

$$\lambda \, a_0 \;\approx\; R_0 \, L \, A_{00} \, a_0 \,. \tag{3.38}$$

After dividing both sides of this last equation by a_0, we obtain

$$\lambda \;\approx\; R_0 \, L \, A_{00} \,, \tag{3.39}$$

where, by coefficient equation (3.30),

$$A_{00} \;=\; \frac{1}{L^2} \int_{-L/2}^{L/2} \int_{-L/2}^{L/2} k(x + c - y) \, dy \, dx \,. \tag{3.40}$$

At the critical speed $c = c^*$, $\lambda = 1$, and we conclude that

$$1 \;=\; \frac{R_0}{L} \int_{-L/2}^{L/2} \int_{-L/2}^{L/2} k(x + c^* - y) \, dy \, dx \,. \tag{3.41}$$

We can often use this last equation to obtain good estimates of the critical speed c^*.

We will refer to equation (3.39) as our $N = 0$ eigenvalue approximation. Equation (3.41) is our $N = 0$ critical-speed equation. The right hand side of these equations is the product

of the net reproductive rate and the average dispersal success [91, 151, 152] of our shifted kernel.

A more precise estimate of the critical speed can be obtained by letting $N = 1$. For $N = 1$, we treat eigenfunctions as linear functions,

$$u(x) \;\approx\; a_0\, X_0(x) \,+\, a_1\, X_1(x) \;=\; a_0 \,+\, \frac{2a_1}{L}\, x\,. \tag{3.42}$$

System (3.36) now reduces to $N = 1$ approximation

$$\lambda \begin{bmatrix} a_0 \\ a_1 \end{bmatrix} = R_0\, L \begin{bmatrix} A_{00} & \dfrac{A_{01}}{3} \\ A_{10} & \dfrac{A_{11}}{3} \end{bmatrix} \begin{bmatrix} a_0 \\ a_1 \end{bmatrix}. \tag{3.43}$$

At the critical speed, $c = c^*$, $\lambda = 1$, and we have that

$$\begin{bmatrix} R_0\, L\, A_{00} \,-\, 1 & \dfrac{1}{3}\, R_0\, L\, A_{01} \\ R_0\, L\, A_{10} & \dfrac{1}{3}\, R_0\, L\, A_{11} \,-\, 1 \end{bmatrix} \begin{bmatrix} a_0 \\ a_1 \end{bmatrix} = \begin{bmatrix} 0 \\ 0 \end{bmatrix}. \tag{3.44}$$

We want nontrivial eigenvectors, and so we require that this system be singular,

$$\begin{vmatrix} R_0\, L\, A_{00} \,-\, 1 & \dfrac{1}{3}\, R_0\, L\, A_{01} \\ R_0\, L\, A_{10} & \dfrac{1}{3}\, R_0\, L\, A_{11} \,-\, 1 \end{vmatrix} = 0. \tag{3.45}$$

This is our $N = 1$ critical-speed equation. It can be used to obtain improved estimates of the critical speed c^*.

We can proceed, in a similar way, for higher N. Often, however, low-order estimates of the critical speed do surprisingly well.

3.5 A simple example

We illustrate the above approximation scheme with a simple example. This is a toy problem that we have chosen for its analytic tractability. We will consider more realistic kernels in a later section.

Consider the symmetric, quadratic kernel

$$k(x) = \begin{cases} \dfrac{3}{4b}\left(1 - \dfrac{x^2}{b^2}\right), & |x| \le b, \\ 0, & |x| > b, \end{cases} \tag{3.46}$$

for $b > 0$. The coefficient at the front of this kernel has been chosen to guarantee that the kernel integrates to one.

If we add the restriction that

$$-b < x + c - y < b \tag{3.47}$$

for all x and y in the closed interval $[-L/2, L/2]$, our kernel is positive over the patch and the conditions for Jentzsch's theorem are satisfied. Eigenvalue problem (3.17) now reduces to

$$\lambda\, u(x) = R_0 \int_{-L/2}^{L/2} \frac{3}{4b}\left[1 - \frac{(x+c-y)^2}{b^2}\right]\, u(y)\, dy\,. \tag{3.48}$$

The kernel of this eigenvalue problem is, in fact, separable. It is easy to show that all eigenfunctions $u(x)$ of this problem are quadratic in x and that system

$$\lambda \begin{bmatrix} a_0 \\ a_1 \\ a_2 \end{bmatrix} = R_0\, L \begin{bmatrix} A_{00} & \dfrac{A_{01}}{3} & \dfrac{A_{02}}{5} \\ A_{10} & \dfrac{A_{11}}{3} & \dfrac{A_{12}}{5} \\ A_{20} & \dfrac{A_{21}}{3} & \dfrac{A_{22}}{5} \end{bmatrix} \begin{bmatrix} a_0 \\ a_1 \\ a_2 \end{bmatrix}, \tag{3.49}$$

with coefficients

$$\begin{gathered} A_{00} = \frac{3}{4b} - \frac{1}{8b^3}(L^2 + 6c^2), \\ A_{10} = -\frac{3cL}{4b^3},\ \ A_{01} = \frac{3cL}{4b^3}, \\ A_{20} = -\frac{L^2}{8b^3},\ \ A_{11} = \frac{3L^2}{8b^3},\ \ A_{02} = -\frac{L^2}{8b^3}, \\ A_{21} = A_{12} = A_{22} = 0 \end{gathered} \tag{3.50}$$

gives exact eigenvalues.

Nevertheless, equations (3.39) and (3.43) give us good approximations for the dominant eigenvalue. For $N = 0$ approximation (3.39),

$$\lambda \approx R_0\, L\, A_{00} = R_0\, L\, \left[\frac{3}{4b} - \frac{1}{8b^3}(L^2 + 6c^2)\right]\,. \tag{3.51}$$

Setting $\lambda = 1$ and solving for c gives us

$$c^* \approx \pm\sqrt{b^2\left(1 - \frac{4b}{3R_0 L}\right) - \frac{L^2}{6}}\,. \tag{3.52}$$

For two-row, two-column ($N = 1$) approximation (3.43),

$$\lambda \begin{bmatrix} a_0 \\ a_1 \end{bmatrix} = R_0\, L \begin{bmatrix} \frac{3}{4b} - \frac{1}{8b^3}(L^2 + 6c^2) & \frac{cL}{4b^3} \\ -\frac{3cL}{4b^3} & \frac{L^2}{8b^3} \end{bmatrix} \begin{bmatrix} a_0 \\ a_1 \end{bmatrix}, \tag{3.53}$$

the characteristic equation is

$$\lambda^2 + \frac{3R_0 L}{4b^3}(c^2 - b^2)\lambda + \frac{R_0^2\, L^4}{64b^6}\left[6(c^2 + b^2) - L^2\right] = 0\,. \tag{3.54}$$

Setting $\lambda = 1$ and solving for c gives us

$$c^* \approx \pm\sqrt{\frac{(R_0\, L^3 - 8\, b^3)(R_0\, L^3 - 6\, b^2\, R_0\, L + 8\, b^3)}{6\, R_0\, L\, (R_0\, L^3 + 8\, b^3)}}\,. \tag{3.55}$$

Finally, for $N = 2$, the characteristic equation is

$$\lambda^3 + \frac{3(c^2 - b^2)R_0\, L}{4\, b^3}\lambda^2 + \frac{3R_0^2\, L^4\left[5(c^2 + b^2) - L^2\right]}{160\, b^6}\lambda + \frac{R_0^3\, L^9}{2560\, b^9} = 0\,. \tag{3.56}$$

Setting $\lambda = 1$ and solving for c gives us

$$c^* = \pm\sqrt{\frac{(8\, b^3 - R_0\, L^3)(R_0^2\, L^6 - 40\, b^3 R_0\, L^3 + 240\, b^5 R_0\, L - 320\, b^6)}{240\, b^3 R_0\, L(R_0\, L^3 + 8\, b^3)}}\,. \tag{3.57}$$

In Figure 3.2, $N = 0$ approximation (3.52), $N = 1$ approximation (3.55), and the exact ($N = 2$) value of the critical speed, equation (3.57), are plotted against the net reproductive rate R_0. Since kernel (3.46) is symmetric, the curves in Figure 3.4 are symmetric with respect to the R_0 axis. Shifting the patch to the right or left has the same effect on population persistence. For $N = 0$, equation (3.52) gives a good approximation to the true critical-speed curve for R_0 small. $N = 1$ approximation (3.55) is, in turn, visually indistinguishable from the exact critical-speed curve for both low and high values of R_0.

3.6 A simplifying approximation

In the above example, our $N = 0$ and $N = 1$ expansions both generated good estimates of the critical range-shift speed. Our kernel, moreover, were sufficiently simple that we could easily solve for c^*. For many kernels, unfortunately, it is much harder to solve for c^*.

For sufficiently smooth kernels, we will therefore expand the kernel $k(x + c - y)$ in a Taylor series in $c^* - y$. If the kernel is locally quadratic, we can then keep the first three

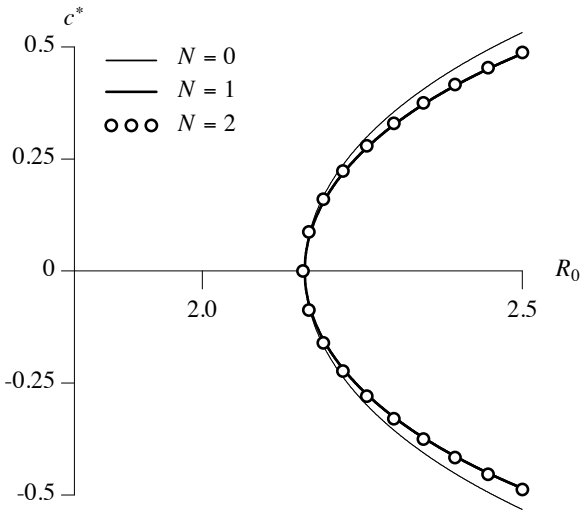

Figure 3.2: The critical speed c^* plotted as a function of the net reproductive rate R_0 for quadratic kernel (3.46). The three curves depict $N = 0$ approximation (3.52), $N = 1$ approximation (3.55), and exact solution (3.57). Since kernel (3.46) is symmetric, these curves are symmetric about the R_0 axis. The $N = 1$ approximation is visually indistinguishable from the exact solution. Here, $b = 1.5$ km, and $L = 1$ km; we restricted $|c| < 0.5$ km/yr in order to satisfy equation (3.47).

terms in our Taylor series and approximate c^* using the quadratic formula. We illustrate the procedure for $N = 0$. This procedure gives us a simple formula for c^* that should be accurate for small critical speeds.

For $N = 0$,

$$\lambda \;\approx\; \frac{R_0}{L}\int_{-L/2}^{L/2}\int_{-L/2}^{L/2} k(x+c-y)\,dy\,dx\,. \tag{3.58}$$

Rewriting $k(x+c-y)$ as a Taylor series about x yields

$$\lambda \;\approx\; \frac{R_0}{L}\sum_{n=0}^{\infty}\frac{1}{n!}\left[\int_{-L/2}^{L/2}\int_{-L/2}^{L/2} k^{(n)}(x)(c-y)^n\,dy\,dx\right]\,. \tag{3.59}$$

If we keep the first three terms in the Taylor series and set $\lambda = 1$, we obtain

$$\begin{aligned} 1 \;\approx\; & R_0\int_{-L/2}^{L/2} k(x)\,dx + \frac{R_0}{L}\int_{-L/2}^{L/2} k\,'(x)\,dx\left[\int_{-L/2}^{L/2}(c^*-y)dy\right] \\ & + \frac{R_0}{L}\int_{-L/2}^{L/2} k\,''(x)\,dx\left[\frac{1}{2}\int_{-L/2}^{L/2}(c^*-y)^2\,dy\right]. \end{aligned} \tag{3.60}$$

After calculating the integrals in y, we obtain the quadratic equation (in c^*)

$$\alpha c^{*2} + 2\beta c^* + \gamma + \frac{L^2\alpha}{12} - \frac{1}{R_0} \approx 0\,, \tag{3.61}$$

where

$$\alpha = \frac{1}{2}\left[k\,'\left(\frac{L}{2}\right) - k\,'\left(-\frac{L}{2}\right)\right], \qquad \beta = \frac{1}{2}\left[k\left(\frac{L}{2}\right) - k\left(-\frac{L}{2}\right)\right], \tag{3.62}$$

and

$$\gamma = \int_{-\frac{L}{2}}^{\frac{L}{2}} k(x)\,dx\,. \tag{3.63}$$

We can now use the quadratic formula to solve for the critical speed

$$c^* \approx -\frac{\beta}{\alpha} \pm \frac{1}{\alpha}\sqrt{\beta^2 - \alpha(\gamma + L^2\alpha/12 - 1/R_0)}\,. \tag{3.64}$$

The coefficient β of the linear term in quadratic equation (3.61) vanishes when the kernel $k(x)$ is symmetric. Indeed, for symmetric kernels,

$$k\left(\frac{L}{2}\right) = k\left(-\frac{L}{2}\right), \qquad \text{and} \qquad k\,'\left(\frac{L}{2}\right) = -k\,'\left(-\frac{L}{2}\right). \tag{3.65}$$

Approximation (3.61) then reduces to

$$\alpha\, c^{*2} + \gamma + \frac{L^2\alpha}{12} - \frac{1}{R_0} \;\approx\; 0\,. \tag{3.66}$$

Solving for c^*, we obtain the remarkably simple formula

$$c^* \approx \pm\sqrt{\frac{1}{R_0\alpha} - \frac{\gamma}{\alpha} - \frac{L^2}{12}}\,. \tag{3.67}$$

Thus, for symmetric kernels, our quadratic approximation preserves the symmetry of c^* with respect to R_0.

3.7 Realistic kernels

Let us now apply our numerical procedures and/or our analytical approximations to some realistic redistribution kernels. We will look at three well-known workhorses: the Gaussian, Laplace, and Cauchy distributions. In addition, we will look at modified Bessel kernel (3.3).

3.7.1 Gaussian distribution

Let us first consider the Gaussian kernel

$$k(x) = \frac{1}{\sqrt{2\pi\sigma^2}} e^{-x^2/(2\sigma^2)}\,, \tag{3.68}$$

with standard deviation $\sigma > 0$. The Gaussian is the archetypal mesokurtic distribution; it has a special role in the theory of dispersal because of its strong connection to both the diffusion equation and the central limit theorem.

For this kernel, eigenvalue problem (3.17) reduces to

$$\lambda u(x) = R_0 \int_{-L/2}^{L/2} \frac{1}{\sqrt{2\pi\sigma^2}} e^{-(x+c-y)^2/(2\sigma^2)} u(y)\, dy\,. \tag{3.69}$$

The Gaussian kernel is not separable; we must, therefore, rely on numerical or analytical approximations to calculate the critical range-shift speed for this kernel [161].

Since kernel (3.68) is symmetric, let us first consider Taylor-series approximation (3.67). For this symmetric kernel,

$$\alpha = k'\left(\frac{L}{2}\right) = -\frac{L}{2\sigma^3\sqrt{2\pi}} e^{-L^2/(8\sigma^2)} \tag{3.70}$$

and

$$\gamma = \int_{-L/2}^{L/2} k(x)\, dx = \operatorname{erf}\left(\frac{\sqrt{2}L}{4\sigma}\right), \tag{3.71}$$

where the error function, erf(x), is given by the integral

$$\mathrm{erf}(x) = \frac{2}{\sqrt{\pi}} \int_0^x e^{-z^2}\, dz\,. \tag{3.72}$$

Formula (3.67) thus yields

$$c^* \;\approx\; \pm\sqrt{\frac{2\sigma^3\sqrt{2\pi}\left[R_0\,\mathrm{erf}\left(\sqrt{2}\,L/(4\sigma)\right)-1\right]}{R_0\,L\,e^{-L^2/(8\sigma^2)}} - \frac{L^2}{12}}. \tag{3.73}$$

For the Gaussian distribution, we can no longer extract c^* from critical-speed equations (3.41) and (3.45) analytically. We did, however, extract critical speeds from these equations numerically, for comparison, by evaluating the coefficients A_{00}, A_{10}, A_{01}, and A_{11} as Riemann sums and by then solving for c^* using a simple root-finding method, the method of bisection. The Riemann sums were calculated using a 100×100 grid; the method of bisection was run with a tolerance of 1×10^{-6} .

Finally, we determined c^* from eigenvalue problem (3.17) numerically, using both the power method and Nyström's method (see section 3.3). For the power method, we iterated 250 times, for each value of R_0, using an FFT-assisted implementation of the extended trapezoidal rule with 2^{10} nodes. For Nyström's method, we used MATLAB's *eigs* command, with 100 grid points, and a root finder, the method of bisection, with tolerance 10^{-8}. The two numerical approaches gave identical answers; we illustrate our results using output from the power method.

Figure 3.3 shows plots of the critical speed c^*, as a function of R_0, for a Gaussian kernel with standard deviation $\sigma = 3.0$ km and patch width $L = 2.0$ km. The curves were obtained using, from top to bottom, $N = 0$ and $N = 1$ critical-speed equations (3.41) and (3.45), the power method, and Taylor-series approximation (3.73). Roots of the $N = 0$ equation slightly overestimate the true critical speed, but the roots of the $N = 1$ equation are visually indistinguishable from the numerical output of the power method. Taylor-series approximation (3.73) provides good estimates of c^* for small critical speeds, but underestimates c^* for large critical speeds.

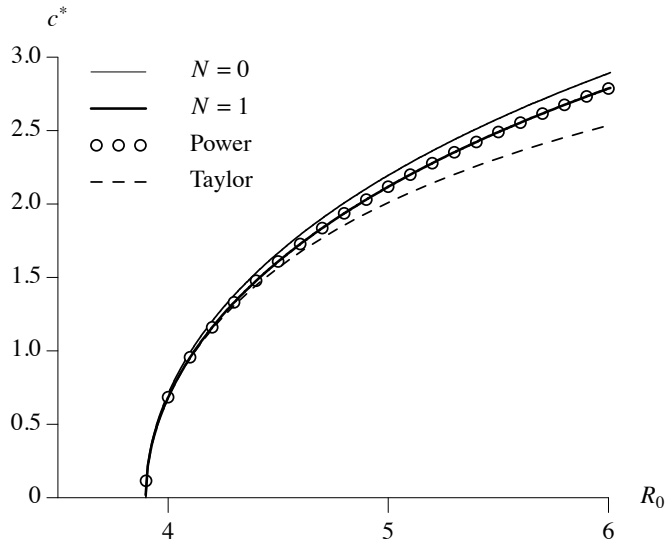

Figure 3.3: The critical speed c^* plotted as a function of the net reproductive rate R_0 for Gaussian kernel (3.68). The four curves depict roots of $N = 0$ and $N = 1$ critical-speed equations (3.41) and (3.45), the numerical output of the power method, and Taylor-series approximation (3.73). Here, $\sigma = 3.0$ km, and $L = 2.0$ km. The $N = 0$ roots overestimate, but the $N = 1$ roots agree with, the power-method curve. Taylor-series approximation (3.73) provides good estimates of c^* for small critical speeds, but underestimates c^* for large critical speeds.

3.7.2 Laplace distribution

The Laplace distribution,

$$k(x) \;=\; \frac{1}{2b} e^{-|x|/b}\,, \tag{3.74}$$

is a symmetric, leptokurtic dispersal kernel that is frequently encountered in empirical studies (e.g., [101, 143, 146]). It can also arise, in models, from a combination of diffusion and settling or advection and settling [92, 105]. Kotz et al. [73] have written the definitive treatise analyzing the Laplace distribution from a statistical viewpoint.

For the Laplace distribution, eigenvalue problem (3.17) reduces to

$$\lambda u(x) \;=\; R_0 \int_{-L/2}^{L/2} \frac{1}{2b}\, e^{-|x+c-y|/b}\, u(y)\, dy\,. \tag{3.75}$$

Since the Laplace distribution is not separable and is not differentiable at the origin, we must rely on numerical methods to calculate the critical range-shift speed.

Figure 3.4 shows plots of the critical speed c^*, as a function of R_0, for a Laplace dispersal kernel with $b = 3.0$ km and patch width $L = 2.0$ km. These curves were obtained using (from top to bottom) $N = 0$ and $N = 1$ critical-speed equations (3.41) and (3.45) and the power method. Since the Laplace distribution is not differentiable at the origin, we do not plot Taylor-series approximation (3.67) for this distribution. The plotted curves were produced in the same manner as for the Gaussian kernel. Roots of the $N = 0$ equation slightly overestimate the true critical speed, but roots of the $N = 1$ equation are, once again, visually indistinguishable from the numerical output of the power method.

3.7.3 Cauchy distribution

The Cauchy distribution,

$$k(x) = \frac{1}{\pi b \left(1 + \frac{x^2}{b^2}\right)}, \tag{3.76}$$

is a symmetric, fat-tailed distribution with no mean, variance, or higher moments. The Cauchy distribution, and related power law models, have proven important in studies of spore dispersal gradients [39], long-distance dispersal [139], and the spread of plant diseases [15, 93, 138].

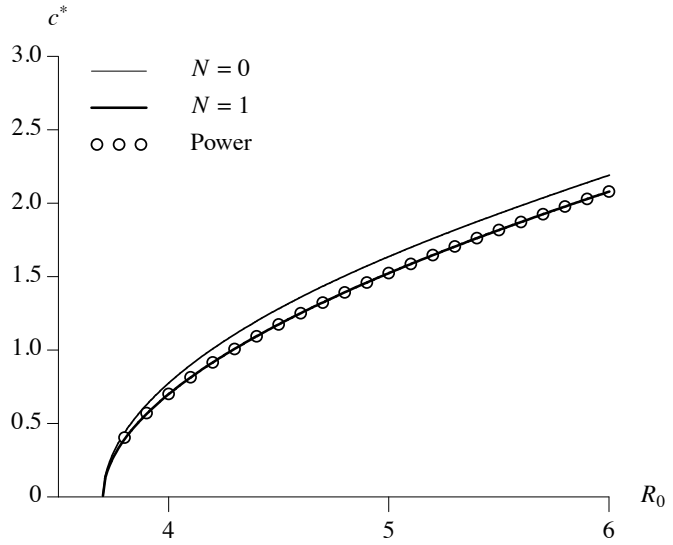

Figure 3.4: The critical speed c^* plotted as a function of the net reproductive rate R_0 for Laplace kernel (3.74). The three curves depict roots of $N = 0$ and $N = 1$ critical-speed equations (3.41) and (3.45) and the numerical output of the power method. Here, $b = 3.0$ km, and $L = 2.0$ km. The $N = 0$ roots overestimate, but the $N = 1$ roots agree with, the power-method curve. Since the Laplace distribution is not differentiable at the origin, we do not plot a Taylor-series approximation for this example.

For the Cauchy distribution, eigenvalue problem (3.17) reduces to

$$\lambda u(x) \;=\; R_0 \int_{-L/2}^{L/2} \frac{u(y)}{\pi b \left[1 + \frac{(x+c-y)^2}{b^2}\right]}\, dy\,. \tag{3.77}$$

Since the Cauchy distribution is not separable, we must rely on numerical or analytical approximations to calculate the critical range-shift speed.

In this instance,

$$\alpha \;=\; k'\left(\frac{L}{2}\right) \;=\; -\frac{bL}{\pi\left(b^2 + \frac{L^2}{4}\right)^2}\,. \tag{3.78}$$

and

$$\gamma \;=\; \int_{-L/2}^{L/2} k(x)\, dx \;=\; \frac{2}{\pi}\, \arctan\frac{L}{2b}\,. \tag{3.79}$$

Taylor-series approximation (3.67) now produces

$$c^* \;\approx\; \pm\sqrt{\frac{[2R_0 \arctan\left(L/2b\right) - \pi]\,(4b^2 + L^2)^2}{16\, R_0\, bL} - \frac{L^2}{12}}. \tag{3.80}$$

Figure 3.5 shows plots of the critical speed c^*, as a function of R_0, for a Cauchy dispersal kernel with $b = 2.0$ km and patch width $L = 2.0$ km. These curves were obtained using (from top to bottom) $N = 0$ and $N = 1$ critical-speed equations (3.41) and (3.45), the power method, and Taylor-series approximation (3.80). These curves were produced in the same manner as for the Gaussian kernel. Roots of the $N = 0$ equation slightly overestimate the true critical speed, but roots of the $N = 1$ equation are, once again, visually indistinguishable from the numerical output of the power method. The Taylor-series approximation, equation (3.80), once again provides good estimates of c^* for small critical speeds, but underestimates c^* for large critical speeds.

3.7.4 Modified Bessel distribution

The modified Bessel distribution,

$$k(x) = \frac{\alpha}{\pi}\, K_0(\alpha|x|), \tag{3.81}$$

arises as the marginal distribution of a 2D distribution whose 1D distribution of dispersal distances is the exponential distribution [162]. More generally, this distribution is the product distribution for two normally distributed variates [27, 36].

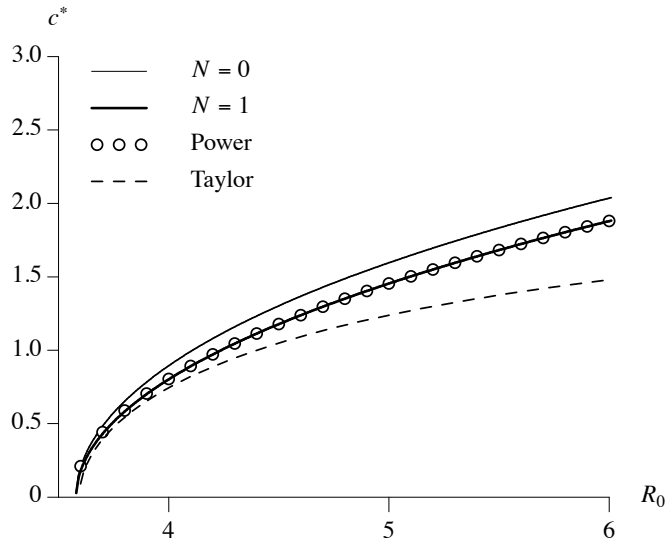

Figure 3.5: The critical speed c^* plotted as a function of the net reproductive rate R_0 for Cauchy kernel (3.76). The four curves depict roots of $N = 0$ and $N = 1$ critical-speed equations (3.41) and (3.45), the numerical output of the power method, and Taylor-series approximation (3.80). Here, $b = 2.0$ km, and $L = 2.0$ km. The $N = 0$ roots overestimate, but the $N = 1$ roots agree with, the power-method curve. Taylor-series approximation (3.80) provides good estimates of c^* for small critical speeds, but underestimates c^* for large critical speeds.

For this kernel, eigenvalue problem (3.17) reduces to

$$\lambda u(x) = R_0 \int_{-L/2}^{L/2} \frac{\alpha}{\pi} K_0 \left(\alpha|x + c - y|\right)\, u(y)\, dy. \tag{3.82}$$

Since the modified Bessel distribution is not separable, we must again rely on numerical or analytical approximations to calculate the critical range-shift speed.

Figure 3.6 shows the critical speed c^*, as a function of R_0, for modified Bessel function (3.81) for $\alpha = 2.5,\ 6,\ 12$ km^{-1} and patch width $L = 0.5$ km. These curves were obtained using Nyström's method with MATLAB's *eigs* command, with 100 grid points, and a root finder, the method of bisection, with tolerance 10^{-8}. The curves cross in several places and are consistent with the dynamics in Figure 3.1.

3.8 Discussion

Climate change is altering the distributions of wildlife species at a fast rate. To estimate this rate, [86] introduced and estimated an index of velocity of temperature change; this index has a global (geometric) mean of 0.42 km/yr. Parmesan et al. [117], in turn, analyzed data for 1700 species and estimated the average speed of significant poleward range shifts to be 6.1 kilometers per decade. Can species keep up with this rate of climate change? In this chapter, we used an integrodifference equation to model the dynamics of a population that resides in a patch that shifts with speed c. In describing our model, we focused on butterflies, but our model can be applied to many animals and plants. We found that our model has a critical shift speed c^* beyond which the population goes extinct. The critical shift speed c^* depends sensitively on the dispersal ability of the species.

In section 3.2, we reduced the problem of finding the critical shift speed c^* to an eigenvalue problem. We then showed that c^* can be estimated using numerical methods (section 3.3) or analytical approximations (sections 3.4 and 3.6). Simple analytic approximations frequently yield results that are surprisingly close to numerical output. The biggest drawback of our analytical approach is that we must approximate our redistribution kernels with positive functions if we wish to satisfy Jentzsch's theorem. This positivity is easily broken.

Our analyses of the critical speed c^* show that a species' dispersal ability has a profound but complicated impact on its success. When we plotted the critical speed c^* with respect

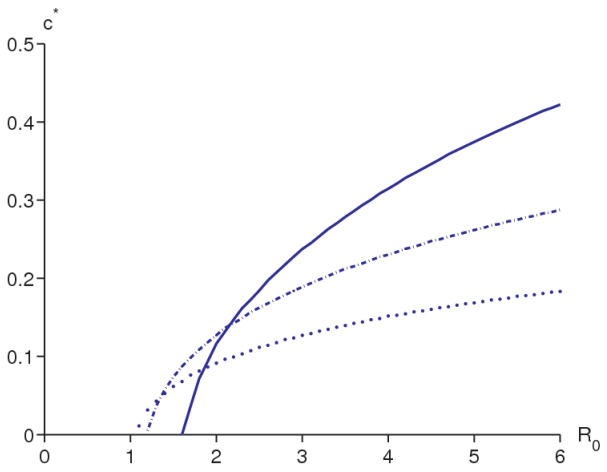

Figure 3.6: The critical speed c^* plotted as a function of the net reproductive rate R_0 for modified Bessel kernel (3.81) and patch size $L = 0.5$ km. The solid curve represents a sedentary population ($\alpha = 2.5$ km^{-1}) , the dot-dashed curve represents an intermediate population ($\alpha = 6$ km^{-1}), and the dotted curve is a vagile population ($\alpha = 12$ km^{-1}). The dotted curve has both a smaller R_0 intercept and a lower c^* asymptote, implying that the sedentary population does comparatively better for small shift speeds but comparatively worse for high shift speeds. These curves were obtained using Nyström's method with MATLAB's *eigs* command, with 100 grid points, and a root finder, the method of bisection, with tolerance 10^{-8}.

to the net reproductive rate R_0 for butterflies, in section 3.7.4, we found that the curves (for different dispersal parameters) cross at many points (Figure 3.6). Sedentary populations do better (can survive for lower R_0) for low shift speeds, intermediate populations do better for intermediate shift speeds, and vagile populations do better at high shift speeds, but the loci of these transitions depend on where the curves intersect.

These observations suggest different conservation strategies for different dispersal classes. Sedentary species experiencing rapid habitat shifts may benefit from assisted dispersal. For vagile species experiencing slow habitat shifts but severe habitat fragmentation, restoration of degraded habitat may be of greater benefit.

The shape of the redistribution kernel also matters. The kernels in Figures 3.3, 3.4, and 3.5 have similar median absolute deviations (MAD $= \sigma/1.4826 = 2.02$, MAD $= b \ln 2 = 2.08$, and MAD $= b = 2$). In spite of this, if we superimpose the critical speed curves for the three kernels (data not shown), they intersect at numerous points. Cauchy distribution (3.76) and Laplace distribution (3.74) have smaller R_0 intercepts, presumably because more propagules pile up near the origin for these two distributions.

We hope to extend our analyses in new directions. In section 3.2, we performed a linear stability analysis for the trivial solution $n^*(\bar{x}) = 0$. This was appropriate because we were only interested in population persistence. For more complicated growth functions, studying the stability of nontrivial traveling pulses may also reveal interesting dynamics. Needless to say, this is a harder problem. One must first determine the nontrivial pulse.

In addition, we have only analyzed a single-species model. Recent studies suggest that species-specific responses to climate change may sunder ecological communities [10, 136]. Studying multi-species models should thus prove interesting.

Finally, in our model, eggs hatch and grow and adults emerge only if they are in the climate-shifted patch for year t. Thus climate change only affects reproductive processes. We have built our model in this way because of the demonstrated effect of climate change on phenology and reproductive biology [22, 41, 81, 100, 115, 153].The observed dynamics could be quite different if climate change has a direct effect on dispersal. These are all interesting and open problems that merit future research.

3.9 Appendix A: Legendre polynomials

The Legendre polynomials are the orthogonal polynomials formed by applying the Gram-Schmidt orthogonalization process to the functions 1, x, $x^2, ...$ on the interval $[-1, 1]$ with the usual inner product. These polynomials are commonly used to approximate probability density functions (along with their derivatives, integrals, and convolutions) [4, 43, 85, 137] and to solve integral equations [76, 79, 155, 160].

The Legendre polynomials are given by

$$P_i(x) \;=\; \frac{1}{2^i i!}\,\frac{d^i}{dx^i}\,[(x^2-1)^i] \tag{3.83}$$

for $i = 0, 1, 2, ...$ The first few Legendre polynomials are

$$P_0(x) = 1\,, \quad P_1(x) = x\,, \quad P_2 = \frac{1}{2}(3x^2-1)\,, \quad P_3(x) = \frac{1}{2}(5x^3-3x)\,. \tag{3.84}$$

Additional Legendre polynomials can be generated using the recurrence relation

$$P_{i+1}(x) \;=\; \frac{2i+1}{i+1}x\,P_i \;-\; \frac{i}{i+1}P_{i-1}(x)\,. \tag{3.85}$$

The Legendre polynomials are even functions for n even and odd functions for i odd. Each of the $P_i(x)$ has i distinct and real roots on the interval $(-1, 1)$. For our purposes, the most important property of the Legendre polynomials is that they form an orthogonal system on $[-1, 1]$ with

$$\int_{-1}^{1} P_i(x)\,P_j(x)\,dx \;=\; \frac{2}{2i+1}\,\delta_{ij}\,. \tag{3.86}$$

Here, δ_{ij} is the Kronecker delta, which equals 1 if $i = j$ and 0 if $i \neq j$.

Because the Legendre polynomials form a complete, orthogonal system over the interval $[-1, 1]$, we may expand a function $f(x)$ on this interval in a Legendre (or Fourier-Legendre) series of the form

$$f(x) \;=\; \sum_{i=0}^{\infty} a_i\,P_i(x)\,. \tag{3.87}$$

Please see [59] and [128] for convergence conditions. It is easy to show, using orthogonality condition (3.86), that the coefficients a_i satisfy

$$a_i \;=\; \frac{2i+1}{2}\int_{-1}^{1} f(x)\,P_i(x)\,dx\,. \tag{3.88}$$

In a similar way, we can expand a bivariate function, $f(x,\, y)$, in a double series of the form

$$f(x,\, y) \;=\; \sum_{i\,=\,0}^{\infty} \sum_{j\,=\,0}^{\infty} A_{ij}\, P_i(x)\, P_j(y)\,. \tag{3.89}$$

The coefficients A_{ij} in this series satisfy

$$A_{ij} \;=\; \frac{(2i+1)\,(2j+1)}{4} \int_{-1}^{1} \int_{-1}^{1} f(x,\, y)\, P_i(x)\, P_j(y)\, dy\, dx\,. \tag{3.90}$$

The problem that we are interested in, equation (3.17), involves an integral over the interval $[-L/2,\, L/2]$. Rather than rescaling our problem, we find it convenient to follow [128] by introducing Legendre polynomials relative to the interval $[-L/2,\, L/2]$,

$$X_i(x) \;=\; P_i\left(\frac{2x}{L}\right)\,. \tag{3.91}$$

In light of this transformation, our orthogonality condition, equation (3.86), now takes the form

$$\int_{-L/2}^{L/2} X_i(x)\, X_j(x)\, dx \;=\; \frac{L}{2i+1}\, \delta_{\,ij}\,. \tag{3.92}$$

When we write a function, $f(x)$, in a series of Legendre polynomials relative to the interval $[-L/2,\, L/2]$,

$$f(x) \;=\; \sum_{n\,=\,0}^{\infty} a_i\, X_i(x)\,, \tag{3.93}$$

the coefficients a_i now satisfy

$$a_i \;=\; \frac{2i+1}{L} \int_{-L/2}^{L/2} f(x)\, X_i(x)\, dx\,. \tag{3.94}$$

Likewise, when we expand a bivariate function, $f(x,\, y)$, in a double series of Legendre polynomials relative to the interval $[-L/2,\, L/2]$,

$$f(x,\, y) \;=\; \sum_{i\,=\,0}^{\infty} \sum_{j\,=\,0}^{\infty} A_{ij}\, X_i(x)\, X_j(y)\,, \tag{3.95}$$

the coefficients A_{ij} now satisfy

$$A_{ij} \;=\; \frac{(2i+1)\,(2j+1)}{L^2} \int_{-L/2}^{L/2} \int_{-L/2}^{L/2} f(x,\, y)\, X_i(x)\, X_j(y)\, dy\, dx\,. \tag{3.96}$$

3.10 Appendix B: Derivation of the modified Bessel kernel

Mark-release-recapture studies are often conducted in two dimensions. For example, they often use the negative exponential distribution

$$f(r) = \exp(-\alpha r), \qquad 0 < \alpha < \infty, \tag{3.97}$$

to represent the complementary cumulative distribution of organism's dispersal distances

$$r = \sqrt{x^2 + y^2}. \tag{3.98}$$

Since our model is one dimensional, we need to calculate the appropriate kernel from the probability distribution functions used in these two dimensional studies. Lewis et al. [83] deduced that, if the data have been collected in terms of propagules per unit length of distance from the source, then the related bivariate probability density function is obtained by rescaling by $2\pi r$. For example, if the complementary cumulative distribution of propagules settling distance r from their source is the negative exponential distribution (3.97), then the probability density function of the frequency of seeds per unit length settling distance r from their source is

$$\tilde{p}(r) = \alpha \, \exp(-\alpha r), \qquad 0 < \alpha < \infty, \tag{3.99}$$

assuming isotropy of the environment. The corresponding probability density function of the frequency of seeds per unit area settling distance r from the source is

$$p(r) = \frac{\alpha}{2\pi r} \, \exp(-\alpha r). \tag{3.100}$$

Since $r = \sqrt{x^2 + y^2}$, distribution (3.100) is really a two-dimensional distribution. Its marginal distribution in, say, direction x is [6]

$$p_{mar}(x) = \frac{\alpha}{\pi} \, K_0(\alpha|x|). \tag{3.101}$$

We therefore derive our kernel from probability density function (3.101), and obtain

$$k(x, y) = \frac{\alpha}{\pi} \, K_0(\alpha|x - y|). \tag{3.102}$$

Note that the parameter α measured in the two-dimensional studies is the same as the α in function (3.101).

Chapter 4

ACCELERATION MATTERS: MODELING RANGE SHIFTS UNDER ACCELERATED CLIMATE WARMING

4.1 Introduction

Recent climate warming has been rapid and extensive [58]. Global average temperatures have increased by 0.13 °C per decade over the last 50 years (1956–2005). This rapid change has had a brutal impact on the Earth's biota. Although species have responded by shifting their geographic ranges, there is empirical evidence that they may not be shifting fast enough to track climate change. Devictor et al. [33] analyzed datasets over two decades (1998−2008) for butterflies and birds in Europe, and estimated that the northward climate change in Europe had outrun the range shifts of butterflies by 135 km and those of birds by 212 km. Bedford et al. [7] also studied 81 butterfly species in Canada, and reported systemic range-shift lags. It is not clear whether these lags, referred to as *climatic debts*, will keep accumulating over time or stabilize at some level.

Many models have shown that the speed of climate warming has a profound impact on species range shifts. Simulations of individual-based models [148], as well as analyses of different mathematical models [9, 161], demonstrate that species may fail to keep pace with climate warming, and thus become extinct, if the warming is too rapid. These models provide useful tools for incorporating population recruitment and dispersal into studies of population dynamics during climate-induced range shifts. One limitation of these models, however, is that they assume constant speeds of climate warming. How will accelerated climate warming affect species range shifts?

This question is especially relevant since the speed of climate warming appears to be increasing. Global temperature increase during 1906−2005 was faster than that during 1901−2000 [58]. For projections of future warming, the IPCC [58] foresees an increase in green house emissions and thus faster warming. If rapid warming prevents species from

keeping up, acceleration of the warming speed is of even greater concern.

In this chapter, I will present an integrodifference model for studying the population dynamics of a single-species population under accelerated climate warming. This model (equation 4.7) incorporates both population recruitment and dispersal. It focuses on organisms with distinct growth and dispersal stages, such as many plants and insects, and is discrete in time. In addition, it includes spatial heterogeneity in recruitment rates. Section (4.2) explains model assumptions and formulations, including different components of the model and their assemblage. Section (4.3) briefly summarizes the mathematical (section 4.3.1) and computational (section 4.3.2) methods utilized in the model analysis. I present details of the mathematical analysis in sections 4.6, 4.7.2, and 4.7.3, and details of computational methods in section 4.8. Results appear in section (4.4), including findings on persistence and speeds of the resulting range shifts (section 4.4.1), accumulated range-shift lags (section 4.4.2), and the impact of acceleration on range-shift lags (section 4.4.3). Finally, the results section is followed by discussions and conclusions (4.5).

4.2 A mathematical model for population dynamics under climate warming

4.2.1 Niche curve and habitat suitability along spatial gradient

I use a mathematical model to derive spatiotemporal population dynamics. Let y be a point along a continuous, one-dimensional spatial gradient. For example, this could be a latitudinal gradient or an altitudinal gradient. Naturally, habitat suitability for population recruitment may vary along this spatial gradient [32, 41], and I use a habitat suitability function $Q(y)$ to prescribe the effect of habitat suitability at point y on *pre-dispersal* population recruitment (e.g., reproduction). Habitat suitability is assumed to vary between 0 and 1. When $Q(y) = 0$ at a certain location y, the environment is completely unsuitable for reproduction at y. On the other hand, locations where $Q(y) = 1$ are optimal locations for reproduction. I chose this *pre-dispersal* formulation of the habitat suitability function, which is different from the *post-dispersal* formulation used by Latore et al. [78], because of the documented impact of climate warming on reproduction [41, 81, 100, 115, 153]. This formulation can be easily adapted if *post-dispersal* habitat suitability is preferred.

For brevity's sake, I will refer to the curve obtained by plotting function $Q(y)$ over the spatial gradient as the *niche curve*. This terminology is reasonable, since $Q(y)$ is determined not only by the environment, but also by the organism's ecological niche [56]. It is also worth mentioning that niche curves are conceptually similar to *fitness curves* [41].

In general, I will consider habitat suitability functions that are *compactly supported*. That is, these functions are only nonzero on intervals of finite lengths. One exception that I will consider as a special example is

$$Q(x) = \exp\left(-\frac{x^2}{\sigma^2}\right). \tag{4.1}$$

Here, the parameter σ affects the width of the Gaussian curve (4.1), and therefore I will refer to σ as the *niche width*. Function (4.1) has the shape of a normal distribution. This distribution prescribes a habitat quality function that is largest at the center of a species' range, and decreases continuously and symmetrically towards the periphery. This smooth, symmetric, and unimodal shape is, of course, only a caricature of reality, and is challenged by many ecologists (see section 4.5.2 of Gaston [41] for a nice review). On the other hand, this shape is a crude approximation. As we shall see later, this example is relatively simple, and provides us with analytic formulas that offer important insights for generalization.

4.2.2 Climate warming

The major novelty of my model is that the niche curve is time-dependent, and is assumed to be shifting in one direction because of climate warming. Although space is continuous, time elapses by discrete steps in the model. The shape of the habitat suitability function $Q(y)$ is assumed to remain the same over time t, but the location $s(t)$ of a reference point on the niche curve evolves over time.

For example, if

$$s(t) = ct, \tag{4.2}$$

the niche curve shifts to the right in each time step for a fixed distance of c, mimicking the impact of a constant-speed climate warming. I will refer to c as the *shift speed*.

The prescription

$$s(t) = c_1 t + \frac{c_2}{2} t^2, \tag{4.3}$$

on the other hand, describes an accelerated-warming scenario, with initial shift speed of c_1, and a constant acceleration c_2 of the shift speed.

Obviously, constant-speed warming (4.2) can be viewed as a special case of accelerated warming (4.3) with zero acceleration. In fact, the constant-speed warming scenario (4.2) provides good insights on population dynamics under more general warming scenarios. Therefore, even though I aim to study scenario (4.3), I will consider scenarios (4.2) as well.

I will also compare the impact of acceleration c_2 on the population by comparing a family of warming scenarios of type (4.3) with different accelerations. To make the comparison fair, the distance of shift, S, over a fixed number of time steps T, is the same for every scenario. Figure (4.1) illustrates the different scenarios I consider. The horizontal line represents the scenario with a constant speed of shift (acceleration = 0), and the slanted lines represent scenarios with different constant accelerations of the shift speed, with thicker lines having higher accelerations. All these lines pass the point $(T/2, \bar{c})$, where $\bar{c}$ is the average speed of shift, S/T, over T time steps.

4.2.3 Population recruitment and dispersal

I will consider a single-species population for a species with distinct growth and dispersal stages, as well as non-overlapping generations. For this type of species, we can simply census the population for each generation. Let $n_t(x)$ be the population density of the t-th generation at location x. It is mapped to the density of propagules after local growth, $f[n_t(x)]$, by the growth function f. During the growth stage, the population does not disperse. A well-known growth function is the right-hand side of the Beverton−Holt stock-recruitment curve,

$$f[n_t] = \frac{R_0 n_t}{1 + [(R_0 - 1)/K] n_t}. \tag{4.4}$$

In this paper, I only consider monotonic growth functions that satisfy

$$f(n) \le f'(0)n, \qquad \text{and} \qquad f(n_1)/n_1 < f(n_2)/n_2 \ \text{ for } \ n_1 > n_2. \tag{4.5}$$

Therefore, the per capita recruitment rate is highest at low population density, and decreases as population becomes denser, but the total recruitment increases for a denser population.

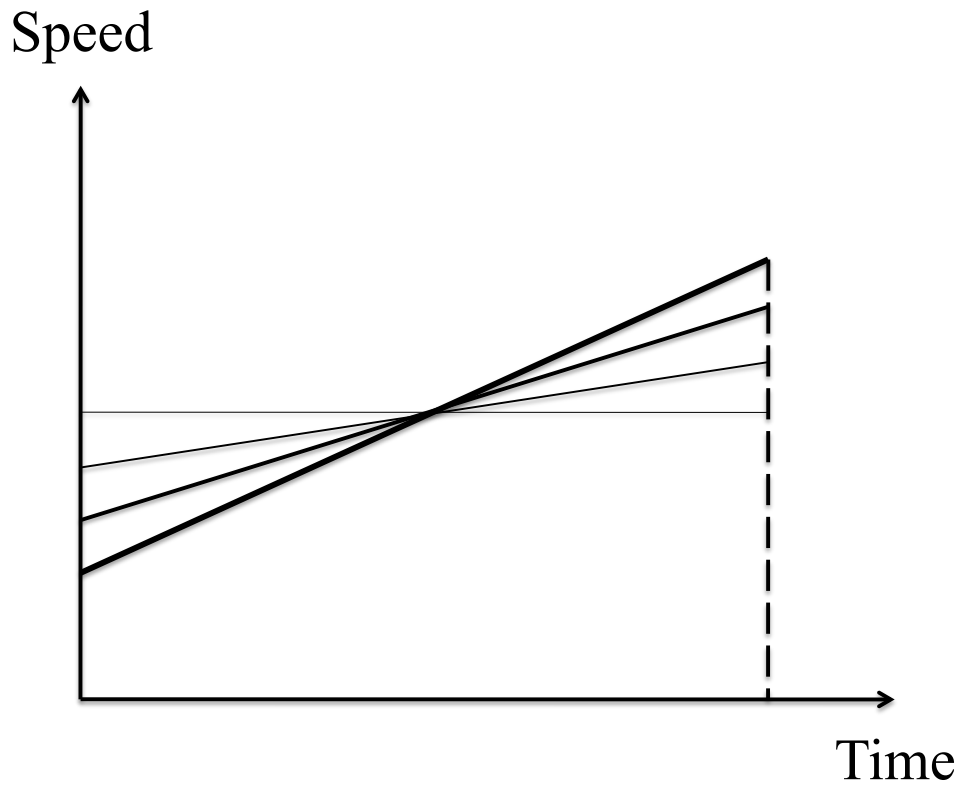

Figure 4.1: Illustration of a family of warming scenarios of type (4.3). In this figure, the horizontal line represents the constant-speed warming scenario (acceleration = 0), and the slanted lines represent scenarios with different accelerations of the shift speed, with thicker lines having higher accelerations. All these lines pass the point $(T/2, \bar{c})$, where $\bar{c}$ is the average speed of shift S/T after T time steps. That is, the distance of shift, S, over a fixed number of time steps T, is the same for every scenario.

These assumptions exclude, for example, recruitment functions with over-compensatory growth [127], or Allee effects [1].

After local recruitment, propagules disperse. Dispersal is quantified by the dispersal kernel $k(x, y)$. For a fixed source y of propagules, the dispersal kernel $k(x, y)$ is a probability density function of the destination x of a propagule from y. Assuming spatial homogeneity and symmetry in dispersal, $k(x, y)$ can be written as the difference kernel $k(x - y)$, where k is symmetric. One common example of the dispersal kernel is the Gaussian kernel

$$k(x-y) = \frac{1}{2\sqrt{\pi D}} \exp\left[-\frac{(x-y)^2}{4D}\right]. \tag{4.6}$$

The population density of the $t + 1$-th generation, $n_{t+1}(x)$, can be calculated with an integral that tallies the propagules. The model I consider is therefore

$$n_{t+1}(x) = \int_{-\infty}^{\infty} k(x-y)Q[y - s(t)]f[n_t(y)]dy. \tag{4.7}$$

Equation (4.7) is an integrodifference-equation model. It is a discrete-time, continuous-space model. When the habitat suitability function $Q(y)$ is a hat function

$$Q(y) = \begin{cases} 1, & y \in [-L/2, L/2], \\ \\ 0, & y \notin [-L/2, L/2], \end{cases} \tag{4.8}$$

and $s(t) = ct$, equation (4.7) reduces to the special case considered in previous chapters, equation (2.4). Equation (4.7) thus extends equation (2.4) to a more universal form. Even though I only considered smooth, symmetric, and unimodal niche curves, model (4.7) itself is much more versatile. If necessary, one can prescribe niche curves of all shapes, including but not limited to examples that Latore et al. [78] considered.

If the population is small, population density $n_t(x)$ will be low, and the nonlinear model (4.7) can be approximated by the linear equation

$$n_{t+1}(x) = f'(0) \int_{-\infty}^{\infty} k(x-y)Q[y - s(t)]n_t(y)\, dy. \tag{4.9}$$

Regardless of population density, the linear equation (4.9) provides an upper bound of the nonlinear equation (4.7) in the sense that, with the same initial population distribution $n_0(x)$, the resulting $n_t(x)$ of the nonlinear model, for any generation t, is no larger than

that of the linear model. Therefore if the population goes extinct under the linear equation, it will also go extinct under the corresponding nonlinear equation.

4.3 Methods

4.3.1 Mathematical analysis

One difficulty in analyzing model (4.7) is that the right hand side expression about $n_t(x)$ depends on time t. This is referred to as nonautonomous. Luckily, this time-dependence is caused only by $s(t)$, the shifting of the niche curve. It is therefore revealing to describe population density $n_t(x)$ in a moving axis, and define a new function $\bar{n}_t(x)$, where

$$\bar{n}_t(x) = n_t(x + s(t)). \tag{4.10}$$

This new function $\bar{n}_t(x)$ can be understood in the following way: if a camera starts at the origin, moves at the same pace with the niche curve, and captures pictures of the population density $n_t(x)$, the photos will show the curve resulting from plotting $y = \bar{n}_t(x)$ in an xy coordinate system. We can then write $n_t(x)$ as

$$n_t(x) = \bar{n}_t(x - s(t)). \tag{4.11}$$

Observing the population in a moving frame reveals important natures of the problem. For constant-speed warming, where $s(t) = ct$, it is shown in Appendix A that the time-dependence can be peeled off by substituting expression (4.11) into model (4.7), and the model can be reduced to an autonomous system about $\bar{n}_t(x)$,

$$\bar{n}_{t+1}(x) = \int_{-\infty}^{\infty} k(x + c - y)Q(y)f[\bar{n}_t(y)]dy. \tag{4.12}$$

Global bifurcation results by Rabinowitz [126] and Hardin [44, 45, 46] (also see Van Kirk and Lewis [151]) can therefore be applied, for compactly-supported $Q(y)$, proving the existence and uniqueness of traveling pulse solutions to equation (4.7), as well as showing that population persistence is determined by whether the dominant eigenvalue of the linear operator

$$K: \qquad u(x) \to f'(0) \int_{-\infty}^{\infty} k(x + c - y)Q(y)u(y)\, dy \tag{4.13}$$

is larger than 1 (see Appendix A for details).

Calculation of the dominant eigenvalue with numerical methods is described in the next section, section (4.3.2). An analytic solution is also available for a special example that uses the Gaussian niche curve (4.1), and the Gaussian kernel (4.6). In this example, when $s(t) = ct$, the function

$$u(x) = a \cdot \exp\left[-\frac{(x-\mu^*)^2}{v^*}\right] \tag{4.14}$$

is an eigenfunction of the linear integral operator (4.13) (see Appendix D), where

$$\mu^* = -c - \frac{\sigma^2 c}{v^*}, \tag{4.15}$$

$$v^* = 2D(1 + \sqrt{1 + \sigma^2/D}), \tag{4.16}$$

and a is an arbitrary nonzero number. The corresponding eigenvalue can then be calculated as

$$\lambda = \sqrt{\frac{\sigma^2 v^*}{\sigma^2 + v^*}} \cdot \exp\left[-\frac{c^2(\sigma^2 + v^*)}{v^{*2}}\right]. \tag{4.17}$$

Numerical computations with the Nyström method indicate that this eigenvalue is actually the dominant eigenvalue of operator (4.13). The eigenvalue λ is equal to 1 when $c = c^*$, smaller than 1 if $c > c^*$, and larger than 1 if $c < c^*$, where

$$c^* = \sqrt{\frac{v^{*2}}{\sigma^2 + v^*} \ln\left[f'(0) \cdot \sqrt{\frac{\sigma^2}{\sigma^2 + v^*}}\right]}. \tag{4.18}$$

General quantitative results of the nonlinear model will require numerical algorithms. For the linear approximation (4.9), analytic results are again available for the special example with the Gaussian niche curve (4.1) and the Gaussian kernel (4.6). This special example can be studied through a three-dimensional dynamical system (see Appendix D). For constant-speed warming scenario $s(t) = ct$, the dynamical system approach confirms results (4.14), (4.15), (4.16), and (4.18). The dynamical system approach is very powerful, and works for more general $s(t)$, such as the accelerated warming scenario (4.3) (see Appendix D).

4.3.2 Numerical calculations

For the nonlinear model, one can resort to numerical schemes to calculate the dominant eigenvalue of operator (4.13). One useful method is the Nyström's method. This method discretizes the integral in operator (4.13), and approximates the eigenvalues of the integral operator with those of a matrix. Appendix E contains details of the method. The numerical results for the special example is compared with the analytic results in Figure (4.10).

Besides analysis of operator (4.13), population density distribution $n_t(x)$ of each generation can also be calculated using the Fast Fourier Transform (FFT) algorithm. From the population density function $n_t(x)$, the center of the population distribution $n_t(x)$ is calculated as

$$\gamma_t = \frac{\int_{-\infty}^{\infty} x n_t(x)\, dx}{\int_{-\infty}^{\infty} n_t(x)\, dx}. \tag{4.19}$$

The distance between this center and the center of the niche curve is referred to as the *niche deficit*, and is calculated as

$$\delta_t = s(t) - \gamma_t. \tag{4.20}$$

4.4 Results

4.4.1 Climate-warming-driven range shifts and their speeds

Constant-speed warming

Model (4.7) captures the range-shift phenomenon under climate warming. For the constant-speed warming scenario $s(t) = ct$, with an initial population distribution $n_0(x)$, the resulting population distributions $n_1(x), n_2(x), \ldots$, for each generation, depending on the model parameters, have two possible fates. Mathematical analysis in Appendix C shows that, for some parameter choices, the population distributions $n_t(x)$ approach a fixed nonzero distribution $\bar{n}^*(x-ct)$ as t increases, regardless of the initial population distribution $n_0(x)$. That is, the population persists and exhibits a steady range shift. Figure (4.2) demonstrates this case for one example with speed $c = 0.06$.

The speed of the resulting range shift approaches the speed, c, of the shifting niche curve (Appendix C). Figure (4.3) demonstrates how the range-shift speed, calculated as the speed

of the population center (4.19), converges to the prescribed speed c for different examples of initial population distributions.

For other choices of model parameters, the population distributions $n_t(x)$, regardless of the initial population distribution $n_0(x)$, approach the zero distribution $n^*(x) \equiv 0$. That is, the population goes extinct over time. Appendix D shows that the population goes extinct if the shift speed c is larger than a critical speed c^* for the analytic example in section 4.7 (also see section 4.3.1). The critical speed c^* can be calculated from the formulas (4.18) and (4.16). For recruitment function (4.4), for example, $f'(0) = R_0$, and

$$c^* = \sqrt{\frac{4D^2(1+\sqrt{1+\sigma^2/D})^2}{\sigma^2+2D(1+\sqrt{1+\sigma^2/D})} \ln\left[R_0 \cdot \sqrt{\frac{\sigma^2}{\sigma^2+2D(1+\sqrt{1+\sigma^2/D})}}\right]}. \tag{4.21}$$

Here, σ is the niche width of the niche curve (4.1), and D is the diffusion rate in the Gaussian kernel (4.6).

Accelerated warming

Under accelerated-warming scenario (4.3), the population center (4.19) shifts at an increasing speed (see Figure 4.4). Figure (4.5) demonstrates how the acceleration of the shifting population center approaches the prescribed acceleration c_2 ($c_2 = 10^{-3}$ in figure 4.5) of the shifting niche curve. This is supported by the analytic example (section 4.7.3).

Unlike the constant-speed warming scenario, the population cannot persist under accelerated warming. For example, with the Gaussian niche curve (4.1), the Gaussian kernel (4.6), and a Gaussian initial-population distribution, analysis of the linear equation (4.9) show that the resulting Gaussian-shaped population distribution approaches the zero distribution because its amplitude approaches 0 (Appendix D). Since population distributions under the nonlinear equation is smaller than that of the linear equation with the same initial conditions, the population also goes extinct under the nonlinear model.

4.4.2 Accumulation of niche deficits

With my model, after a sufficient number of time steps, the population center (4.19) lags behind the center $s(t)$ of the niche curve, regardless of the initial population distribution.

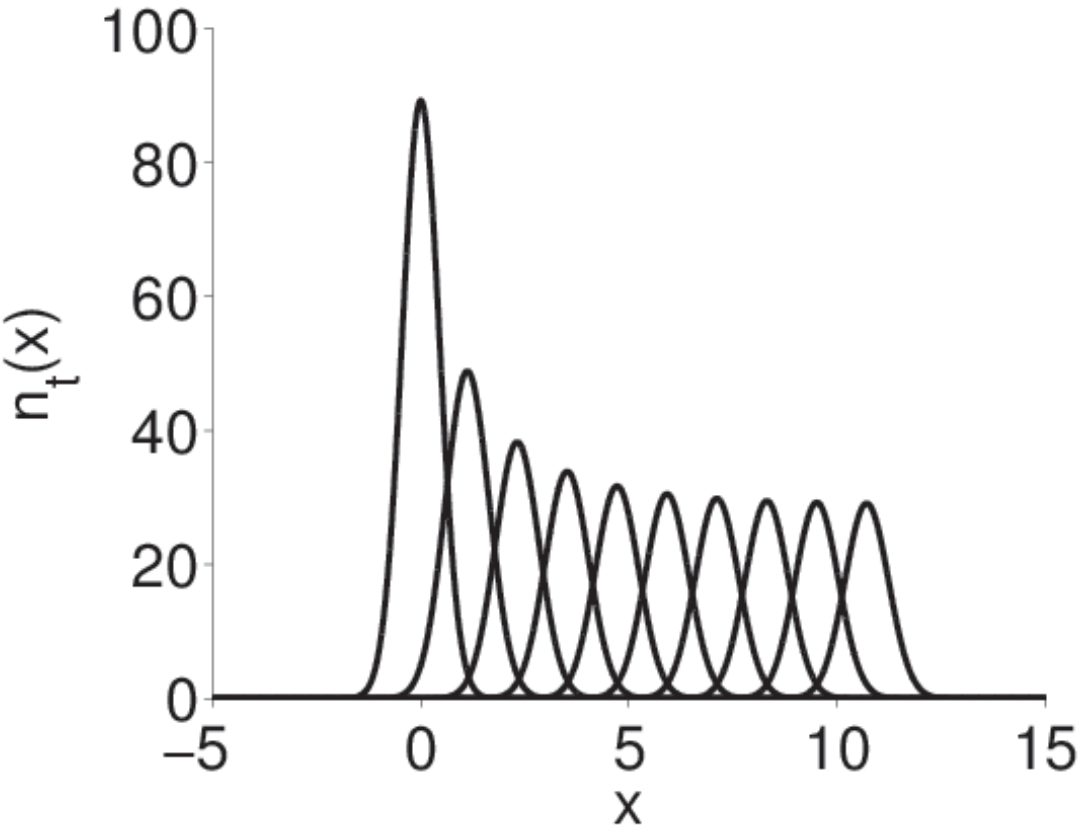

Figure 4.2: Simulations of the population distribution under constant-speed climate warming, obtained by iterating the convolution equation (4.7) with $s(t) = ct$, show that the population distribution may experience a steady shift. In this figure, the initial distribution of the population over space x was $(K/10) \cdot k(x)$, where $k(x)$ is the normal distribution with variance 0.4, and $K = 1000$ is the carrying capacity in the recruitment function (4.4). The net reproductive rate $R_0 = 2$ in (4.4), and the dispersal kernel was the Gaussian kernel (4.6) with diffusion rate $D = 0.2$. The habitat quality function was (4.1), with $\sigma^2 = 0.2$. The speed c was 0.06. The distribution is displayed every 20 generations and was computed using an FFT-assisted implementation of the extended trapezoidal rule with 2^{16} nodes on the interval $[-40, 40]$.

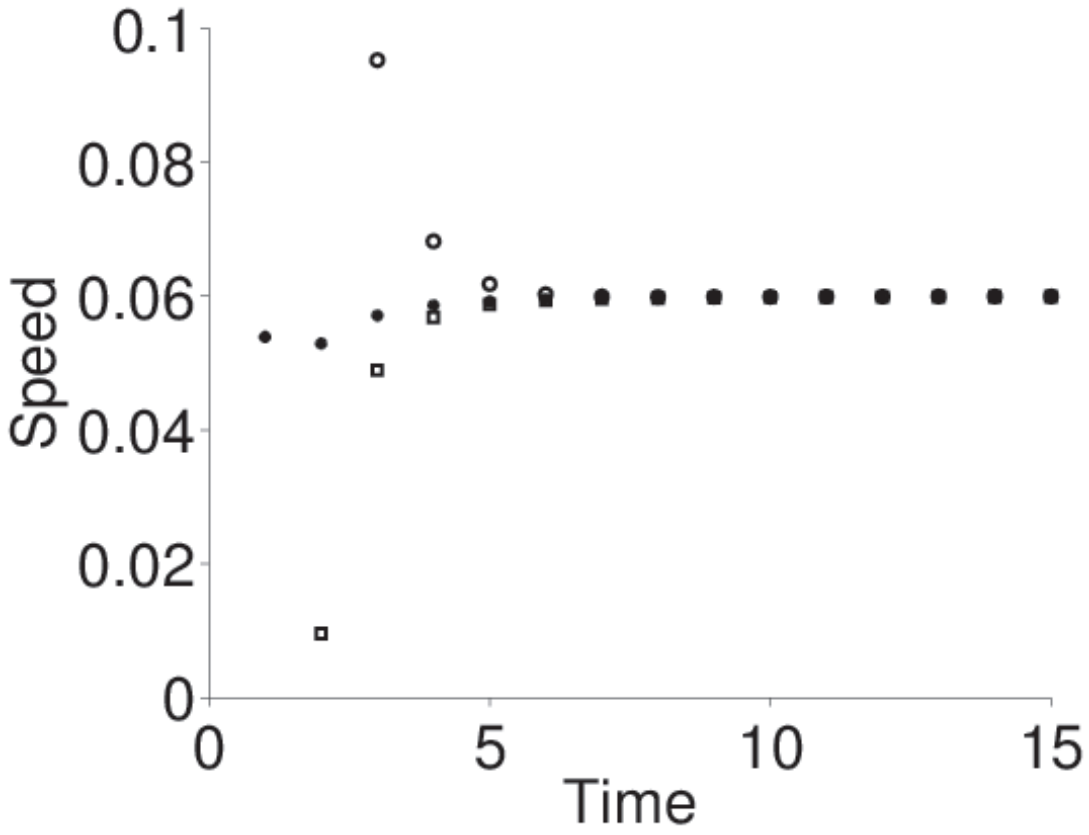

Figure 4.3: Speed of range shifts under constant-speed climate warming, calculated as the speed of the center (4.19) of the population distribution $n_t(x)$ for each generation t. The population distributions $n_t(x)$ was obtained by iterating the convolution equation (4.7) with $s(t) = ct$ using an FFT-assisted implementation of the extended trapezoidal rule with 2^{16} nodes on the interval $[-40, 40]$. The initial population distributions were $K \cdot \exp(-x^2)$ for the solid circles, $K \cdot (\sin(x)+1)$ for the open circles, and $K \cdot \exp[-(x+1)^2] + K \cdot \exp[-(x-2)^2]$ for the squares, where $K = 1000$ is the carrying capacity in the recruitment function (4.4). The net reproductive rate $R_0 = 2$ in (4.4), and the dispersal kernel was the Gaussian kernel (4.6) with diffusion rate $D = 0.2$. The habitat quality function was (4.1), with $\sigma^2 = 0.2$. The speed c was 0.06. For all three initial population distributions over space, populations eventually shift at a constant speed. This shift speed is equal to the prescribed speed c of the shifting niche curve.

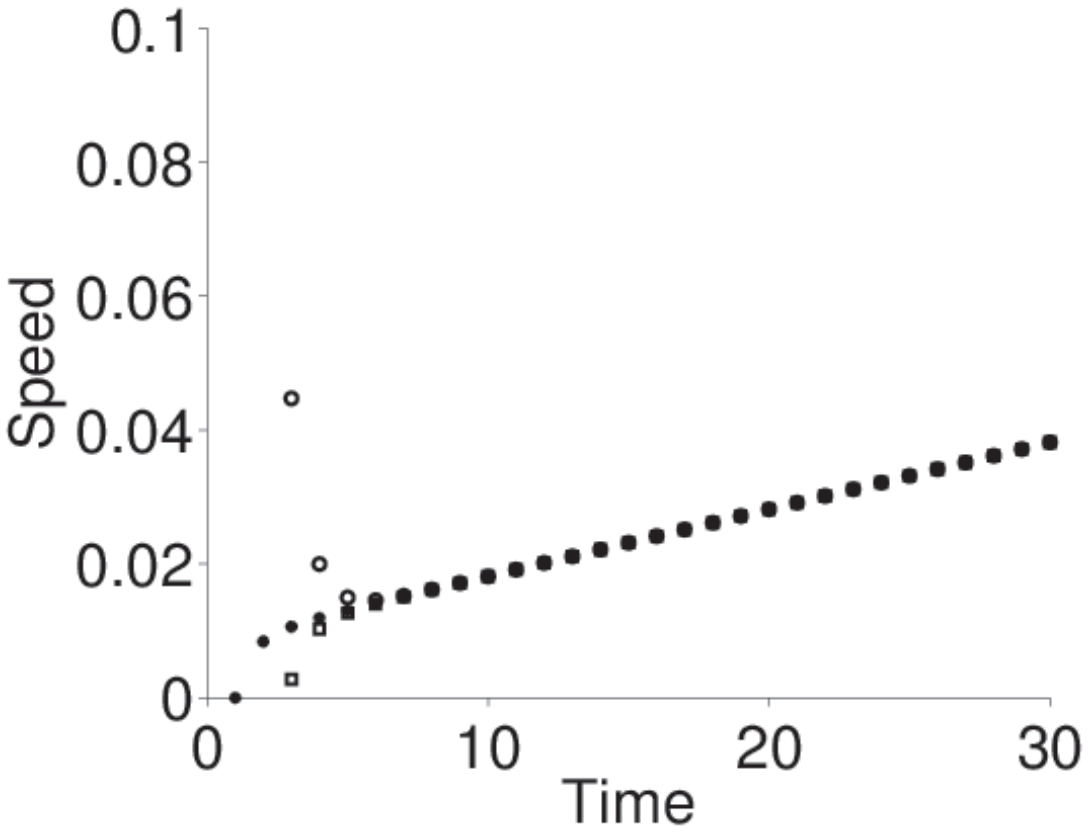

Figure 4.4: Speed of range shifts under accelerated climate warming, calculated as the speed of the center (4.19) of the population distribution $n_t(x)$ for each generation t. The population distributions $n_t(x)$ was obtained by iterating the convolution equation (4.7) with the accelerated-warming scenario, $s(t) = c_1 t + c_2/2t^2$, using an FFT-assisted implementation of the extended trapezoidal rule with 2^{16} nodes on the interval $[-40, 40]$. The initial population distributions were $K \cdot \exp(-x^2)$ for the solid circles, $K \cdot (\sin(x) + 1)$ for the open circles, and $K \cdot \exp[-(x+1)^2] + K \cdot \exp[-(x-2)^2]$ for the squares, where $K = 1000$ is the carrying capacity in the recruitment function (4.4). The net reproductive rate $R_0 = 2$ in (4.4), and the dispersal kernel was the Gaussian kernel (4.6) with diffusion rate $D = 0.2$. The habitat quality function was (4.1), with $\sigma^2 = 0.2$. The initial speed c_1 was 0.01, and the acceleration c_2 was 10^{-3}. For all three initial population distributions over space, populations eventually shift at the same speed. This shift speed is increasing with respect to time.

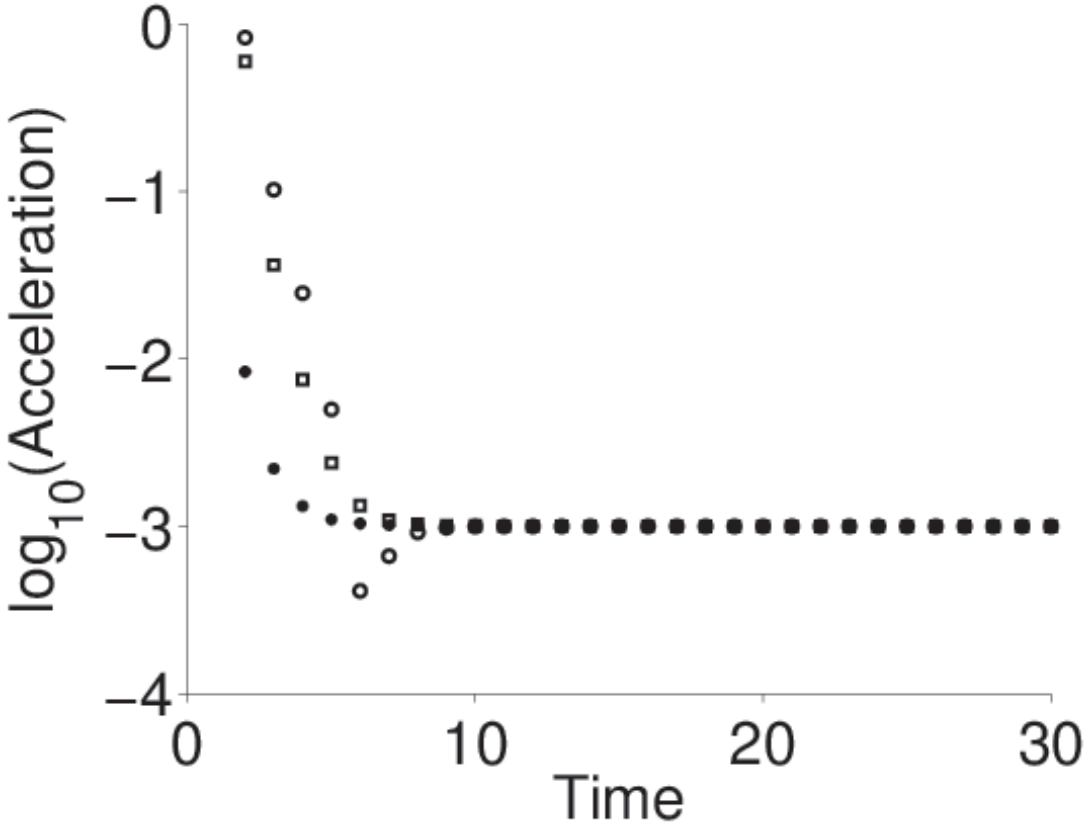

Figure 4.5: Acceleration of range shifts under accelerated climate warming, calculated as the increase of the speed of the center (4.19) of the population distribution $n_t(x)$ for each generation t, plotted on a logarithmic scale. The population distributions $n_t(x)$ was obtained by iterating the convolution equation (4.7) under the accelerated-warming scenario, $s(t) = c_1 t + c_2/2t^2$, using an FFT-assisted implementation of the extended trapezoidal rule with 2^{16} nodes on the interval $[-40, 40]$. The initial population distributions were $K \cdot \exp(-x^2)$ for the solid circles, $K \cdot (\sin(x)+1)$ for the open circles, and $K \cdot \exp[-(x+1)^2] + K \cdot \exp[-(x-2)^2]$ for the squares, where $K = 1000$ is the carrying capacity in the recruitment function (4.4). The net reproductive rate $R_0 = 2$ in (4.4), and the dispersal kernel was the Gaussian kernel (4.6) with diffusion rate $D = 0.2$. The habitat quality function was (4.1), with $\sigma^2 = 0.2$. The initial speed c_1 was 0.01, and the acceleration c_2 was 10^{-3}. For all three initial population distributions over space, populations eventually shift at the same acceleration. This acceleration approaches c_2 over time.

That is, the population carries a positive amount of niche deficit (4.20). Specifically, if the initial population center overlaps with the initial niche center $s(0)$, this result implies that the population shifts less than the niche curve.

The warming scenario has a profound influence on the accumulation of niche deficits. Under constant-speed warming, the niche deficit approaches a constant over time. This constant does not depend on initial population distribution $n_0(x)$. I will refer to this constant as *asymptotic niche deficit*. Analysis of the analytic example provides a formula,

$$\delta_\infty = c \cdot \left(\frac{\sigma^2 + v^*}{v^*} \right), \tag{4.22}$$

for the asymptotic niche deficit under the linear equation (4.9). In formula (4.22), c is the prescribed shift speed, σ is the niche width in niche curve (4.1), and v^* is given by formula (4.16). Since the linear equation (4.9) approximates the nonlinear equation when population density is low, equation (4.22) provides an estimate of the niche deficit in the analytic example for a small population. Computation of the niche deficit under the nonlinear model (4.7) or for more general choices of niche curves and dispersal kernels will require numerical methods. Figure (4.6), obtained by numerical computations, illustrates how the niche deficit for three different initial population distributions approach the same constant amount over time under constant-speed climate warming.

Formula (4.22) implies that the asymptotic niche deficit increases with the shift speed c. Results from the nonlinear model, obtained by numerical computations, imply the same. This dependence of the asymptotic niche deficit on the shift speed c for the nonlinear equation (4.7) is demonstrated in Figure (4.7), for shift speeds varying from 0.01 to 0.1.

Under accelerated warming, the niche deficit will keep accumulating, as demonstrated in Figure (4.8), while the acceleration of the niche deficit approaches a constant. This is supported by the analytic formula

$$\delta_t = 2 \left(\frac{\sigma^2 + v^*}{v^*} \right) c_2 t + \left\{ \left(\frac{\sigma^2 + v^*}{v^*} \right) c_1 + \left[1 - \frac{2(\sigma^2 + v^*)}{v^*} \right] \left(\frac{\sigma^2 + v^*}{v^*} \right) c_2 \right\}, \tag{4.23}$$

which is an estimate of the niche deficit under the linear equation (4.9) for the analytic example. Figure (4.9) shows how the acceleration of the niche deficit approaches a constant over time.

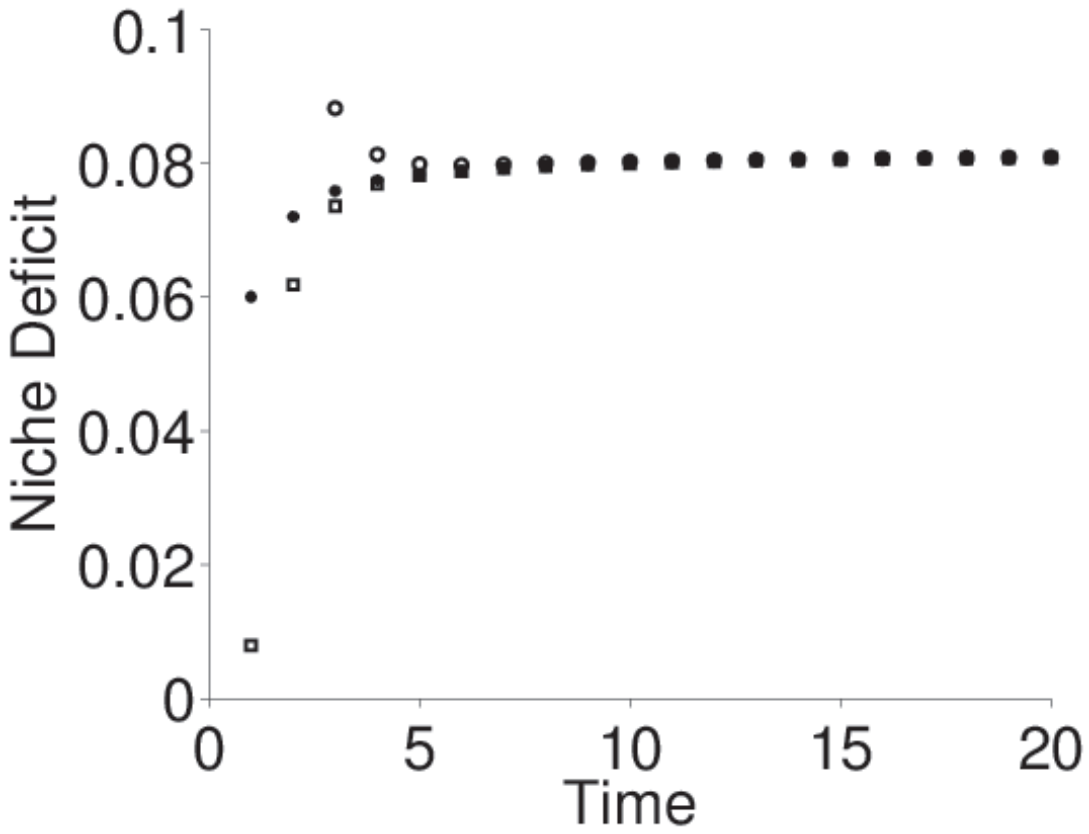

Figure 4.6: Accumulation of niche deficits (4.20) over time for a population under constant-speed climate warming. The population distributions $n_t(x)$ used in eqn. (4.20) was obtained by iterating the convolution equation (4.7) with $s(t) = ct$ using an FFT-assisted implementation of the extended trapezoidal rule with 2^{16} nodes on the interval $[-40, 40]$. The initial population distributions were $K \cdot \exp(-x^2)$ for the solid circles, $K \cdot (\sin(x) + 1)$ for the open circles, and $K \cdot \exp[-(x+1)^2] + K \cdot \exp[-(x-2)^2]$ for the squares, where $K = 1000$ is the carrying capacity in the recruitment function (4.4). The net reproductive rate $R_0 = 2$ in (4.4), and the dispersal kernel was the Gaussian kernel (4.6) with diffusion rate $D = 0.2$. The habitat quality function was (4.1), with $\sigma^2 = 0.2$. The speed c was 0.06. For all three initial population distributions over space, the niche deficits approach a constant over time. This constant is referred to as *asymptotic niche deficit*.

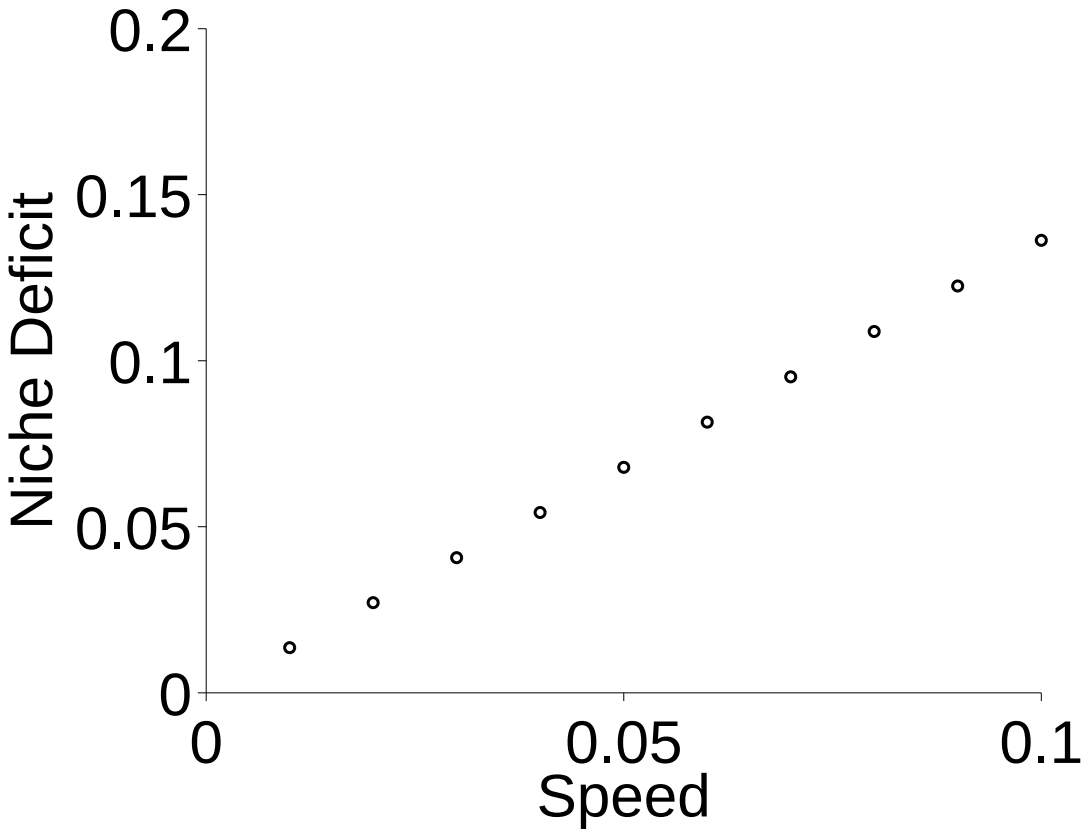

Figure 4.7: Asymptotic niche deficits for a population under constant-speed climate warming, with different shift speed c. To calculate the asymptotic niche deficits, the population distributions $n_t(x)$ used in equation (4.20) was obtained by iterating the convolution equation (4.7) with $s(t) = ct$ over sufficient numbers of generations, so that the niche deficit approaches a constant. The iterations were computed using an FFT-assisted implementation of the extended trapezoidal rule with 2^{16} nodes on the interval $[-40, 40]$. The initial population distributions were $K \cdot \exp(-x^2)$, where $K = 1000$ is the carrying capacity in the recruitment function (4.4). The net reproductive rate $R_0 = 2$ in (4.4), and the dispersal kernel was the Gaussian kernel (4.6) with diffusion rate $D = 0.2$. The habitat quality function was (4.1), with $\sigma^2 = 0.2$. Asymptotic niche deficits were then calculated for shift speeds c from 0.01 to 0.1 with an increment of 0.01.

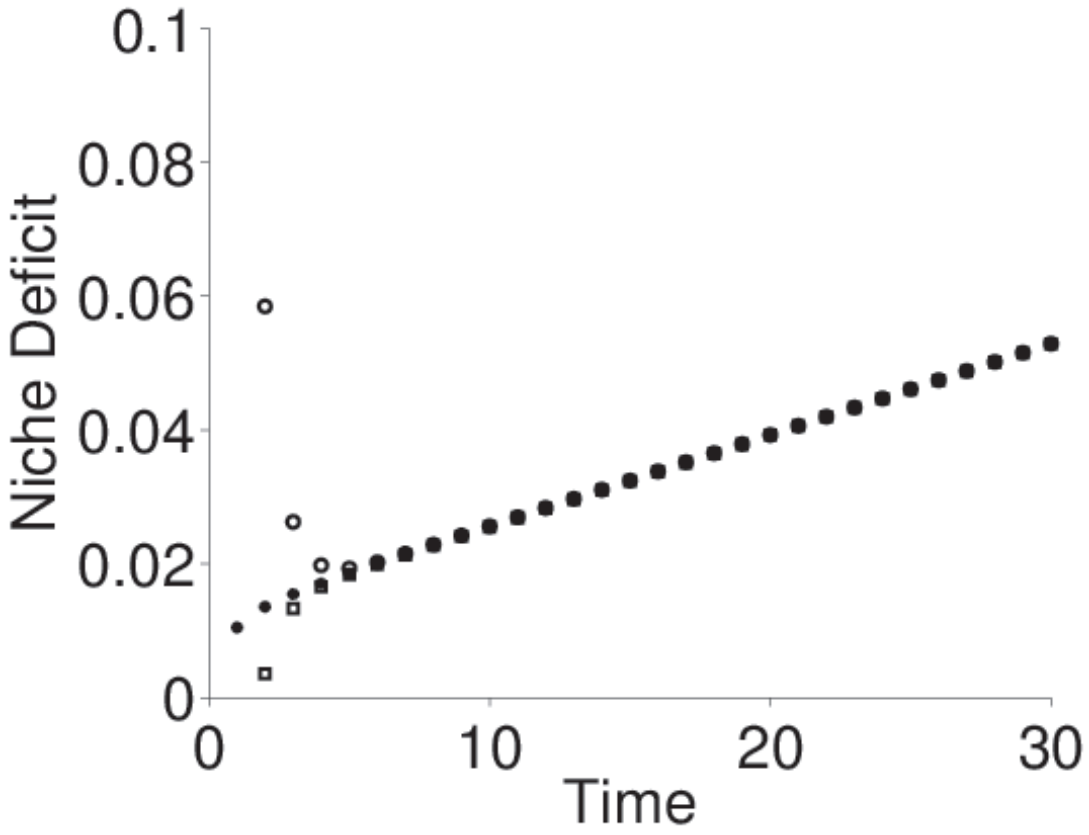

Figure 4.8: Accumulation of niche deficits (4.20) over time for a population under accelerated climate warming. The population distributions $n_t(x)$ used in eqn. (4.20) was obtained by iterating the convolution equation (4.7) with $s(t) = ct$ using an FFT-assisted implementation of the extended trapezoidal rule with 2^{16} nodes on the interval $[-40, 40]$. The initial population distributions were $K \cdot \exp(-x^2)$ for the solid circles, $K \cdot (\sin(x) + 1)$ for the open circles, and $K \cdot \exp[-(x+1)^2] + K \cdot \exp[-(x-2)^2]$ for the squares, where $K = 1000$ is the carrying capacity in the recruitment function (4.4). The net reproductive rate $R_0 = 2$ in (4.4), and the dispersal kernel was the Gaussian kernel (4.6) with diffusion rate $D = 0.2$. The habitat quality function was (4.1), with $\sigma^2 = 0.2$. The initial speed c_1 was 0.01, and the acceleration c_2 was 10^{-3}. For all three initial population distributions over space, the niche deficits become the same over time. This niche deficit increases over time.

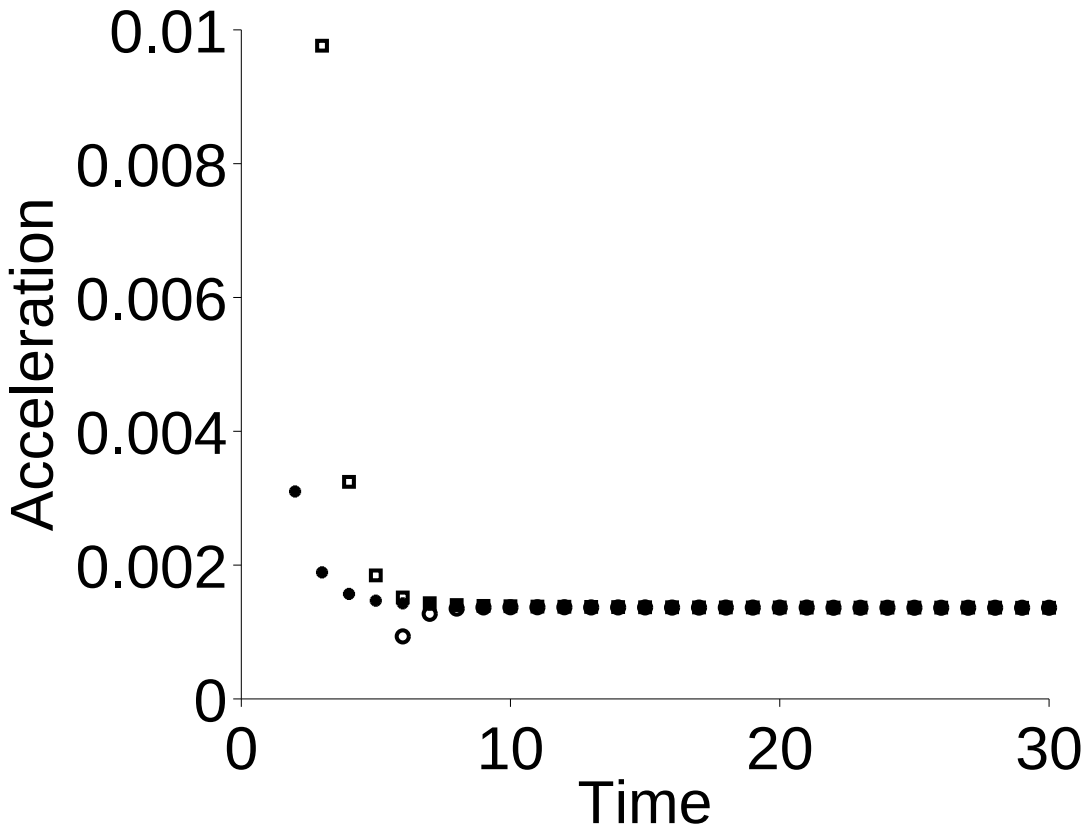

Figure 4.9: Acceleration of niche deficits (4.20) over time for a population under accelerated climate warming. The population distributions $n_t(x)$ used in equation (4.20) was obtained by iterating the convolution equation (4.7) with $s(t) = ct$ using an FFT-assisted implementation of the extended trapezoidal rule with 2^{16} nodes on the interval $[-40, 40]$. The initial population distributions were $K \cdot \exp(-x^2)$ for the solid circles, $K \cdot (\sin(x) + 1)$ for the open circles, and $K \cdot \exp[-(x+1)^2] + K \cdot \exp[-(x-2)^2]$ for the squares, where $K = 1000$ is the carrying capacity in the recruitment function (4.4). The net reproductive rate $R_0 = 2$ in (4.4), and the dispersal kernel was the Gaussian kernel (4.6) with diffusion rate $D = 0.2$. The habitat quality function was (4.1), with $\sigma^2 = 0.2$. The initial speed c_1 was 0.01, and the acceleration c_2 was 10^{-3}. For all three initial population distributions over space, the acceleration of the niche deficits approach the same amount.

4.4.3 Acceleration causes more niche deficit

As illustrated in Figure (4.1), I compare a family of climate-warming scenarios, where the niche curves shift the same distance S over the same number of time steps T, but with different accelerations. The other model parameters, niche curves, dispersal kernels, and initial population distributions were the same within each comparison. Since acceleration is the only difference between these scenarios, this comparison illustrates the impact of acceleration c_2 on the population over a finite period of time.

Niche deficits were compared between these warming scenarios. The analytic example again provides important insight on the comparison. Under the accelerated-warming scenario (4.3), the niche deficit of the T-th generation is

$$\delta_{\text{accelerated}}(T) = \left(\frac{\sigma^2+v^*}{v^*}\right)\left[c_2T + c_1 + \frac{c_2}{2} - \frac{(\sigma^2+v^*)c_2}{v^*}\right] - \left(\frac{\sigma^2}{\sigma^2+v^*}\right)^T(\bar{\mu}_0+\beta), \quad (4.24)$$

where β is given in equation (4.91) in Appendix (4.7.3). In comparison, the niche deficit of the T-th generation under the constant-speed warming scenario (4.2) is

$$\delta_{\text{constant}}(T) = \left(\frac{\sigma^2+v^*}{v^*}\right)\left(c_1 + \frac{c_2T}{2}\right) - \left(\frac{\sigma^2}{\sigma^2+v^*}\right)^T(\bar{\mu}_0+\beta). \quad (4.25)$$

The difference between these two results can be calculated as

$$\delta_{\text{accelerated}}(T) - \delta_{\text{constant}}(T) = c_2\left(\frac{\sigma^2+v^*}{v^*}\right)\left(\frac{T}{2} - \frac{\sigma^2}{v^*} - \frac{1}{2}\right). \quad (4.26)$$

If T is large enough so that

$$T > \frac{2\sigma^2}{v^*} + 1, \quad (4.27)$$

then

$$\delta_{\text{accelerated}}(T) > \delta_{\text{constant}}(T). \quad (4.28)$$

That is, as long as the comparisons are made over a large-enough number of time steps, niche deficits accumulated over an accelerated warming will be larger than that accumulated in a constant-speed warming with the same average speed.

4.5 Discussion and conclusion

Many different mechanisms may induce changes in the spatial distribution of a species. Exotic species introduced into new habitats may, as demonstrated by Kot et al. [70], quickly

spread in space and generate "waves" of invasion. This phenomenon has been broadly studied for more than a decade. Recently, another mechanism has caught the attention of ecologists. Climate warming, as a global change, has evidently [20, 119] caused range shifts in species across the globe. While invasion waves of non-native species are largely driven by the spontaneous reproduction and dispersal of these species, climate-driven range shifts is more of a "forced" shift. Besides the intrinsic traits of the affected species such as reproductive rates and dispersal patterns, the speed of climate warming also plays a crucial role in range shifts. As shown in Figure (4.3), when the niche curve is prescribed to shift at a constant speed c, the population, if persistent, eventually shifts at speed c regardless of its initial distributions. In fact, mathematical analysis in Appendix C implies that a persistent population will shift at speed c regardless of the growth or recruitment function f, and the dispersal kernel $k(x, y)$. When accelerated warming is prescribed, the population eventually shifts with the prescribed acceleration c_2 (see Figure 4.5). Of course, the models bear the simplifying assumption that the niche curve only shifts and does not change in its shape. For example, contractions of the southern boundaries of a northern-hemisphere species are assumed to accompany expansions of its northern boundaries. Range *expansions*, instead of range *shifts*, therefore, invoke different models and future extensions of the presented work.

The forced nature of climate-induced range shifts implies that species may not track climate warming. In this chapter, I articulated two types of "failure to track". One obvious failure occurs, as explained in Appendix C, when the species goes extinct, for example, when the speed c of the shifting niche curve is too rapid (Appendix D). Another "failure to track" occurs when the species lags behind its niche curve, and thus carry a *niche deficit*. A niche deficit can undermine a population's chance to persist. A simple example (Appendix D) clearly points out that larger niche deficits reduce population growth (see equation 4.83) in this example. An intuitive explanation is that, when the population carries a niche deficit, it has less individuals at the fertile, more suitable locations, and therefore under-utilizes the suitable habitats.

Niche deficits depend heavily on the speed of climate warming. Under constant-speed warming, the niche deficit converges to a constant (Figure 4.6). That is, while the population shifts at the same speed of the niche curve, the population center eventually lags behind

for a constant distance. This constant niche deficit increases with the shift speed c (Figure 4.7 and formula 4.80). Under accelerated climate warming, the niche deficit increases over time, and eventually accelerates with the same acceleration, c_2, of the niche curve (Figure 4.9). The ever-increasing niche deficit under accelerated warming causes eventual extinction in the simple example considered in Appendix D.

Acceleration in climate warming also imposes an unexpected burden on the population. In a comparison between climate warming scenarios with the same amount of warming over the same period of time, a positive acceleration produces a larger niche deficit at the end of the time period (equation 4.28), provided that the time period is not too short (equation 4.27), in the analytic example (Appendix D). That is, if we attempt to project niche deficits under a climate warming scenario, we need to consider the acceleration of climate warming, since simply taking the average of the warming speeds may underestimate the niche deficits. With projected increase in warming speed [58], this result is especially concerning.

I would like to point out that models in this chapter are still very simple models. I had intended to tear apart and set aside other mechanisms in range shifts, such as evolution, with the hope that the simple models will provide a useful foundation for more complex models. With evolutionary adaptations under climate warming, the population may benefit from an evolutionary rescue [8], and admit other interesting dynamics. Also, the analytic example in Appendix D can be easily extended to consider range shifts on a two-dimensional spatial domain, range expansions, periodic range expansions and contractions, stochastic speeds of climate warming, and other interesting scenarios.

4.6 Appendix C: Global bifurcation results for a nonlinear operator

The model (4.7) can be written in the form

$$n_{t+1}(x) = F_t\left[n_t(x)\right], \tag{4.29}$$

where F_t is the nonlinear integral operator

$$F_t: \qquad n(x) \;\; \rightarrow \;\; \int_{-\infty}^{\infty} k(x-y)\, Q(y-s(t))\, f\left[n(y)\right]\, dy, \tag{4.30}$$

that maps $\mathcal{L}_1(\mathbb{R})$ to $\mathcal{L}_1(\mathbb{R})$. Although the dynamical system (4.29) is disguised as a non-autonomous system, one can unveil its autonomous nature by setting up a moving axis. To

show this, let us define a new function $\bar{n}_t(x)$, so that

$$\bar{n}_t(x) = n_t(x + s(t)). \tag{4.31}$$

The function $\bar{n}_t(x)$ portrays the population dynamics relative to a moving observation frame. If a camera that starts at the origin and moves at the same speed c captures pictures of the population density, the photos will show the curve resulting from plotting $y = \bar{n}_t(x)$ in an xy coordinate system. Replacing $n_t(x)$ with

$$n_t(x) = \bar{n}_t(x - s(t)) \tag{4.32}$$

in equation (4.7), one obtains

$$\bar{n}_{t+1}(x - s(t+1)) = \int_{-\infty}^{\infty} k(x-y)Q(y - s(t))f\left[\bar{n}_t(y - s(t))\right]\, dy. \tag{4.33}$$

Using a simple substitution of variable $\bar{y} = y - s(t)$, equation (4.33) becomes

$$\bar{n}_{t+1}(x - s(t+1)) = \int_{-\infty}^{\infty} k(x - s(t) - \bar{y})Q(\bar{y})f\left[\bar{n}_t(\bar{y})\right]\, d\bar{y}. \tag{4.34}$$

Since $\bar{y}$ is the integration variable in equation (4.34), its notation does not matter, and the bar can be dropped without causing any confusion. Then, comparing the x arguments on both sides, it is clear that

$$\bar{n}_{t+1}(x) = \int_{-\infty}^{\infty} k(x + s(t+1) - s(t) - y)Q(y)f\left[\bar{n}_t(y)\right]\, dy. \tag{4.35}$$

For the constant-speed warming scenario, $s(t) = ct$, and $s(t+1) - s(t) = c$. Hence

$$\bar{n}_{t+1}(x) = \int_{-\infty}^{\infty} k(x + c - y)Q(y)f\left[\bar{n}_t(y)\right]\, dy. \tag{4.36}$$

Thus, under constant-speed warming, the population dynamics $\bar{n}_t(x)$ relative to a moving coordinate system is governed by the autonomous system

$$\bar{n}_{t+1}(x) = F\left[\bar{n}_t(x)\right], \tag{4.37}$$

where $F : \mathcal{L}_1(\mathbb{R}) \to \mathcal{L}_1(\mathbb{R})$ is the nonlinear integral operator defined by the right hand side of equation (4.36).

For habitat suitability functions $Q(x)$ that are compactly-supported, the integral operator F is compact. Its corresponding linear operator

$$K: \qquad u(x) \to f'(0) \int_{-\infty}^{\infty} k(x+c-y)Q(y)u(y)\,dy \tag{4.38}$$

is also compact. The spectrum of K therefore consists of its eigenvalues and the number 0 [57]. Eigenvalues of K form a discrete set that may be empty, finite, or countably infinite [57, 65]. Since the support of $Q(x)$ is continuous and finite, Jentzsch's (1912) theorem [61] (also see [53, 75]) may be invoked. Jentzsch's theorem extends the Perron−Probenius theorem for positive matrices to integral equations with positive kernels. The theorem concludes that K has a simple and positive dominant eigenvalue with a positive eigenfunction. Global bifurcation theorems by Rabinowitz [126] (also see [30] for a nice summary) can then be applied to conclude that, when the dominant eigenvalue $\lambda_{\max}$ of the linear operator K is larger than 1, equation

$$\bar{n}^*(x) = F\left[\bar{n}^*(x)\right] \tag{4.39}$$

has a positive solution $\bar{n}^*(x)$. When the dominant eigenvalue $\lambda_{\max}$ of operator K is less than 1, equation (4.39) only has a zero solution.

Since operator K has a positive dominant eigenvalue, and its spectrum only consists of eigenvalues and the number 0, $r(K) = \lambda_{\max}$. Since

$$r(K) = \lim_{t\to\infty} ||K^t||^{1/t}, \tag{4.40}$$

where $||K^t||$ is the norm of the operator K^t,

$$\lambda_{\max} = \lim_{t\to\infty} ||K^t||^{1/t} \tag{4.41}$$

for the compact linear operator K. Hardin's results [44] on asymptotic properties of integrodifference equations (also see conclusions from Vankirk and Lewis [151]) can therefore be applied to conclude that, if $\lambda_{\max} > 1$, the sequence $\{\bar{n}_t(x)\}$, with any arbitrary initial condition $\bar{n}_0(x)$, will converge to a unique positive fixed-point $\bar{n}^*(x)$ of system (4.37), which is a unique positive solution of equation (4.39). Therefore the population, with any nonzero, nonnegative initial density distribution, will approach a unique traveling solution $n_t(x) = \bar{n}^*(x - ct)$ that shifts at the prescribed speed c. In other words, the population

will be able to persist and shift its range steadily. The niche deficit will also converge to a constant calculated as

$$\begin{aligned}\frac{\int_{-\infty}^{\infty} x\bar{n}^*(x-ct)dx}{\int_{-\infty}^{\infty}\bar{n}^*(x-ct)dx} - ct &= \frac{\int_{-\infty}^{\infty}(x+ct)\bar{n}^*(x)dx}{\int_{-\infty}^{\infty}\bar{n}^*(x)dx} - ct \\ &= \frac{\int_{-\infty}^{\infty} x\bar{n}^*(x)dx}{\int_{-\infty}^{\infty}\bar{n}^*(x)dx} + \left(\frac{\int_{-\infty}^{\infty}\bar{n}^*(x)dx}{\int_{-\infty}^{\infty}\bar{n}^*(x)dx}\right)ct - ct \\ &= \frac{\int_{-\infty}^{\infty} x\bar{n}^*(x)dx}{\int_{-\infty}^{\infty}\bar{n}^*(x)dx}.\end{aligned} \tag{4.42}$$

If $\lambda_{\max} < 1$, the sequence $\{\bar{n}_t(x)\}$ will converge to the trivial solution $\bar{n}^*(x) \equiv 0$ of equation (4.39) with any arbitrary initial condition $\bar{n}_0(x)$, and the population collapses and goes extinct eventually.

If the support of $Q(x)$ is non-compact, K and F may not be compact. I therefore only consider one special example of non-compactly-supported $Q(x)$ (4.1) for the linear equation (4.9), where other approaches are available without invoking the global bifurcation theorem (see section 4.7).

4.7 Appendix D: An analytic example

For a special example, analytic results are available. In this example, the niche curve is the Gaussian curve,

$$Q(x) = \exp\left(-\frac{x^2}{\sigma^2}\right), \tag{4.43}$$

and the dispersal kernel in this special example is the Gaussian kernel

$$k(x-y) = \frac{1}{2\sqrt{\pi D}}\exp\left[-\frac{(x-y)^2}{4D}\right], \tag{4.44}$$

where the "diffusion rate" D is half of the variance of this normal distribution. It is worth mentioning that, for habitat suitability functions $Q(x)$ and dispersal kernels $k(x)$ that satisfy

$$\begin{aligned}&\int_{-\infty}^{\infty} k(x+c-y)Q(y)\,dy < \infty, \\ &\int_{-\infty}^{\infty} |k(x+c-y)Q(y)|\,dy \to \infty \text{ as } x \to \infty, \text{ and} \\ &\int_{-\infty}^{\infty} |k(x+c-y)Q(y) - k(x'+c-y)Q(y)|\,dy \to 0, \text{ as } x' \to x,\end{aligned} \tag{4.45}$$

the linear operator K is compact [3, 19], even though $Q(x)$ is not compactly-supported. Thus the linear operator K is compact for habitat suitability function (4.43) and dispersal kernel (4.44. The spectral radius of K is equal to its dominant eigenvalue $\lambda_{\max}$, which is a positive real number.

4.7.1 Eigenfunction when warming speed is constant

When $s(t) = ct$, an eigenfunction of the linear integral operator (4.13) for this special example is found to be

$$u(x) = a \cdot \exp\left[-\frac{\left(x + c + \dfrac{\sigma^2 c}{v^*}\right)^2}{v^*}\right], \tag{4.46}$$

where

$$v^* = 2D(1 + \sqrt{1 + \sigma^2/D}), \tag{4.47}$$

and a is an arbitrary nonzero number. Eigenfunction (4.46) can be found by guessing a Gaussian ansatz

$$u(x) = a \cdot \exp\left[-\frac{(x-\mu)^2}{v}\right], \tag{4.48}$$

with undetermined coefficients a, μ, and v. For ansatz (4.48) to be an eigenfunction, it must satisfy the equation

$$\lambda u(x) = f'(0) \int_{-\infty}^{\infty} \frac{1}{2\sqrt{\pi D}} \exp\left[-\frac{(x+c-y)^2}{4D}\right] \cdot \exp\left(-\frac{y^2}{\sigma^2}\right) u(y)\, dy. \tag{4.49}$$

Substituting the ansatz (4.48) into equation (4.49), and calculating the right hand side integral, I obtain

$$\lambda a \cdot \exp\left[-\frac{(x-\mu)^2}{v}\right] = \frac{a \cdot \sqrt{\dfrac{\sigma^2 v}{\sigma^2 + v}}}{\sqrt{4D + \dfrac{\sigma^2 v}{\sigma^2 + v}}} \cdot \exp\left[-\frac{\mu^2}{\sigma^2 + v} - \frac{\left(x + c - \dfrac{\sigma^2 \mu}{\sigma^2 + v}\right)^2}{4D + \dfrac{\sigma^2 v}{\sigma^2 + v}}\right]. \tag{4.50}$$

For equation (4.50) to hold for all x, we must have

$$v = 4D + \frac{\sigma^2 v}{\sigma^2 + v}, \tag{4.51}$$

$$\mu = \frac{\sigma^2 \mu}{\sigma^2 + v} - c, \tag{4.52}$$

and

$$\lambda = \frac{a\sqrt{\frac{\sigma^2 v}{\sigma^2 + v}}}{\sqrt{4D + \frac{\sigma^2 v}{\sigma^2 + v}}} \cdot \exp\left[-\frac{\mu^2}{\sigma^2 + v}\right]. \tag{4.53}$$

Solving eqn. (4.51) for v yields solution (4.47), and solving eqn. (4.52) for μ yields

$$\mu = -c - \frac{\sigma^2 c}{v^*}. \tag{4.54}$$

Substituting solutions (4.47) and (4.54) into eqn. (4.53) simplifies eqn. (4.53) to

$$\lambda = \sqrt{\frac{\sigma^2 v^*}{\sigma^2 + v^*}} \cdot \exp\left[-\frac{c^2(\sigma^2 + v^*)}{v^{*2}}\right]. \tag{4.55}$$

This eigenvalue λ decreases as speed c increases. When $c = c^*$, where

$$c^* = \sqrt{\frac{v^{*2}}{\sigma^2 + v^*} \ln\left[f'(0) \cdot \sqrt{\frac{\sigma^2}{\sigma^2 + v^*}}\right]}, \tag{4.56}$$

the eigenvalue $\lambda = 1$. If λ is the dominant eigenvalue $\lambda_{\max}$ of operator (4.13), then c^* is the critical speed above which the population cannot persist. Numerical computation of c^* with the Nyström's method, which matches very well with the analytic result (4.56), indicates that this is indeed the case (see Figure 4.10).

4.7.2 Dynamical system approach for constant-speed warming

When $s(t) = ct$, if the linear equation (4.9) is iterated with a Gaussian-shaped initial condition

$$n_0(x) = a_0 \exp\left(-\frac{x^2}{\sigma_0^2}\right), \tag{4.57}$$

every n_t will be in the shape of a Gaussian pulse

$$n_t(x) = a_t \exp\left[-\frac{(x - \mu_t)^2}{v_t}\right], \tag{4.58}$$

where v_t, μ_t, and a_t describe the variance, mean, and amplitude of the Gaussian pulse.

Substituting the ansatz (4.58) into the linear equation (4.9), we can see that $n_{t+1}(x)$ keeps the Gaussian shape

$$n_{t+1}(x) = a_{t+1} \exp\left[-\frac{(x-\mu_{t+1})^2}{v_{t+1}}\right], \tag{4.59}$$

where its shape parameters are

$$\begin{cases} v_{t+1} &= 4D + \dfrac{\sigma^2 \cdot v_t}{\sigma^2 + v_t}, \\ \mu_{t+1} &= \dfrac{\sigma^2 \mu_t + v_t \cdot ct}{\sigma^2 + v_t}, \\ a_{t+1} &= \dfrac{a_t \cdot f'(0)\sqrt{\sigma^2 v_t}}{\sqrt{4\sigma^2 D + (\sigma^2 + 4D)v_t}} \exp\left[-\dfrac{(\mu_t - ct)^2}{\sigma^2 + v_t}\right]. \end{cases} \tag{4.60}$$

Growth or decay of the perturbation n_t can thus be studied through the discrete-time dynamical system (4.60).

Linear system (4.60) is very nice in that its first equation is decoupled from the other two equations, and the first two equations are decoupled from the third equation. The first equation,

$$v_{t+1} = 4D + \frac{\sigma^2 \cdot v_t}{\sigma^2 + v_t} = \phi(v_t), \tag{4.61}$$

has a positive and asymptotically stable equilibrium

$$v^* = 2D[1 + \sqrt{1 + \sigma^2/D}] \tag{4.62}$$

because

$$\phi'(v) = \frac{\sigma^2}{\sigma^2 + v} - \frac{\sigma^2 v}{(\sigma^2 + v)^2}, \tag{4.63}$$

and

$$0 < \phi'(v^*) = \frac{\sigma^4}{\left[\sigma^2 + 2D + 2\sqrt{D(D+\sigma^2)}\right]^2} < 1. \tag{4.64}$$

The other equilibrium of equation (4.61),

$$v_-^* = 2D[1 - \sqrt{1 + \sigma^2/D}], \tag{4.65}$$

is negative and unstable. Therefore, regardless of the initial pulse variance v_0, the variance of the Gaussian pulses n_t for each t converges swiftly to v^*.

In fact, equation (4.61) can be exactly solved by substituting v_t with $w_t + v^*$, followed by the substitution $u_t = 1/w_t$, so that

$$w_{t+1} = \frac{(4D + \sigma^2 - v^*)w_t}{(\sigma^2 + v^*) + w_t}, \tag{4.66}$$

and

$$u_{t+1} = \left(\frac{\sigma^2 + v^*}{4D + \sigma^2 - v^*}\right) u_t + \frac{1}{4D + \sigma^2 - v^*}. \tag{4.67}$$

From eqn. (4.67), we can see that

$$u_{t+1} + \frac{1}{2v^* - 4D} = \left(\frac{\sigma^2 + v^*}{4D + \sigma^2 - v^*}\right)\left(u_t + \frac{1}{2v^* - 4D}\right). \tag{4.68}$$

Therefore

$$u_t = \left(\frac{\sigma^2 + v^*}{4D + \sigma^2 - v^*}\right)^t \left(u_0 + \frac{1}{2v^* - 4D}\right) - \frac{1}{2v^* - 4D}. \tag{4.69}$$

Transforming the variables back reveals the solution

$$v_t = v^* + \left[\left(\frac{\sigma^2 + v^*}{4D + \sigma^2 - v^*}\right)^t \left(\frac{1}{v_0 - v^*} + \frac{1}{2v^* - 4D}\right) - \frac{1}{2v^* - 4D}\right]^{-1}. \tag{4.70}$$

The second equation in system (4.60),

$$\mu_{t+1} = \frac{\sigma^2\mu_t + v_t \cdot ct}{\sigma^2 + v_t} = \left(\frac{\sigma^2}{\sigma^2 + v_t}\right)\mu_t + \left(\frac{v_t}{\sigma^2 + v_t}\right) ct, \tag{4.71}$$

makes it clear that μ_{t+1} is a weighted average between μ_t and the niche optimum ct. After v_t converges to v^*, eqn. (4.71) becomes the linear difference equation

$$\mu_{t+1} = \left(\frac{\sigma^2}{\sigma^2 + v^*}\right)\mu_t + \left(\frac{v^*}{\sigma^2 + v^*}\right) ct, \tag{4.72}$$

or equivalently,

$$\mu_{t+1} = \left(\frac{\sigma^2}{\sigma^2 + v^*}\right)(\mu_t - ct) + ct. \tag{4.73}$$

Equation (4.72) can be analytically solved. To see this, notice that equation (4.72) can be rewritten as

$$\delta_{t+1} - c\left(\frac{\sigma^2 + v^*}{v^*}\right) = \left(\frac{\sigma^2}{\sigma^2 + v^*}\right)\left[\delta_t - c\left(\frac{\sigma^2 + v^*}{v^*}\right)\right], \tag{4.74}$$

where δ_t is the niche deficit

$$\delta_t = ct - \mu_t. \tag{4.75}$$

Therefore

$$\delta_t = \left(\frac{\sigma^2}{\sigma^2+v^*}\right)^t \cdot \left(\delta_0 - c\cdot\frac{\sigma^2+v^*}{v^*}\right) + c\cdot\left(\frac{\sigma^2+v^*}{v^*}\right). \tag{4.76}$$

Since $\sigma^2 > 0$ and $v^* > 0$, the fraction

$$0 < \left(\frac{\sigma^2}{\sigma^2+v^*}\right) < 1. \tag{4.77}$$

As a result, if $\delta_0 < c(\sigma^2+v^*)/v^*$, then δ_t is monotonically increasing. If $\delta_0 > c(\sigma^2+v^*)/v^*$, δ_t is monotonically decreasing. As $t\to\infty$,

$$\delta_t \to c\cdot\left(\frac{\sigma^2+v^*}{v^*}\right), \tag{4.78}$$

and

$$\begin{aligned}\mu_t &= ct - \left(\frac{\sigma^2}{\sigma^2+v^*}\right)^t \cdot \left(\delta_0 - c\cdot\frac{\sigma^2+v^*}{v^*}\right) - c\cdot\left(\frac{\sigma^2+v^*}{v^*}\right)\\ &\to ct - c\cdot\left(\frac{\sigma^2+v^*}{v^*}\right).\end{aligned} \tag{4.79}$$

The asymptotic behavior (4.79) of μ_t implies that the Gaussian pulse (4.58) eventually travels at the same speed c of climate warming, but the center of the pulse is behind the niche optimum ct for a distance of

$$\delta_\infty = c\cdot\left(\frac{\sigma^2+v^*}{v^*}\right). \tag{4.80}$$

The niche deficit δ_∞ quantifies the mismatch between the population distribution and the niche curve when t is infinite. Since $c > 0$, $\sigma^2 > 0$, and $v^* > 0$, it is obvious that $\delta_\infty > 0$, and that the center of the Gaussian pulse (4.58) lags behind the niche optimum ct after a long time has elapsed.

Similarly, δ_t quantifies this mismatch for each t. Such a mismatch, as we shall see in the analysis of the third equation in system (4.60), undermines the population's recruitment. The larger δ_t is, the less the population recruits in the t-th generation. As I have analyzed, $\bar{\mu}_t$ monotonically increases if the population distribution was not too much ahead of the niche curve at the beginning. Thus the population keeps lagging behind more as climate change progresses, and the niche deficit accumulates.

The damage of a niche deficit is clear once we examine the third equation in system (4.60),

$$a_{t+1} = a_t \cdot \frac{f'(0)\sqrt{\sigma^2 v_t}}{\sqrt{4\sigma^2 D + (\sigma^2+4D)v_t}} \exp\left[-\frac{(\mu_t - ct)^2}{\sigma^2+v_t}\right]. \tag{4.81}$$

For large t, v_t converges to v^*, and equation (4.81) becomes

$$a_{t+1} = a_t \cdot \frac{f'(0)\sqrt{\sigma^2 v^*}}{\sqrt{4\sigma^2 D + (\sigma^2 + 4D)v^*}} \exp\left[-\frac{(\mu_t - ct)^2}{\sigma^2 + v^*}\right]. \tag{4.82}$$

Equation (4.82) is an affine equation about a_t with a positive coefficient. Thus the amplitude a_t of the Gaussian pulse either increases or decreases, depending on whether the coefficient

$$\Psi_t = \frac{f'(0)\sqrt{\sigma^2 v^*}}{\sqrt{4\sigma^2 D + (\sigma^2 + 4D)v^*}} \exp\left[-\frac{(\mu_t - ct)^2}{\sigma^2 + v^*}\right]. \tag{4.83}$$

is larger than or smaller than 1. Notice that Ψ_t depends square exponentially on the niche deficit $\delta_t = ct - \mu_t$. Thus a larger niche deficit δ_t reduces population growth in the t-th generation.

Since the niche deficit $\bar{\mu}_t$ converges to $\bar{\mu}^*$ as $t \to \infty$, equation (4.82) becomes the homogeneous linear difference equation

$$a_{t+1} = a_t \cdot \frac{f'(0)\sqrt{\sigma^2 v^*}}{\sqrt{4\sigma^2 D + (\sigma^2 + 4D)v^*}} \exp\left[-\frac{\delta_\infty^2}{\sigma^2 + v^*}\right]. \tag{4.84}$$

Thus the persistence of a small Gaussian perturbation depends on the coefficient

$$\Psi = \frac{f'(0)\sqrt{\sigma^2 v^*}}{\sqrt{4\sigma^2 D + (\sigma^2 + 4D)v^*}} \exp\left[-\frac{\delta_\infty^2}{\sigma^2 + v^*}\right]. \tag{4.85}$$

If $\Psi > 1$, the Gaussian perturbation grows; if $\Psi < 1$, the Gaussian perturbation declines and $a_t \to 0$ as $t \to \infty$. The threshold situation occurs when $\Psi = 1$.

Given parameters σ^2, D, and $f'(0)$, the coefficient Ψ depends negatively on the shift speed c. The coefficient Ψ drops below 1 as c rises through the threshold, or critical speed c^*, where

$$c^* = \sqrt{\frac{v^* 2}{\sigma^2 + v^*} \ln\left(f'(0)\sqrt{\frac{\sigma^2}{\sigma^2 + v^*}}\right)}. \tag{4.86}$$

The critical speed formula (4.86) is obtained by substituting the climate deficit expression (4.80) into equation (4.85), and solving for c in the equation $\Psi = 1$. The solid curve in Figure 4.10 illustrates how the critical speed c^* increases as the net reproductive rate $R_0 = f'(0)$ increases according the analytic formula (4.86).

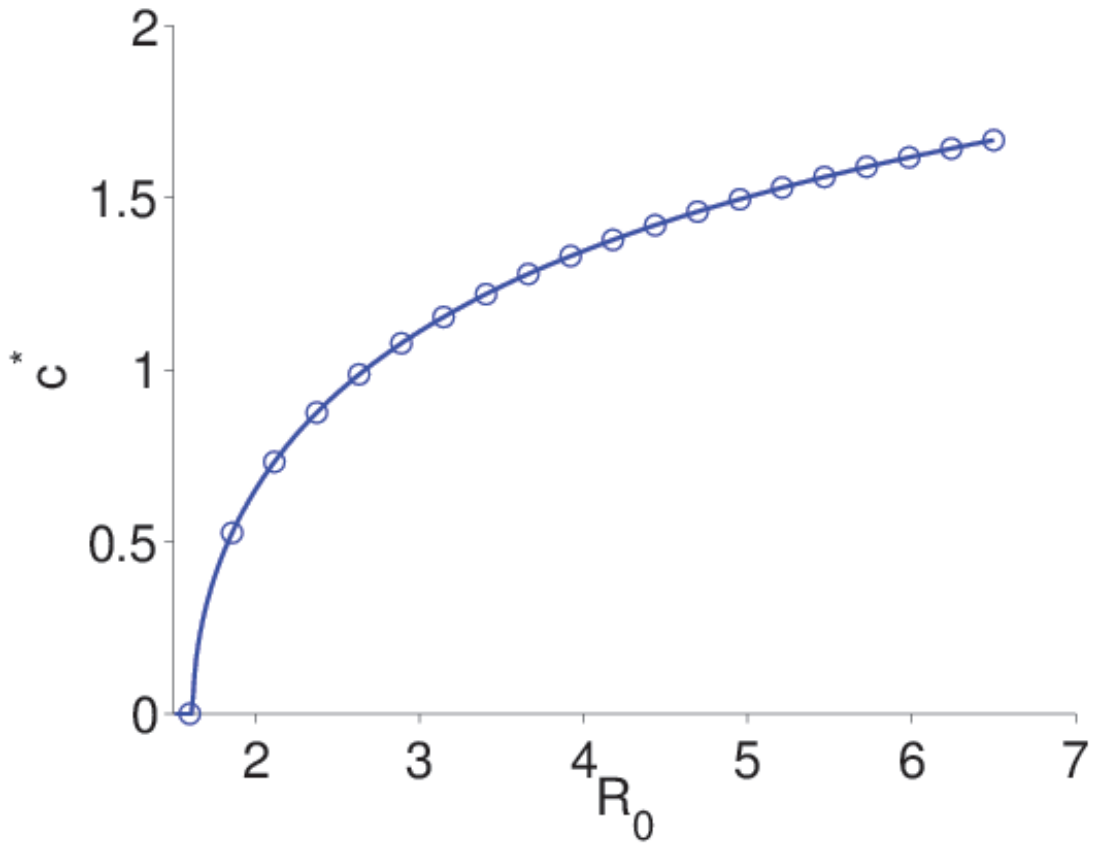

Figure 4.10: The critical speed c^*, plotted as a function of the net reproductive rate R_0, for the analytic example with habitat suitability function (4.43) and dispersal kernel (4.44). The niche variance $\sigma^2 = 2$, and the diffusion rate in dispersal kernel (4.44) was $D = 0.5$. The solid curve was obtained by employing the Nyström's method to compute the dominant eigenvalue of the linear operator (4.38), and then using the bisection method with tolerance 10^{-8} to determine the critical speed c^* that made the dominant eigenvalue equal to 1. Points marked by empty circles were obtained by the analytic formula (4.86).

4.7.3 Dynamical system approach for accelerated warming

For general $s(t)$, dynamical system (4.60) becomes

$$\begin{cases} v_{t+1} &= 4D + \dfrac{\sigma^2 \cdot v_t}{\sigma^2 + v_t}, \\ \mu_{t+1} &= \dfrac{\sigma^2 \mu_t + v_t \cdot s(t)}{\sigma^2 + v_t}, \\ a_{t+1} &= \dfrac{a_t \cdot f'(0)\sqrt{\sigma^2 v_t}}{\sqrt{4\sigma^2 D + (\sigma^2 + 4D)v_t}} \exp\left\{-\dfrac{[\mu_t - s(t)]^2}{\sigma^2 + v_t}\right\}. \end{cases} \tag{4.87}$$

Notice that the speed or acceleration of shift does not affect the first equation. That is, the width of the resulting pulse still converges to v^*, as given in equation (4.62).

After v_t converges to v^*, the second equation in system (4.87) becomes the linear equation

$$\mu_{t+1} = \left(\frac{\sigma^2}{\sigma^2 + v^*}\right)\mu_t + \left(\frac{v^*}{\sigma^2 + v^*}\right) \cdot s(t). \tag{4.88}$$

For the accelerated-warming scenario, $s(t) = c_1 t + c_2/2t^2$, and the solution of equation (4.88) can be obtained as

$$\mu_t = s(t) + \left(\frac{\sigma^2}{\sigma^2 + v^*}\right)^t (\mu_0 + \beta) - \alpha t - \beta, \tag{4.89}$$

where

$$\alpha = 2\left(\frac{\sigma^2 + v^*}{v^*}\right) c_2, \tag{4.90}$$

and

$$\beta = \left(\frac{\sigma^2 + v^*}{v^*}\right) c_1 + \left[1 - \frac{2(\sigma^2 + v^*)}{v^*}\right]\left(\frac{\sigma^2 + v^*}{v^*}\right) c_2. \tag{4.91}$$

The niche deficit

$$\delta_t = s(t) - \mu_t, \tag{4.92}$$

and we can see that, as $t \to \infty$,

$$\delta_t \to \alpha t + \beta. \tag{4.93}$$

Since α and β are constants, we can see that the resulting Gaussian pulse (4.58) asymptotically travels at the same acceleration c_2, but its speed lags behind that of the niche curve by α. Therefore, the niche deficit in this example keeps growing larger and approaches ∞ as $t \to \infty$.

The third equation from system (4.87), as $t \to \infty$, becomes

$$a_{t+1} = \frac{a_t \cdot f'(0)\sqrt{\sigma^2 v^*}}{\sqrt{4\sigma^2 D + (\sigma^2 + 4D)v^*}} \exp\left\{-\frac{[\mu_t - s(t)]^2}{\sigma^2 + v^*}\right\}, \tag{4.94}$$

and it can be seen that the niche deficit in this example still negatively affects the recruitment rate in each generation in a square exponential manner. Therefore, as $t \to \infty$, the small perturbation $n_0(x) \to 0$ regardless of any parameter choice. This is not surprising, because the stress on the population created by an accelerated warming keeps progressing.

Since the population is doomed if $t \to \infty$, we naturally ask, how big is the damage of an accelerated warming climate over a finite period of time? I will answer this question by comparing scenarios of warming with the same average speed but different accelerations. Figure (4.1) illustrates the different scenarios of warming I consider. The horizontal line represents the scenario with a constant speed of shift (acceleration = 0), and the slanted lines represent scenarios with different constant accelerations of the shift speed, with thicker lines having higher accelerations. All these lines pass the point $(T/2, \bar{c})$. That is the speed of shift reaches the same speed $\bar{c}$. Therefore the average speed between time 0 and time T for all scenarios of shift speed are the same, which is

$$\bar{c} = c_1 + c_2 T/2. \tag{4.95}$$

Let us assume the same initial condition for all scenarios. As I have shown in this analytic example, with constant acceleration, the niche deficit at time T for large T is

$$\begin{aligned} \delta_{\text{accelerated}}(T) &= \alpha T + \beta - \left(\frac{a}{a+g^*}\right)^T (\delta_0 + \beta) \\ &= \left(\frac{\sigma^2 + v^*}{v^*}\right)\left(c_2 T + c_1 + \frac{c_2}{2} - \frac{(\sigma^2 + v^*)c_2}{v^*}\right) - \left(\frac{\sigma^2}{\sigma^2 + v^*}\right)^T (\bar{\mu}_0 + \beta), \end{aligned} \tag{4.96}$$

where β is given in eqn. (4.91). For the constant-speed scenario, the niche deficit is

$$\begin{aligned} \delta_{\text{constant}}(T) &= \frac{a+g^*}{g^*}\bar{c} - \left(\frac{a}{a+g^*}\right)^T \left(\frac{a+g^*}{g^*}\right)\bar{c} \\ &= \left(\frac{\sigma^2 + v^*}{v^*}\right)\left(c_1 + \frac{c_2 T}{2}\right) - \left(\frac{\sigma^2}{\sigma^2 + v^*}\right)^T (\delta_0 + \beta). \end{aligned} \tag{4.97}$$

The difference between these two results can be calculated as

$$\delta_{\text{accelerated}}(T) - \delta_{\text{constant}}(T) = c_2 \left(\frac{\sigma^2 + v^*}{v^*} \right) \left(\frac{T}{2} - \frac{\sigma^2}{v^*} - \frac{1}{2} \right). \tag{4.98}$$

If T is large enough so that

$$T > \frac{2\sigma^2}{v^*} + 1, \tag{4.99}$$

then

$$\delta_{\text{accelerated}}(T) > \delta_{\text{constant}}(T). \tag{4.100}$$

That is, as long as the comparisons are made over a large-enough number of time steps, niche deficits accumulated over an accelerated warming will be larger than that accumulated in a constant-speed warming with the same average speed.

4.8 Appendix E: Nyström's method

For more general examples of habitat quality function and dispersal kernels, analytical formulae of the critical speed c^* may not be available, but we may resort to numerical approaches, such as the Nyström scheme to compute the dominant eigenvalue of the compact operator K defined in equation (4.13),

$$K[\eta(x)] = \int_{-\infty}^{\infty} k(x + c - y) Q(y) \eta(y)\, dy. \tag{4.101}$$

Nyström's method approximates the integral in eqn. (4.101) with a numerical quadrature, and thereby approximates the eigenvalues of the integral operator K with eigenvalues of a matrix system. For example, if we choose the repeated trapezoidal rule to approximate the integral with

$$K[\,\eta(x_i)] \approx f'(0)\, \frac{\Delta \bar{x}}{2} \sum_{j=1}^{N-1} [\, k(x_i + c - y_j)\, Q(y)\, \eta(y_j) + k(x_i + c - y_{j+1})\, Q(y)\, \eta(y_{j+1})\,], \tag{4.102}$$

then we can reduce the eigenvalue problem to that of the matrix system

$$\lambda\, c_i = f'(0) \sum_{j=1}^{N} A_{ij}\, c_j \tag{4.103}$$

with matrix elements

$$A_{i1} = \frac{\Delta x}{2}\, k(x_i + c - y_1)Q(y_1), \tag{4.104}$$

$$A_{ij} = \Delta\bar{x}\, k(\bar{x}_i + c - \bar{y}_j)Q(y_j),\ 2 \le j \le N-1, \tag{4.105}$$

$$A_{iN} = \frac{\Delta\bar{x}}{2}\, k(\bar{x}_i + c - \bar{y}_N)Q(y_N), \tag{4.106}$$

and

$$c_i = \eta(x_i), \qquad i = 1, \ldots, N. \tag{4.107}$$

The circled points in Figure 4.10 illustrates numerical results of the critical speeds c^* for different net reproductive rates R_0 obtained by the Nyström's scheme. These numerical results match with the analytical results (solid line in Figure 4.10) very well.

BIBLIOGRAPHY

[1] W. C. Allee. *The Social Life of Animals*. Norton, New York, 1938.

[2] E. Anderson, Z. Bai, C. Bischof, S. Blackford, J. Demmel, J. Dongarra, J. Du Croz, A. Greenbaum, S. Hammarling, A. McKenney, and D. Sorensen. *LAPACK User's Guide*. Society for Industrial and Applied Mathematics, Philadelphia, 1999.

[3] P. M. Anselone and I. H. Sloan. Integral equations on the half line. *Journal of Integral Equations*, 9:3–23, 1985.

[4] R. D. Badinelli. Approximating probability density functions and their convolutions using orthogonal polynomials. *European Journal of Operational Research*, 95:211–230, 1996.

[5] M. Bakkenes, J.R.M. Alkemade, F. Ihle, R. Leemans, and J.B. Latour. Assessing effects of forecasted climate change on the diversity and distribution of European higher plants for 2050. *Global Change Biology*, 8:390–407, 2002.

[6] N. Balakrishnan and C.-D. Lai. *Continuous Bivariate Distributions*. Springer, Dordrechet, Netherlands, 2009.

[7] E. F. Bedford, R. J. Whittaker, and J.T. Kerr. Systemic range shift lags among a pollinator species assemblage following rapid climate change. *Botany*, 90(7):587–597, 2012.

[8] Graham Bell and Andrew Gonzalez. Evolutionary rescue can prevent extinction following environmental change. *Ecology Letters*, 12(9):942–948, 2009.

[9] H. Berestycki, O. Diekmann, C. J. Nagelkerke, and P. A. Zegeling. Can a species keep pace with a shifting climate? *Bulletin of Mathematical Biology*, 71:399–429, 2009.

[10] M. P. Berg, E. T. Kiers, G. Driessen, M. Van Der Heijden, B. W. Kooi, F. Kuenen, M. Liefting, H. A. Verhoef, and J. Ellers. Adapt or disperse: understanding species persistence in a changing world. *Global Change Biology*, 16:587–598, 2010.

[11] A. S. Best, K. Johst, Münkemüller, and J. M.J. Travis. Which species will succesfully track climate change? the influence of intraspecific competition and density dependent dispersal on range shifting dynamics. *Oikos*, 116:1531–1539, 2007.

[12] R. J. H. Beverton and S. J. Holt. *On the Dynamics of Exploited Fish Populations*. Her Majesty's Stationery Office, London, 1957.

[13] E. O. Box. *Macroclimate and Plant Forms: an Introduction to Predictive Modeling in Phytogeography*. Dr. W. Junk, The Hague, 1981.

[14] R. P. Brent. *Algorithms for Minimization Without Derivatives*. Prentice-Hall, Inc., Englewood Cliffs, 1973.

[15] J. K. M. Brown and M. S. Hovmoller. Aerial dispersal of pathogens on the global and continental scales and its impact on plant disease. *Science*, 297:537–541, 2002.

[16] L. B. Buckley. Linking traits to energetics and population dynamics to predict lizard ranges in changing environments. *The American Naturalist*, 171:E1–E19, 2008.

[17] M. B. Bush and H. Hooghiemstra. Tropical biotic responses to climate change. In T. E. Lovejoy and L. Hannah, editors, *Climate Change and Biodiversity*. Yale University Press, New Haven, 2005.

[18] R. S. Cantrell and C. Cosner. *Spatial Ecology via Reaction-Diffusion Equations*. J. Wiley, Chichester, 2003.

[19] S. N. Chandler-Wilde, B. Zhang, and C. R. Ross. On the solvability of second kind integral equations on the real line. *Journal of Mathematical Analysis and Applications*, 245(1):28–51, 2000.

[20] I-C. Chen, J. K. Hill, R. Ohlemüller, D. B. Roy, and C. D. Thomas. Rapid range shifts of species associated with high levels of climate warming. *Science*, 333:1024–1026, 2011.

[21] I-C. Chen, J-J. Shiu, B. Suzan, J. D. Holloway, V. K. Chey, H. S. Barlow, J. K. Hill, and C. D. Thomas. Elevation increases in moth assemblages over 42 years on a tropical mountain. *Proceedings of the National Academy of Sciences of the United States of America*, 106:1479–1483, 2009.

[22] I. Chuine. Why does phenology drive species distribution? *Philosophical Transaction of the Royal Society B*, 365:3149–3160, 2010.

[23] J. S. Clark. Why trees migrate so fast: confronting theory with dispersal biology and the paleorecord. *The American Naturalist*, 152:204–224, 1998.

[24] R. Cousens, C. Dytham, and R. Law. *Dispersal in Plants: A Population Perspective*. Oxford University Press, Oxford, UK, 2008.

[25] R. D. Cousens. When will plant morphology affect the shape of a seed dispersal "kernel"? *Journal of Theoretical Biology*, 211:229–238, 2001.

[26] M. J. R. Cowley, C. D. Thomas, D. B. Roy, R. J. Wilson, J. L. Leon-Cortes, D. Gutierrez, C. R. Bulman, R. M. Quinn, D. Moss, and K. J. Gaston. Density-distribution relationships in British butterflies. I. The effect of mobility and spatial scale. *Journal of Animal Ecology*, 70:410–425, 2001.

[27] C. C. Craig. On the frequency function of xy. *Annals of Mathematical Statistics*, 7:1–15, 1936.

[28] E. E. Crone and C. B. Schultz. Movement behavior and minimum patch size for butterfly population persistence. In C. L. Boggs, W. B. Watt, and P. R. Ehrlich, editors, *Butterflies: Ecology and Evolution Taking Flight*, pages 561–576. University of Chicago Press, Chicago, 2003.

[29] E. E. Crone and C. B. Schultz. Old models explain new observations of butterfly movement at patch edges. *Ecology*, 89:2061–2067, 2008.

[30] J. M. Cushing. *An Introduction to Structured Population Dynamics*. Society for Industrial and Applied Mathematics, Philadelphia, 1998.

[31] L. M. Delves and J. Walsh. *Numerical Solution of Integral Equations*. Clarendon Press, Oxford, 1974.

[32] C. A. Deutsch, J. J. Tewksbury, R. B. Huey, K. S. Sheldon, C. K. Ghalambor, D. C. Haak, and P. R. Martin. Impacts of climate warming on terrestrial ectotherms across latitude. *Proceedings of the National Academy of Sciences*, 105(18):6668–6672, 2008.

[33] V. Devictor, C. van Swaay, T. Brereton, D. Chamberlain, J. Heliölä, S. Herrando, R. Julliard, M. Kuussaari, Å. Lindström, D.B. Roy, O. Schweiger, J. Settele, C. Stefanescu, A. Van Strien, C. Van Turnhout, Z. Vermouzek, M. WallisDeVries, I. Wynhoff, and F. Jiguet. Differences in the climatic debts of birds and butterflies at a continental scale. *Nature Climate Change*, 2(2):121–124, 2012.

[34] G. Dwyer and W. F. Morris. Resource-dependent dispersal and the speed of biological invasions. *The American Naturalist*, 167:165–176, 2006.

[35] R. Engler and A. Guisan. MIGCLIM: Predicting plant distribution and dispersal in a changing climate. *Diversity and Distributions*, 15:590–601, 2009.

[36] B. Epstein. Some applications of the Mellin transform in statistics. *Annals of Mathematical Statistics*, 19:370–379, 1948.

[37] W. F. Fagan, M. Lewis, M. G. Neubert, C. Aumann, J. L. Apple, and J. G. Bishop. When can herbivores slow or reverse the spread of an invading plant? a test case from Mount St. Helens. *The American Naturalist*, 166:669–685, 2005.

[38] R. A. Fisher. The wave of advance of advantageous genes. *Annals of Eugenics*, 7:355–369, 1937.

[39] B. D. L. Fitt, P. H. Gregory, A. D. Todd, H. A. McCartney, and O. C. MacDonald. Spore dispersal and plant disease gradients: a comparison between two empirical models. *Journal of Phytopathology*, 118:227–242, 1987.

[40] M. Galassi, J. Davies, J. Theiler, B. Gough, G. Jungman, P. Aiken, M. Booth, and F. Rossi. *GNU Scientific Library: Reference Manual*. Network Theory Ltd., Bristol, 2009.

[41] K. J. Gaston. *The Structure and Dynamics of Geographic Ranges*. Oxford University Press, Oxford, 2003.

[42] A. Guisan and W. Thuiller. Predicting species distribution: offering more than simple habitat models. *Ecology Letters*, 8:993–1009, 2005.

[43] P. Hall. Comparison of two orthogonal series methods of estimating a density and its derivatives on an interval. *Journal of Multivariate Analysis*, 12:432–449, 1982.

[44] D. P. Hardin, P. Takac, and G. F. Webb. Asymptotic properties of a continuous-space discrete-time population model in a random environment. *Journal of Mathematical Biology*, 26:361–374, 1988.

[45] D. P. Hardin, P. Takac, and G. F. Webb. A comparison of dispersal strategies for survival of spatially heterogeneous populations. *SIAM Journal on Applied Mathematics*, 48:1396–1423, 1988.

[46] DP Hardin, P Takáč, and GF Webb. Dispersion population models discrete in time and continuous in space. *Journal of mathematical biology*, 28(1):1–20, 1990.

[47] S. Harrison, D.D. Murphy, and P.R. Ehrlich. Distribution of the bay checkerspot butterfly, *Euphydryas editha bayensis*: Evidence for a metapopulation model. *The American Naturalist*, 132:360–382, 1988.

[48] D. R. Hart and R. H. Gardner. A spatial model for the spread of invading organisms subject to competition. *Journal of Mathematical Biology*, 35:935–948, 1997.

[49] A. Hastings, K. Cuddington, K. F. Davies, C. J. Dugaw, S. Elmendorf, A. Freestone, S. Harrison, M. Holland, J. Lambrinos, U. Malvadkar, B. A. Melbourne, K. Moore, C. Taylor, and D Thomson. The spatial spread of invasions: new developments in theory and evidence. *Ecology Letters*, 8:91–101, 2005.

[50] A. Hastings and K. Higgins. Persistence of transients in spatially structured ecological models. *Science*, 263:1133–1136, 1994.

[51] R. Hickling, D. B. Roy, J. K. Hill, R. Fox, and C. D. Thomas. The distributions of a wide range of taxonomic groups are expanding polewards. *Global Change Biology*, 12:450–455, 2006.

[52] O. Honnay, K. Verheyen, J. Butaye, H. Jacquemyn, B. Bossuyt, and M. Hermy. Possible effects of habitat fragmentation and climate change on the range of forest plant species. *Ecology Letters*, 5:525–530, 2002.

[53] T. Horiguchi and Y. Fukui. A variation of the Jentzsch theorem for a symmetric integral kernel and its application. *Interdisciplinary Information Sciences*, 2:139–144, 1996.

[54] L. Hughes. Biological consequences of global warming: is the signal already apparent? *Trends in Ecology & Evolution*, 15:56–61, 2000.

[55] B. Huntley. North temperate responses. In T.E. Lovejoy and L. Hannah, editors, *Climate Change and Biodiversity*. Yale University Press, New Haven, 2005.

[56] G.E. Hutchinson. Concluding remarks. *Cold Spring Harbor Symposia on Quantitative Biology*, 22:415–427, 1957.

[57] V. Hutson and J. S. Pym. *Applications of Functional Analysis and Operator Theory*. Academic Press, London, 1980.

[58] IPCC. Climate Change 2007: Synthesis Report. Contribution of Working Groups I, II and III to the Fourth Assessment Report of the Intergovernmental Panel on Climate Change. Core Writing Team and Pachauri, R. K. and Reisinger, A., IPCC, Geneva, 2007.

[59] D. Jackson. *The Theory of Approximation*. American Mathematical Society, New York, New York, USA, 1930.

[60] C.E. Jeffree and E.P. Jeffree. Redistribution of the potential geographical ranges of mistletoe and Colorado beetle in Europe in response to the temperature component of climate change. *Functional Ecology*, 10:562–577, 1996.

[61] R. Jentzsch. Über integralgleichungen mit positivem kern. *Journal für die Reine und Angewandte Mathematik*, 141:235–244, 1912.

[62] R. Kadmon, O. Farber, and A. Danin. A systematic analysis of factors affecting the performance of climatic envelope models. *Ecological Applications*, 13:853–867, 2003.

[63] Y. Kang, D. Armbruster, and Y. Kuang. Dynamics of a plant–herbivore model. *Journal of Biological Dynamics*, 2:89–101, 2008.

[64] P. Kareiva. Population dynamics in spatially complex environments: theory and data. *Philosophical Transactions: Biological Sciences*, 330:175–190, 1990.

[65] S. Karlin. The existence of eigenvalues for integral operators. *Transactions of the American Mathematical Society*, 113:1–17, 1964.

[66] M. Keeling. Spatial models of interacting populations. In J. M. McGlade, editor, *Advanced Ecological Theory: Principles and Applications*, pages 64–99. Blackwell Science, Malden, 1999.

[67] A. E. Kelly and M. L. Goulden. Rapid shifts in plant distribution with recent climate change. *Proceedings of the National Academy of Sciences of the United States of America*, 105:11823–11826, 2008.

[68] A. Komonen, A. Grapputo, V. Kaitala, J. S. Kotiaho, and J. Päivinen. The role of niche breadth, resource availability and range position on the life history of butterflies. *Oikos*, 105:41–54, 2004.

[69] M. Kot. Discrete-time travelling waves: ecological examples. *Journal of Mathematical Biology*, 30:413–436, 1992.

[70] M. Kot, M. A. Lewis, and P. Van Den Driessche. Dispersal data and the spread of invading organisms. *Ecology*, 77:2027–2042, 1996.

[71] M. Kot, J. Medlock, T. Reluga, and D. B. Walton. Stochasticity, invasions, and branching random walks. *Theoretical Population Biology*, 66:175–184, 2004.

[72] M. Kot and W. M. Schaffer. Discrete-time growth-dispersal models. *Mathematical Biosciences*, 80:109–136, 1986.

[73] S. Kotz, T. J. Kozubowski, and K. Podgorski. *The Laplace Distribution and Generalizations: A Revisit with Applications to Communications, Economics, Engineering, and Finance*. Birkhauser, Boston, Massachusetts, USA, 2001.

[74] E. Kreyszig. *Introductory Functional Analysis with Applications*. John Wiley and Sons, New York, 1978.

[75] S. Krzemiński. Comment on 'A simple proof of the Perron–Frobenius theorem for positive symmetric matrices'. *Journal of Physics A: Mathematical and General*, 10:1437–1438, 1977.

[76] H. Kschwendt. Numerical solution of integral equations using Legendre polynomials. *Journal of Mathematical Physics*, 10:1964–1968, 1969.

[77] J. Latore, P. Gould, and A. M. Mortimer. Spatial dynamics and critical patch size of annual plant populations. *Journal of Theoretical Biology*, 190:277–285, 1998.

[78] J. Latore, P. Gould, and A. M. Mortimer. Effects of habitat heterogeneity and dispersal strategies on population persistence in annual plants. *Ecological Modelling*, 123:127–139, 1999.

[79] T.-T. Lee and Y.-F. Chang. Solutions of convolution integral and integral equations via double general orthogonal polynomials. *International Journal of Systems Science*, 19:415–430, 1988.

[80] J. Lenoir, J. C. Gégout, P. A. Marquet, P. de Ruffray, and H. Brisse. A significant upward shift in plant species optimum elevation during the 20th Century. *Science*, 320:1768–1771, 2008.

[81] T. M. Letcher. *Climate Change: Observed Impacts on Planet Earth*. Elsevier, Amsterdam, 2009.

[82] M. A. Lewis. Variability, patchiness, and jump dispersal in the spread of an invading population. In D. Tilman and P. Kareiva, editors, *Spatial Ecology: The Role of Space in Population Dynamics and Interspecific Interactions*, pages 46–69. Princeton University Press, Princeton, 1997.

[83] M. A. Lewis, M. G. Neubert, H. Caswell, J. S. Clark, and K. Shea. A guide to calculating discrete-time invasion rates from data. In M. W. Cadotte, S. M. McMahon, and T. Fukami, editors, *Conceptual Ecology and Invasions Biology: Reciprocal Approaches to Nature*, pages 169–192. Springer, Dordrecht, 2006.

[84] T.-Y. Li and J. A. Yorke. Period three implies chaos. *The American Mathematical Monthly*, 82(10):985–992, 1975.

[85] X. B. Li and F. Q. Gong. A method for fitting probability distributions to engineering properties of rock masses using Legendre orthogonal polynomials. *Structural Safety*, 31:335–343, 2009.

[86] S. R. Loarie, P. B. Duffy, H. Hamilton, G. P. Asner, C. B. Field, and D. D. Ackerly. The velocity of climate change. *Nature*, 462(24):1052–1055, 2009.

[87] D. R. Lockwood, A. Hastings, and L. W. Botsford. The effects of dispersal patterns on marine reserves: Does the tail wag the dog? *Theoretical Population Biology*, 61:297–309, 2002.

[88] T. E. Lovejoy and L. Hannah. *Climate Change and Biodiversity*. Yale University Press, New Haven, 2005.

[89] R. Lui. Existence and stability of travelling wave solutions of a nonlinear integral operator. *Journal of Mathematical Biology*, 16:199–220, 1983.

[90] F. Lutscher. Density-dependent dispersal in integrodifference equations. *Journal of Mathematical Biology*, 56:499–524, 2008.

[91] F. Lutscher and M. A. Lewis. Spatially-explicit matrix models. *Journal of Mathematical Biology*, 48:293–324, 2004.

[92] F. Lutscher, E. Pachepsky, and M. A. Lewis. The effect of dispersal patterns on stream populations. *SIAM Journal on Applied Mathematics*, 65:1305–1327, 2005.

[93] L. V. Madden, G. Hughes, and F. van den Bosch. *The Study of Plant Disease Epidemics*. American Phytopathological Society, St. Paul, Minnesota, USA, 2007.

[94] R. M. May. On relationships among various types of population models. *The American Naturalist*, 107:46–57, 1973.

[95] R. M. May. Biological populations with nonoverlapping generations: stable points, stable cycles, and chaos. *Science*, 186(4164):645–647, 1974.

[96] R. M. May. Biological populations obeying difference equations: stable points, stable cycles, and chaos. *Journal of Theoretical Biology*, 51:511–524, 1975.

[97] R. M. May. Simple mathematical models with very complicated dynamics. *Nature*, 261(5560):459–467, 1976.

[98] R. M. May, M. P. Hassell, R. M. Anderson, and D. W. Tonkyn. Density dependence in host–parasitoid models. *Journal of Animal Ecology*, 50:855– 865, 1981.

[99] J. Maynard Smith. *Mathematical Ideas in Biology*. Cambridge University Press, London, 1968.

[100] J. P. McCarty. Ecological consequences of recent climate change. *Conservation Biology*, 15:320–331, 2001.

[101] T. E. X. Miller and B. Tenhumberg. Contributions of demography and dispersal parameters to the spatial spread of a stage-structured insect invasion. *Ecological Applications*, 20:620–633, 2010.

[102] V. Mitikka, R. K. Heikkinen, M. Luoto, M. B. Araújo, K. Saarinen, J. Pöyry, and S. Fronzek. Predicting range expansion of the map butterfly in Northern Europe using bioclimatic models. *Biodiversity and Conservation*, 17:623–641, 2008.

[103] D. D. Murphy, N. Wahlberg, I. Hanski, and P. R. Ehrlich. Introducing checkerspots: Taxonomy and ecology. In P. R. Ehrlich and I. Hanski, editors, *On the Wings of Checkerspots: A Model System for Population Biology*, pages 17–33. Oxford University Press, Oxford, 2004.

[104] M. G. Neubert and H. Caswell. Demography and dispersal: calculation and sensitivity analysis of invasion speed for structured populations. *Ecology*, 81:1613–1628, 2000.

[105] M. G. Neubert, M. Kot, and M. A. Lewis. Dispersal and pattern formation in a discrete-time predator-prey model. *Theoretical Population Biology*, 48:7–43, 1995.

[106] M. G. Neubert, M. Kot, and M. A. Lewis. Invasion speeds in fluctuating environments. *Proceedings of the Royal Society of London B*, 267:1603–1610, 2000.

[107] M. G. Neubert and I. M. Parker. Projecting rates of spread for invasive species. *Risk Analysis*, 24:817–831, 2004.

[108] A. J. Nicholson. The balance of animal populations. *Journal of Animal Ecology*, 2:132–178, 1933.

[109] A. Okubo. *Diffusion and Ecological Problems: Mathematical Models*. Springer, Berlin, 1980.

[110] P. Opdam and D. Wascher. Climate change meets habitat fragmentation: linking landscape and biogeographical scale levels in research and conservation. *Biological Conservation*, 117:285–297, 2004.

[111] J. L. Osborne, H. D. Loxdale, and I. P. Woiwod. Monitoring insect dispersal: methods and approaches. In J. M. Bullock, R. E. Kenward, and R. S. Hails, editors, *Dispersal Ecology: The 42nd Symposium of the British Ecological Society held at the University of Reading 2-5 April 2001*, pages 24–49. Blackwell Science, Malden, 2002.

[112] W. A. Ozinga, C. Römermann, R. M. Bekker, A. Prinzing, W. L. M. Tamis, J. H. J. Schaminée, S. M. Hennekens, K. Thompson, P. Poschlod, M. Kleyer, J. P. Bakker, and J. M. van Groenendael. Dispersal failure contributes to plant losses in NW Europe. *Ecology Letters*, 12:66–74, 2009.

[113] C. Parmesan. Climate and species' range. *Nature*, 382:765–766, 1996.

[114] C. Parmesan. Detection at multiple levels: *Euphydryas editha* and climate change. In T. E. Lovejoy and L. Hannah, editors, *Climate Change and Biodiversity*, pages 56–60. Yale University Press, New Haven, 2005.

[115] C. Parmesan. Ecological and evolutionary responses to recent climate change. *Annual Review of Ecology, Evolution, and Systematics*, 37:637–669, 2006.

[116] C. Parmesan, N. Ryrholm, C. Stefanescu, J.K. Hill, C.D. Thomas, H. Descimon, B. Huntley, L. Kaila, J. Kullberg, T. Tammaru, W.J. Tennent, J.A. Thomas, and M. Warren. Poleward shifts in geographical ranges of butterfly species associated with regional warming. *Nature*, 399:579–583, 1999.

[117] C. Parmesan and G. Yohe. A globally coherent fingerprint of climate change impacts across natural systems. *Nature*, 421:37–42, 2003.

[118] R. G. Pearson and T. P. Dawson. Predicting the impacts of climate change on the distribution of species: are bioclimate envelope models useful? *Global Ecology and Biogeography*, 12:361–371, 2003.

[119] A. L. Perry, P. J. Low, J. R. Ellis, and J. D. Reynolds. Climate change and distribution shifts in marine fishes. *Science*, 308:1912–1915, 2005.

[120] A. T. Peterson, M. A. Ortega-Huerta, J. Bartley, V. Sánchez-Cordero, J. Soberón, R. H. Buddemeier, and D. R. B. Stockwell. Future projections for Mexican faunas under global climate change scenarios. *Nature*, 416:626–629, 2002.

[121] A. C. Pipkin. *A Course on Integral Equations*. Springer-Verlag, New York, 1991.

[122] A. B. Potapov and M. A. Lewis. Climate and competition: the effect of moving range boundaries on habitat invasibility. *Bulletin of Mathematical Biology*, 66:975–1008, 2004.

[123] J. Pöyry, M. Luoto, R. K. Heikkinen, M. Kuussaari, and K. Saarinen. Species traits explain recent range shifts of Finnish butterflies. *Global Change Biology*, 15:732–743, 2009.

[124] W. H. Press, S. A. Teukolsky, W. T. Vetterling, and B. P. Flannery. *Numerical Recipes in C: the Art of Scientific Computing*. Cambridge University Press, Cambridge, 1992.

[125] R. B. Primack and S. L. Miao. Dispersal can limit local plant distribution. *Conservation Biology*, 6:513–519, 1992.

[126] P. H. Rabinowitz. Some global results for nonlinear eigenvalue problems. *Journal of Functional Analysis*, 7(3):487–513, 1971.

[127] W. E. Ricker. Stock and recruitment. *Journal of the Fisheries Research Board of Canada*, 11:559–623, 1954.

[128] G. Sansone. *Orthogonal Functions*. Dover Publications, Inc., Mineola, New York, USA, 2004.

[129] C. B. Schultz. Dispersal behavior and its implications for reserve design in a rare oregon butterfly. *Conservation Biology*, 12:284–292, 1998.

[130] C. B. Schultz and E. E. Crone. Burning prairie to restore butterfly habitat: a modeling approach to management tradeoffs for the Fender's blue. *Restoration Ecology*, 6:244–252, 1998.

[131] C. B. Schultz and E. E. Crone. Edge-mediated dispersal behavior in a prairie butterfly. *Ecology*, 82:1879–1892, 2001.

[132] C. B. Schultz and P. C. Hammond. Using population viability analysis to develop recovery criteria for endangered insects: Case study of the Fender's blue butterfly. *Conservation Biology*, 17:1372–1385, 2003.

[133] C. B. Schultz, P. C. Hammond, and M. V. Wilson. Biology of the Fender's blue butterfly(*Icaricia icarioides fenderi Macy*), an endangered species of western Oregon native prairies. *Natural Areas Journal*, 23:61–71, 2003.

[134] F. M. Schurr, G. F. Midgley, A. G. Rebelo, G. Reeves, P. Poschlod, and S. I. Higgins. Colonization and persistence ability explain the extent to which plant species fill their potential range. *Global Ecology and Biogeography*, 16:449–459, 2007.

[135] M. W. Schwartz. Modelling effects of habitat fragmentation on the ability of trees to respond to climatic warming. *Biodiversity and Conservation*, 2:51–61, 1992.

[136] O. Schweiger, J. Settele, O. Kudrna, S. Klotz, and I. Kühn. Climate change can cause spatial mismatch of trophically interacting species. *Ecology*, 89:3472–3479, 2008.

[137] T. A. Severini. *Elements of Distribution Theory*. Cambridge University Press, New York, New York, USA, 2005.

[138] M. Shaw. Modeling stochastic processes in plant pathology. *Annual Review of Phytopathology*, 32:523–544, 1994.

[139] M. W. Shaw. Simulation of population expansion and spatial pattern when individual dispersal distributions do not decline exponentially with distance. *Proceedings of the Royal Society of London B*, 259:243–248, 1995.

[140] N. Shigesada and K. Kawasaki. *Biological Invasions: Theory and Practice*. Oxford University Press, Oxford, 1997.

[141] N. Shigesada and K. Kawasaki. Invasion and the range expansion of species: effects of long-distance dispersal. In J.M. Bullock, R.E. Kenward, and R.S. Hails, editors, *Dispersal Ecology*, pages 350–373. Blackwell Science, Oxford, 2002.

[142] J. G. Skellam. Random dispersal in theoretical populations. *Biometrika*, 38:196–218, 1951.

[143] C. A. Smith, I. Giladi, and Y.-S. Lee. A reanalysis of competing hypotheses for the spread of the California sea otter. *Ecology*, 90:2503–2512, 2009.

[144] V. M. Stevens, C. Turlure, and M. Baguette. A meta-analysis of dispersal in butterflies. *Biological Reviews*, 85:625–642, 2010.

[145] C. M. Taylor and A. Hastings. Allee effects in biological invasions. *Ecology Letters*, 8:895–908, 2005.

[146] M. T. Tinker, D. F. Doak, and J. A. Estes. Using demography and movement behavior to predict range expansion of the southern sea otter. *Ecological Applications*, 18:1781–1794, 2008.

[147] A. Trakhtenbrot, R. Nathan, G. Perry, and D. M. Richardson. The importance of long-distance dispersal in biodiversity conservation. *Diversity and Distributions*, 11:173–181, 2005.

[148] J. M. J. Travis. Climate change and habitat destruction: a deadly anthropogenic cocktail. *Proceedings of the Royal Society of London B*, 270:467–473, 2003.

[149] P. Turchin. *Quantitative Analysis of Movement*. Sinauer Associates, Inc., Sunderland, 1998.

[150] U.S. Fish and Wildlife Service. Endangered and threatened wildlife and plants; endangered status for *Erigeron decumbens* var. *decumbens* (Willamette daisy) and Fender's blue butterfly (*Icaricia icarioides fenderi*) and threatened status for *Lupinus sulphureus ssp. kincaidii* (Kincaid's lupine). Federal Register, 65:3875–3890, 2000.

[151] R. W. Van Kirk and M. A. Lewis. Integrodifference models for persistence in fragmented habitats. *Bulletin of Mathematical Biology*, 59:107–137, 1997.

[152] R. W. Van Kirk and M. A. Lewis. Edge permeability and population persistence in isolated habitat patches. *Natural Resource Modeling*, 12:37–64, 1999.

[153] G. R. Walther, E. Post, P. Convey, A. Menzel, C. Parmesan, T. J. C. Beebee, J. M. Fromentin, O. Hoegh-Guldberg, and F. Bairlein. Ecological responses to recent climate change. *Nature*, 416:389–395, 2002.

[154] M. H. Wang, M. Kot, and M. G. Neubert. Integrodifference equations, Allee effects, and invasions. *Journal of Mathematical Biology*, 44:150–168, 2002.

[155] M.-L. Wanga, R.-Y. Changa, and S.-Y. Yanga. Double generalized orthogonal polynomial series for the solution of integral equations. *International Journal of Systems Science*, 19:459–470, 1988.

[156] H. F. Weinberger. Asymptotic behavior of a model in population genetics. *Lecture Notes in Mathematics*, 648:47–96, 1978.

[157] H. F. Weinberger. Long-time behavior of a class of biological models. *SIAM Journal on Mathematical Analysis*, 13:353–396, 1982.

[158] A. L. Westerling, H. G. Hidalgo, D. R. Cayan, and T. W. Swetnam. Warming and earlier spring increase western U.S. forest wildfire activity. *Science*, 313:940–943, 2006.

[159] M. V. Wilson, T. Erhart, P. C. Hammond, T. N. Kaye, K. Kuykendall, A. Liston, A. F. Robinson Jr., C. B. Schultz, and P. M. Severns. Biology of Kincaid's lupine(*Lupinus sulphureus ssp. kincaidii* [Smith] Phillips), a threatened species of western Oregon native prairies, USA. *Natural Areas Journal*, 23:72–83, 2003.

[160] S. Yalcinbas, M. Aynigul, and T. Akkaya. Legendre series solutions of Fredholm integral equations. *Mathematical and Computational Applications*, 15:371–381, 2010.

[161] Y. Zhou and M. Kot. Discrete-time growth-dispersal models with shifting species ranges. *Theoretical Ecology*, 4:13–25, 2011.

[162] Y. Zhou and M. Kot. The role of the modified Bessel distribution in dispersal models. *In preparation.*, 2012.